



NTNU – Trondheim
Norwegian University of
Science and Technology

Stress Induced Stability Assessment of the Underground Caverns for Moglicë Hydropower Project, Albania

Martin Flåten

Geotechnology

Submission date: June 2015

Supervisor: Krishna Kanta Panthi, IGB

Co-supervisor: Bent Aagaard, Sweco Norge AS

Norwegian University of Science and Technology
Department of Geology and Mineral Resources Engineering



Your ref.: MS/N21T31/IGB/MFKKP

Date: 13.01.2015

TGB4930 INGGEOL/BERGMEK - MSc thesis

for

Eng. geo. Student Martin Flåten

**STRESS INDUCED STABILITY ASSESSMENT OF THE UNDERGROUND CAVERNS FOR
MOGLICE HYDROPOWER PROJECT, ALBANIA**

Background

The powerhouse and transformer hall of the Moglice Hydropower Project in Albania are placed underground. The powerhouse cavern has a size with length, width (span) and height of 61m x 17m x 28m that houses generating units, control room and service facilities. In addition, a 45m x 20m x 14m underground transformer hall is placed parallel to the powerhouse cavern. Optimization of cavern placement, orientation, spacing between two caverns are of major importance for the successful execution of this project. In addition, in-depth stability assessment of the underground caverns is of prime importance.

MSc thesis task

Hence, this MSc thesis is to focus on the overall optimization of the placement, orientation of the two caverns and spacing between them. In addition, detailed stability assessment of the underground powerhouse and transformer caverns must be carried out with following scope of work:

- Review existing theory on the stability issues for large underground caverns.
- Briefly describe Moglice Hydropower Project and review on the engineering geological investigations carried out at the project.
- Document mechanical and engineering geological parameters of the rocks and rock masses and in-situ stress conditions for the powerhouse and transformer caverns.
- Carry out assessment on the placement of underground caverns.
- Carry out analysis to optimize spacing between two caverns.

- Carry out stability assessment of these caverns using empirical, analytical and numerical analysis. Discuss and model the influence of high rock stresses on the design and rock support of the caverns.
- Optimize rock support needed to secure the cavern stability.
- Discuss the analysis results from empirical, analytical and numerical approaches.

Relevant computer software packages

Candidate shall use *roc-science package* and other relevant computer software for the master study.

Background information for the study

- Relevant information about the project such as reports, maps, information and data received from Sweco, Trondheim.
- The information provided by the professor about rock engineering and hydropower.
- Scientific papers, reports and books related to geology and tunnelling.
- Scientific papers and books related to international tunnelling cases.
- Literatures in rock engineering, rock support principles, rock mechanics and tunnelling.

Cooperating partner

Sweco Trondheim is the co-operating partner. Relevant project information, geological and engineering geological investigation reports shall be received from Sweco, Trondheim. **Mr. Bent Aagaard** will be the contact person for this project work at Sweco.

The project work is to start on January 15, 2015 and to be completed by June 11, 2015.

The Norwegian University of Science and Technology (NTNU)
Department of Geology and Mineral Resources Engineering

January 13, 2015



Dr. Krishna K. Panthi

Associate Professor of geological engineering, main supervisor

Acknowledgements

This master thesis has been conducted at the Department of Geology and Mineral Resources Engineering, as a part of the Master's Degree Programme, Geotechnology at the Norwegian University of Science and Technology (NTNU). Associate Professor Krishna Kanta Panthi has been my main supervisor. Sweco Norge AS has been the cooperating partner, and provided relevant project information and engineering geological investigation reports. Senior Engineering Geologist Bent Aagaard has been my co-supervisor and contact person at Sweco Trondheim.

I would like to thank my supervisor, Krishna Kanta Panthi. His good guidance have been an essential contribution to this task. Further, I would like to thank my co-supervisor Bent Aagaard and the rest of the Engineering Geologists at Sweco Trondheim for arranging this task and providing the necessary information. I am also grateful to Quac Nghia Trinh for advise regarding numerical modelling in Phase².

Martin Flåten

Trondheim, June 2015

Abstract

As a heavy investment to the Albanian renewable energy production, Devoll hydropower project (DHPP) is under development. DHPP is located in the southeast of Albania and consists of three hydropower plants, where Moglicë is the largest with its 175 MW. The powerhouse and transformer hall of the Moglicë plant will be placed underground. This thesis targets to optimize the location, orientation and spacing between the caverns in the Moglicë plant. To achieve this optimization, engineering geological conditions including rock mass properties and stress situation in the Moglicë area have been evaluated.

The original placement and orientation of the caverns from the background information are assessed. In addition, an alternative placement and orientation is proposed to reduce the length of the appurtenant tunnel system and minimize the impact of stress induced instabilities. These two alternatives are compared throughout the thesis.

An in-depth stability assessment of the underground caverns is carried out, with the scope of evaluating possible stress induced instabilities for the caverns. This analysis includes analytical, empirical and numerical methods. The analysis detected brittle failure in the cavern roofs and tensile fracturing in the cavern walls due to magnitude and anisotropy in the redistributed stresses. Stress induced instabilities will be more extensive in the powerhouse cavern relative to the transformer hall due to its shape and size.

Analytical and empirical studies includes Kirsch's equations and an approach from Hoek & Brown (1980) to assess the redistribution and concentration of stresses in the cavern contour. Spalling potential and depth of brittle failure are estimated based on cavern span, rock mass spalling strength and tangential stresses. These results are compared to estimations of failure depth from numerical analysis using the deviatoric stress criterion and analysis of strength factor with Hoek-Brown brittle parameters in the 2D finite element program, Phase². A reasonable coherence between the methods are found considering the associated uncertainties.

Support measures are proposed based on empirical relations between cavern span and bolt lengths, recommendations from the Q-system and analysis of yielding and deformation from the numerical results.

From the assessment of engineering geological conditions and the in-depth stability analysis, a pillar width of 22 m is suggested for the original placement and orientation, and 26 m pillar for the alternative placement and orientation. It is considered feasible to obtain a satisfactory level of stability for both locations and orientations, considering the rock mass properties and stress condition that are most likely to occur. However, the worst case numerical analysis showed significant stability problems. Placing large scale underground caverns in such conditions is not advisable.

Sammendrag

Som en del av satsningen på fornybar energi i Albania er vannkraftprosjektet Devoll HPP under utvikling. Devoll HPP er lokalisert sørøst i Albania og består av tre vannkraftverk, hvorav Moglicë er det største med sine 175 MW. Kraftstasjonen og transformatorhallen i Moglicë kraftverket skal plasseres i fjell. Denne oppgaven har som mål å optimalisere plassering, orientering og bredde mellom kavernene i Moglicë kraftverket. For å oppnå denne optimaliseringen er det nødvendig å evaluere ingeniørgeologiske forhold som inkluderer bergmassens egenskaper og spenningssituasjonen i det aktuelle området.

Den originale plasseringen og orienteringen av kavernene fra bakgrunnsinformasjonen er vurdert. I tillegg er en alternativ plassering og orientering foreslått for å se på muligheten til å redusere lengden på det tilhørende tunnelsystemet, samt minimere omfanget av spenningsinduserte stabilitetsproblemer. Disse to alternativene er sammenlignet gjennom denne oppgaven.

En dyptgående stabilitetsvurdering er gjennomført for å evaluere mulige spenningsinduserte stabilitetsproblemer. Denne analysen inkluderer analytiske, empiriske og numeriske metoder. Analysen detekterte sprø bruddutvikling i taket på kavernene og tensjonsbrudd i veggene som følge av størrelsen og anisotropien til de omfordelte spenningene i konturen på bergrommet. Spenningsinduserte stabilitetsproblemer vil være mer utbredt for kraftstasjonshallen enn for transformatorhallen på grunn av form og størrelse.

De analytiske og empiriske studiene inkluderer Kirschs ligninger og en metode av Hoek & Brown (1980) for å vurdere omfordeling og konsentrasjon av spenninger i konturen til bergrommene. Mulighet for sprakeberg og brudddybde er estimert basert på bergrommenes spennvidde, bergmassens trykkfasthet og tangensiale spenninger. Resultatene er sammenlignet med estimert brudddybde fra numerisk analyse ved bruk av «spenningsdeviatorkriteriet» og analyse av styrkefaktoren med Hoek-Brown sprø friksjonsparametere i det 2D endelig elementprogrammet Phase². En brukbar sammenheng mellom metodene er funnet med de gjeldende usikkerheter tatt i betraktning.

Sikringsmidler er foreslått basert på empiriske sammenhenger mellom spennvidde og boltelengder, anbefalinger fra Q-systemet og analyse av brudd og deformasjoner fra de numeriske resultatene.

Fra vurderingen av ingeniørgeologiske forhold og stabilitetsanalysen er det foreslått en pillarbredde på 22 m for den originale plasseringen og orienteringen. For den alternative plasseringen og orienteringen er pillarbredden anbefalt å være 26 m. Det anses som mulig å oppnå et tilfredsstillende stabilitetsnivå for begge plasseringer og orienteringer med bergmasseforholdene og spenningene som mest sannsynlig vil finne sted. Når det er sagt, kan spenningene og bergmassekvaliteten i verste fall føre til betydelige stabilitetsproblemer. Å plassere store kaverner i forhold som er gitt av «worst case» -scenarioet er ikke å anbefale.

Contents

ACKNOWLEDGEMENTS	I
ABSTRACT.....	III
SAMMENDRAG.....	V
CONTENTS.....	VII
1. INTRODUCTION	1
1.1 Background.....	1
1.2 Scope	2
1.3 Methodology	3
1.4 Limitations.....	4
2. STABILITY ISSUES FOR CAVERNS	5
2.1 Rock type	5
2.1.1 Strength of intact rock.....	5
2.1.2 Elasticity.....	5
2.2 Jointing	6
2.3 Weakness zones	7
2.4 Rock stresses	8
2.5 Ground water	10
2.6 Considerations regarding large scale caverns.....	11
2.6.1 Large span.....	12
2.6.2 Location	12
2.6.3 Orientation	12
2.6.4 Cavern shape	13
2.6.5 Pillar width.....	14
3. THEORY ON STABILITY ASSESSMENT OF UNDERGROUND CAVERNS.....	17
3.1 Structurally controlled instability.....	17
3.2 Tensile failure	18
3.3 Compressive failure	20
3.4 Failure criteria	21
3.5 Empirical and analytical methods to evaluate stability	23
3.5.1 Estimating stress distribution	23
3.5.2 Classifying rock mass quality	25
3.5.3 Predicting failure and extent	31
3.5.4 Proposing support	36

3.6 Numerical methods	36
3.6.1 Finite element methods	37
3.6.2 Phase ²	37
3.6.3 RocLab	37
4. MOGLIČĚ HYDROPOWER PROJECT	39
4.1 Project Description	39
4.1.1 Project layout features	39
4.1.2 Powerhouse complex design	40
4.2 Engineering Geological Conditions	42
4.2.1 Regional geology.....	42
4.2.2 Ground investigations.....	43
4.2.3 Geology along headrace tunnel.....	44
4.2.4 Geology in the area of the Powerhouse complex	45
4.3 Placement and orientations of Underground Caverns	50
4.3.1 Original placement and orientation	50
4.3.2 Alternative placement and orientation	51
4.4 Location of unlined pressure shaft.....	52
5. EMPIRICAL AND ANALYTICAL ANALYSIS.....	55
5.1 Stress distribution.....	55
5.2 Rock mass quality	56
5.3 Failure and extent.....	57
5.4 Support.....	58
6. NUMERICAL MODELLING	61
6.1 Model set up and input data	61
6.1.1 Geometry and excavation stages	61
6.1.2 Mesh and displacement	62
6.1.3 In-situ stresses.....	62
6.1.4 Material properties	65
6.1.5 Support.....	67
6.3 Numerical modelling results	68
6.3.1 Spacing between caverns	68
6.3.2 Stress distribution	70
6.3.3 Failure and extent	72
6.3.4 Support.....	76
6.4 Discussion on model results and sensitivity analysis.....	77
7. DISCUSSION.....	83
7.1 Stress situation	83
7.2 Placement and orientation of the caverns	83
7.2.1 Placement.....	83
7.2.2 Orientation	84

7.3 Spacing between caverns.....	84
7.4 Stability analysis	85
7.4.1 Stress distribution.....	85
7.4.2 Failure and extent.....	86
7.4.3 Rock mass quality and rock support	87
8. CONCLUSIONS AND FURTHER WORK	89
8.1 Conclusions.....	89
8.2 Further work.....	91
9. BIBLIOGRAPHY.....	93
APPENDICES	97
Appendix A: Guidelines for estimating disturbance factor D (Hoek, 2007)	99
Appendix B: The RMR-system and guidelines for support (Hoek, 2007)	101
Appendix C: The Q-system (NGI, 2013).....	103
Appendix D: Tectonic scheme of the Albanides (DHP, 2011)	105
Appendix E: Longitudinal section of the Moglicë waterway (DHP, 2011).....	107
Appendix F: Stereo plots of joints in the ophiolite complex	109
Appendix G: Values of the constant m_i for intact rock (Hoek, 2007)	111

1. Introduction

1.1 Background

In light of the increasing world focus on preventing climate changes, renewable resources will play an important role. As for today and until 2020 the European Union (EU) targets a 20% market share for renewable energy sources (Erbach, 2015). The Albanian president, Bujar Faik Nishani, reports in the Climate Summit 2014 that Albania has implemented climate policies in line with EU regulations (IISD, 2014). As a heavy investment to Albanian renewable energy production, the Devoll hydropower project (DHPP) is under development.

DHPP is located in the southeast of Albania, approximately 70 km southeast of the capital, Tirana (Figure 1.1). When the power plant is completed and at full capacity, it will make a significant contribution to the Albanian electricity production. Devoll Hydropower Sh.A, which is an Albanian registered company, owned and operated by the Norwegian power company Statkraft AS, are going to build, own, operate and transfer the project (DHP, 2013). Sweco Norge AS is contracted as consultants in the planning procedure, and this thesis is written in cooperation with Sweco Norge AS.

DHPP consists of three hydropower plants. Banjë and Molicë are under development, while the investment decision for the third plant, Kokël, will be taken when the other two are completed. The plants will have a total installed capacity of 278 MW, with an average production of about 800 GWh annually. This will increase the Albanian electricity production by almost 20 per cent (Statkraft, 2015).

Moglicë HPP (175 MW) is the upper and largest power plant in the project. It utilizes a head of 300 meters between 650 and 350 m.a.s.l approximately. The powerhouse and transformer hall for the Moglicë plant will be placed underground. Optimal location, orientation and spacing between the caverns are crucial to a successful execution of this project. As a result, this thesis will assess these parameters, in addition to an in-depth stability analysis.

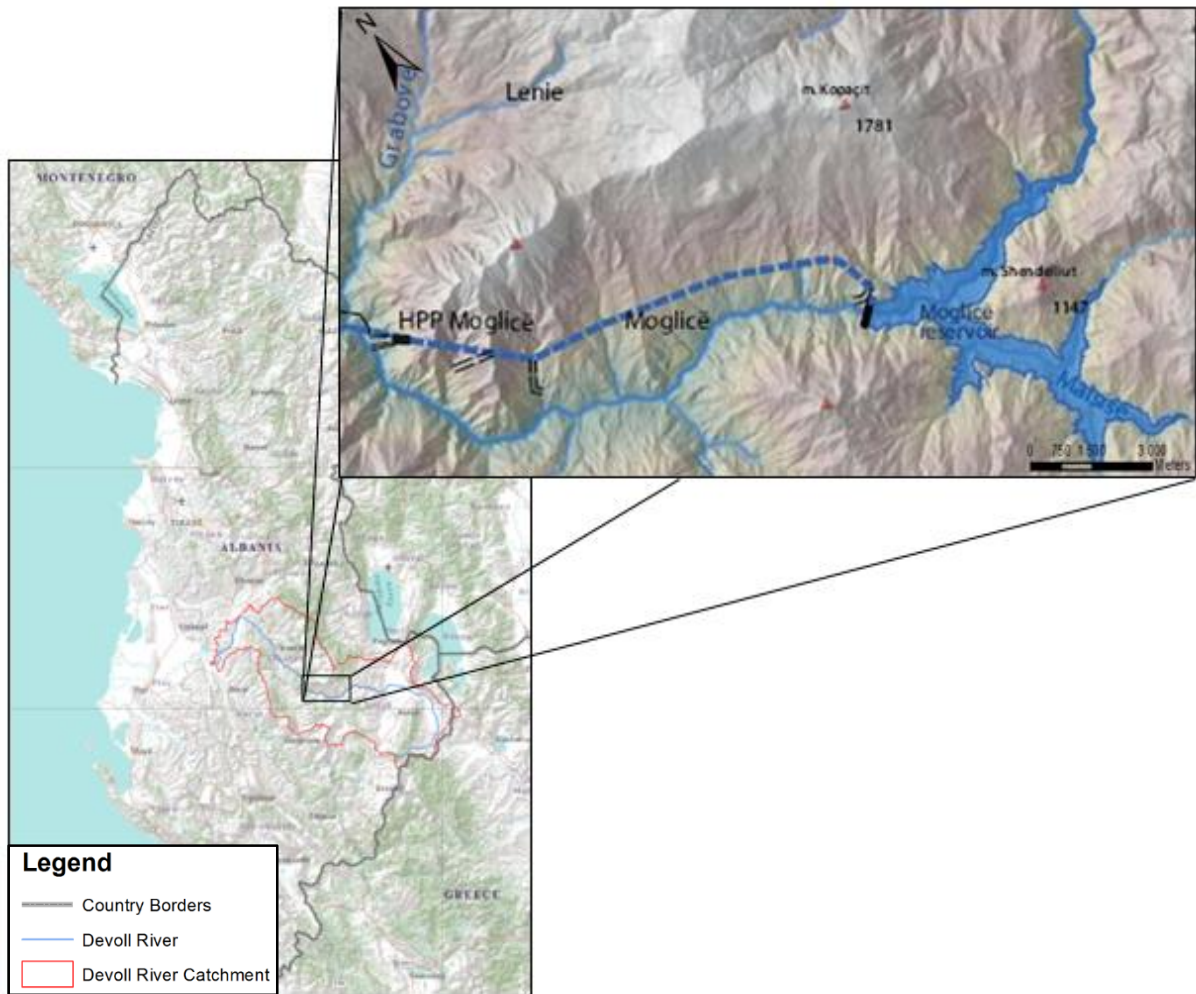


Figure 1. 1: Overview of the Moglicë Hydropower plant, Albania. Modified from DHP (2015).

The main engineering geologic challenges related to establishment of underground caverns in the area of Moglicë, are tectonically disturbed rock mass and high tectonic stresses which are capable of inducing brittle failure in the rock mass. In addition, practical and economic conditions has to be taken into account when evaluating location and orientation.

1.2 Scope

This thesis is to focus on the optimization of placement and orientation of the underground caverns of Moglicë HPP. The other main objective is an overall stability analysis of the powerhouse and transformer hall, which includes assessment of support and spacing between the caverns.

The scope of the thesis can be listed as follows:

- Review existing theory on stability issues for large underground caverns.
- Briefly describe Moglicë HPP and review the engineering geological investigations carried out at the project.
- Document mechanical and engineering geological parameters of the rocks and rock masses and in-situ stress conditions for the powerhouse and transformer caverns.

- Carry out assessment on the placement, orientation and spacing between the underground caverns.
- Analyse the global stability of the caverns using analytical, empirical and numerical methods.
- Discuss and model the influence of high rock stresses on the cavern stability.
- Optimize rock support needed to secure the cavern stability.
- Discuss the analysis results from empirical, analytical and numerical approaches.

1.3 Methodology

The methodology in the work has principally followed the structure below.

Literature review:

The literature review is the basis for the theory and methods in this thesis. Scientific articles and literature constitutes the bulk of the references. Most of the literature is found through databases in the university library of the Norwegian university of science and technology. The search engine in the Compendex database has been used frequently to systematically narrow down the search to the most relevant scientific articles. The main topics for the literature review have been:

- Stability issues for large underground caverns
- Failure mechanism in brittle rocks
- Analytical and empirical methods to assess stability for underground excavations
- Support principles for underground caverns

Study of Moglicë HPP:

Reports and project descriptions have been studied to get an overview of the Devoll project, with special considerations to Moglicë HPP. Evaluation of engineering geologic reports, containing data from field investigation, laboratory tests and stress measurements have been crucial to the assessment of cavern placement and stability. In addition, it has been important to get an overview of the project layout and the topography in the area of the powerhouse caverns. This is to make sure that possible adjustments to the placement do not interfere with practical feasibility.

Cavern placement and orientation:

In this thesis two different alternatives for placement and orientation has been analysed. One is based on background information provided by Sweco Norge AS. This alternative is planned for Moglicë HPP, and will in the further be referred to as “the original placement”. The other alternative is a solution proposed by the author where the caverns are moved 150 m towards the valley and where the length axis is oriented N48°E, rather than N120°E that is the original orientation. This solution will be referred to as “the alternative placement”. A stability assessment is carried out on both alternatives.

Stability assessment:

The stability assessment has been carried out with different techniques:

1. Analytical methods
2. Empirical methods
3. Numerical methods

The analytical and empirical methods recapitulated in one chapter. This is because the methods used are often combinations of analytical and empirical approaches. The following techniques have been used to assess stability of the caverns:

- Kirsch's equations and an empirical approach introduced by Hoek and Brown (1980) are utilised to estimate the redistribution of stresses around the excavation contours.
- The rock mass is classified by the "little q" system. In addition, the GSI value is converted to RMR- and Q-values to describe the rock mass quality.
- Extent of brittle failure is estimated after classification developed by Hoek and Brown (1980) based on the major principle stress and the UCS.
- Spalling potential is estimated by methods from Diederichs (2007), Martin & Christiansson (2009) and Cai & Kaiser (2014)
- Depth of brittle failure is calculated using formulas by Martin & Christiansson (2009), Kaiser et al. (1996) and Martin et al. (1999).
- A collection of empirical formulas are used to estimate required bolt lengths based on excavation span.
- Support is proposed based on RMR and Q-values converted from GSI, together with recommendations from the "little-q" system.

A numerical stability assessment is carried out through modelling of both elastic and plastic material. The elastic model has its purpose to obtain information about the distribution of secondary stress, stress concentration in the pillar between the caverns and also to estimate depth of spalling. Depth of spalling is analysed with Hoek-Brown brittle parameters and with the deviatoric stress criterion. The plastic model has been important to predict deformations, yielded elements and to estimate rock support.

1.4 Limitations

The thesis is focusing on stress induced stability issues. Hence, the in depth stability assessment is based on stress related problems and the assessment of structurally controlled instabilities is limited.

Proposing a new location for a hydropower plant involves changes in design for the related tunnel system. This new design have been roughly worked out in this thesis, but details in the tunnel design are left out.

Due to practical difficulties in conducting a field trip to the site, this project has been carried out as a desk study. This has not been a major problem since field observations and laboratory test have already been executed and documented in reports. That being said, second hand information will always be a slight restriction, especially when assessing the location of the caverns.

2. Stability issues for caverns

Several factors affects the stability of an underground cavern. Most of these elements are generally important for excavations in rock. When dealing with large scale underground caverns, there are special considerations that need to be taken into account.

2.1 Rock type

As the rock mass is the building material for an underground excavation, the mechanical properties of the rock is crucial to the stability of the opening. These characteristics describes the ability the rock has to withstand stress and deformation (Panthi, 2006). In addition, the anisotropy and weathering of the rock will affect the stability.

2.1.1 Strength of intact rock

The strength of rocks is of great importance regarding stability assessments. Strength can be measured by various methods and procedures. A common way to represent the rock strength is by uniaxial compressive strength. This test is carried out by loading a core sample of a rock, in the axial direction, until failure occurs. The pressure needed to induce failure is referred to as the uniaxial compressive strength of the rock (σ_c). Standard procedures for this test are given by the International society for rock mechanics (ISRM), and the following table can be used for classification (Nilsen & Palmström, 2000):

Table 2. 1: Classification based on uniaxial compressive strength (ISRM, 1978). The table is modified from Nilsen & Palmström (2000).

Type	Classification	Uniaxial compressive strength, UCS [MPa]
<i>Soil</i>		< 0,25
<i>Rock</i>	Extremely low strength	0,25 – 1
	Very low strength	1 – 5
	Low strength	5 – 25
	Medium strength	25 – 50
	High strength	50 – 100
	Very high strength	100 – 250
	Extremely high strength	> 250

2.1.2 Elasticity

Another substantial mechanical property of the rock is the elasticity parameters. In elastic deformation, there are constants that relate the magnitude of the strain response to the applied stress. Young's modulus (E) is the gradient of the stress-strain curve in the linear area of elastic deformation. Hooke's law gives the formula for E:

$$\sigma = E\varepsilon \quad [2.1.1]$$

(Nilsen & Palmström, 2000)

When a cylinder of rock is compressed axially, it will expand in the radial direction. The ratio of radial strain (ε_r) to axial strain (ε_a) is defined as Poisson's ratio (ν).

$$\nu = -\frac{\varepsilon_r}{\varepsilon_a} \quad [2.1.2]$$

(Myrvang, 2001)

Information about the elasticity of the rock is important regarding which failure mode to expect. High E-modulus yields a stiff rock and a brittle failure mode. Low E-modulus results in more deformation, and squeezing can occur. This influences the post failure behaviour. Information about post failure behaviour is valuable regarding estimation of permanent rock support. Typical post-failure behaviour for different quality rock is represented in a stress-strain diagram in figure 2.1.

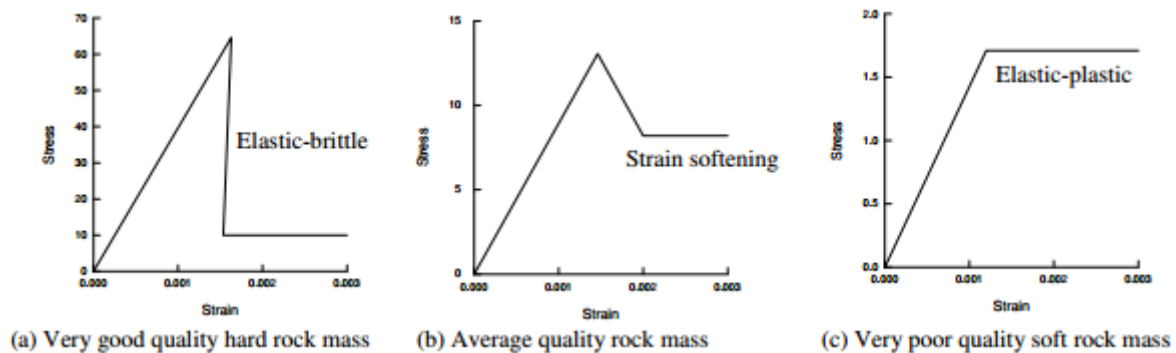


Figure 2. 1: Stress-strain diagrams of typical post-failure behaviour for different quality rock. Modified after Hoek (2007).

2.2 Jointing

The properties of the in-situ rock mass will largely be governed by the properties of joints and discontinuities. This is the case, even for strong and hard rocks. Joints transfer compressive and shear forces, but not tensile forces. It is essential to understand the jointing in order to understand the behaviour of the rock mass (Nilsen & Thidemann, 1993). Joints are often defined, based on their origin (e.g. tectonic joints, exfoliation joints, bedding joints etc.) or based on size and composition (e.g. partings, cracks, fissures, seams etc.) (Nilsen & Palmström, 2000).

Joints delineate blocks. Their dimensions and shapes are determined by the joint spacing, by the number of joint sets and random joints. Block size is a very important parameter regarding stability, especially in areas with low gripping tension. Hence, information about the degree and characteristics of jointing is essential (Nilsen & Palmström, 2000).

There are different methods for measuring the degree of jointing. The most common are:

- Joint spacing
- Density of joints
- Block size, on surfaces
- Rock quality designation (RQD), in drill cores

(Nilsen & Palmström, 2000)

In addition to the degree of jointing, several characteristics influence the stability of the rock mass. The main characteristics are:

- Roughness, waviness of the joint wall
- Alteration of wall rock or occurrence of coating
- Presence of possible filling
- Length and continuity of the joint

Their properties influence the stability affecting the shear strength of the joints, as well as the amount of water that can flow through the rock mass (Nilsen & Palmström, 2000). The properties and characteristics will vary greatly from one type of joint to another, since their formation, age and history of development are fundamentally different. The effect of joints on rock mass behaviour calls for special attention to these features when characterising rock masses for practical applications (Palmström & Stille, 2010).

2.3 Weakness zones

It is essential to avoid weakness zones when deciding the location of an underground cavern. In an engineering geological context, it is useful to divide weakness zones in two main groups: weak rock layers and tectonic faults (Figure 2.2) (Nilsen & Broch, 2011).

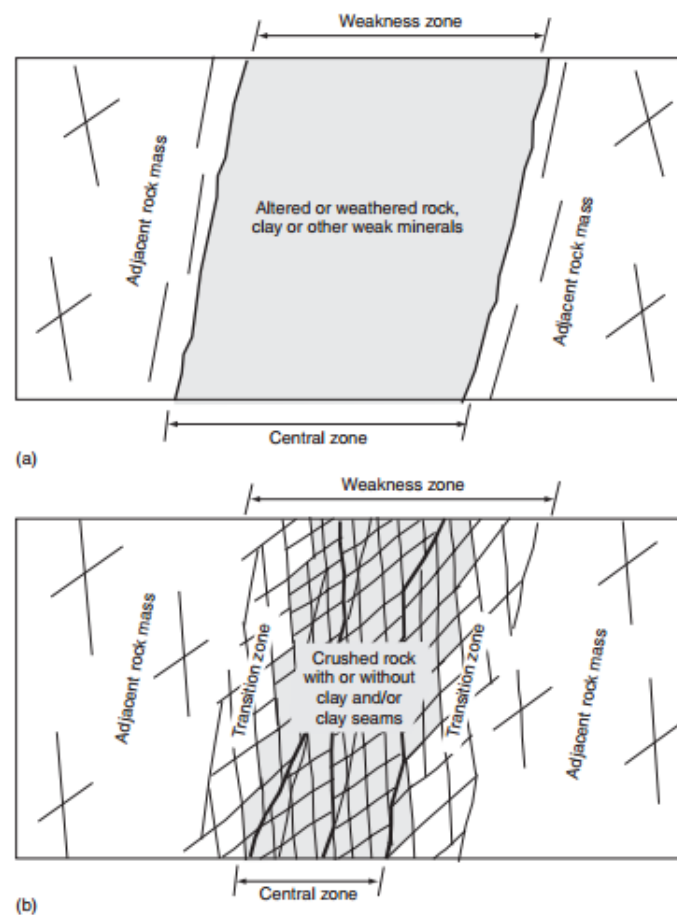


Figure 2. 2: Weakness zones divided into two main groups: weak rock layers (a) and tectonic faults (b) (Palmström & Stille, 2010).

Weak rock layers consist of rock masses with significantly weaker mechanical properties than the surrounding rock mass. Such layers often consists of an anisotropic structure, either formed primarily or during metamorphism. Chemical weathering may cause weak rock layers, particularly by forming of clay minerals (Nilsen & Broch, 2011).

Tectonic faults are zones where relative movement, caused by tectonic activity have taken place. The grain size in such zones will often vary from block to clay due to crushing. Important factors for tectonic faults regarding stability are grade of disintegration and amount of prospective clay minerals (Nilsen & Broch, 2011).

Hydrothermal activity and other processes may cause alteration of minerals into clays, often with swelling properties. Weakness zones often contain materials quite different from the “host” rock. Such zones can vary a lot in structure and composition. The fact that weakness zones of significant size can have a huge impact on the stability of an underground opening, means that special attention, follow-up and investigations often are necessary to predict and avoid such events (Palmström & Stille, 2010).

2.4 Rock stresses

Rock stresses can lead to significant stability problems, but they are also vital to obtain a self-bearing construction with the rock mass as building material. According to convention, compressive stress is positive and tensile stress is negative.

Principal stresses are useful in stress analysis. These are the normal stresses on planes with no shear stress. Knowledge about the in-situ stresses in the rock mass, can along with information about the opening geometry, provide means to evaluate the magnitudes and directions of the redistributed stresses surrounding the opening. If the rock mass properties are known, it is possible to assess potential stress induced stability problems. Hence, also the need for rock support and possibilities for optimising the excavation geometry (Nilsen & Palmström, 2000).

The virgin rock stress generally represents the resultant of the following components:

- Gravitational stresses
- Tectonic stresses
- Topographic stresses
- Residual stresses

(Nilsen & Thidemann, 1993)

The gravity induced vertical (σ_v) and horizontal stresses (σ_h) are related through the following equations:

$$\sigma_v = \gamma \times H \quad [2.4.1]$$

$$\sigma_h = \frac{\nu}{1-\nu} \times \gamma \times H \quad [2.4.2]$$

Where, γ is the specific weight of the rock mass, and H is the depth and ν is the Poisson's ratio (Panthi, 2006).

Measurements of mining and civil engineering projects around the world are plotted in figure 2.3. This shows an average ratio of 0,027 between vertical stress (in MPa) and depth below surface (in meters).

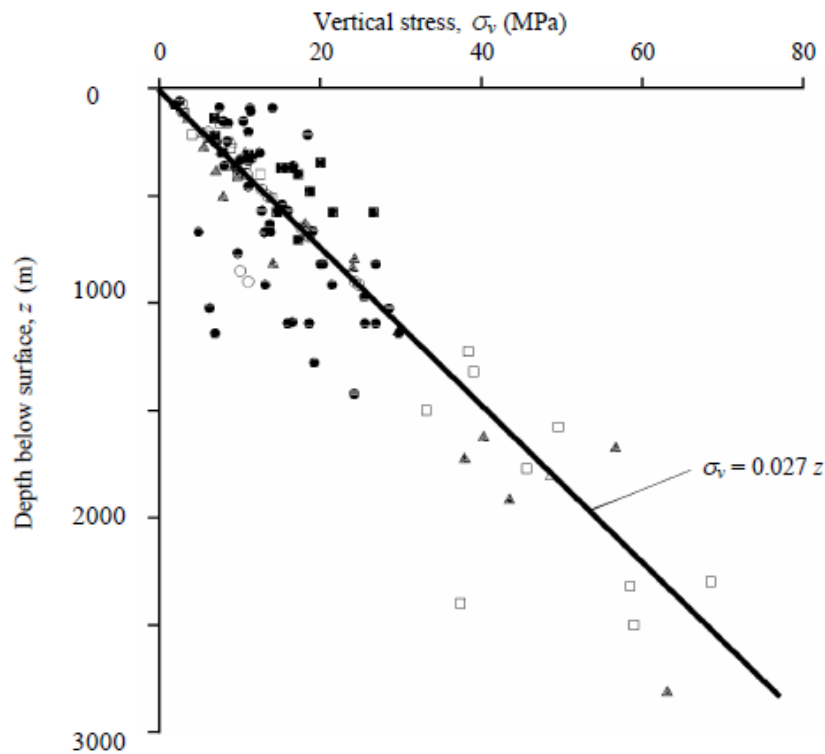


Figure 2. 3: Vertical stress measurements from mining and civil engineering projects around the world (Hoek et al., 1995).

The horizontal stress induced by gravity is commonly about 1/3 of the vertical stress. However, the horizontal stress induced by gravity will normally constitute to only a small part of the total horizontal stress (Nilsen & Palmström, 2000). This is often mainly due to tectonic stresses. Figure 2.4 shows the results of a large number of rock stress measurements from different parts of the world. This illustrates the variations in the ratio between horizontal and vertical stresses.

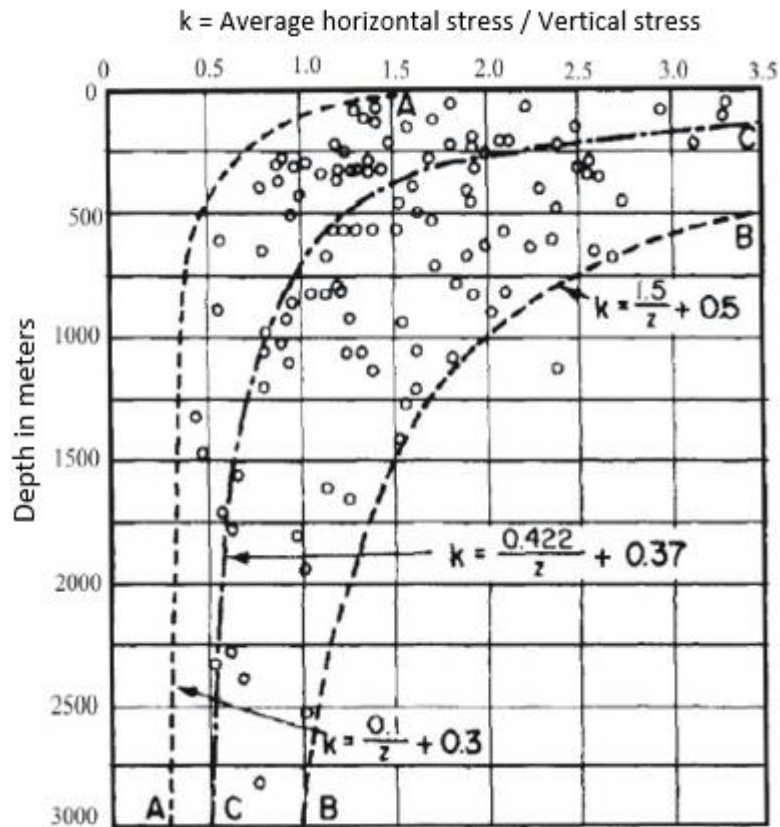


Figure 2. 4: Variation in the ratio between average horizontal to vertical stress as a function of depth below surface (Panthi, 2006).

When the surface is dipping, the stress situation will be greatly influenced by topographic stresses. In high valley sides, topographic effects near the surface will dominate the stress situation. The largest principal stress will be directed more or less parallel to the surface (Nilsen & Palmström, 2000).

Residual stresses have been locked into the rock material during earlier stages of its geological history. Variation in concentration of a cooling rock melt can lead to residual stresses (Nilsen & Palmström, 2000). The residual stresses are hard to predict without explicit stress measurements.

2.5 Ground water

Groundwater is freely moving water that occurs below the groundwater table. The groundwater table is the level below which the geologic formation is fully saturated. Subsurface water is in large extent consisting of groundwater. Water may also occur as:

- chemically bounded to the crystal structure (e.g. in gypsum $\text{CaSO}_4 \cdot \text{H}_2\text{O}$)
- absorbed, by the crystal structure in some minerals (e.g. smectite)
- capillary, in thin fissures and pore systems

(Palmstöm & Stille, 2010)

Some rocks, such as young sandstones and certain limestones, may contain large volumes of capillary water. However, in majority of the cases, it is freely moving groundwater that affects the excavation conditions and long-term stability (Palmström & Stille, 2010).

Groundwater in rock masses is a part of the hydrologic cycle (Figure 2.5). The groundwater is capable of travelling long distances through a rock mass. Hence, it is important to consider the regional geology and the overall groundwater pattern when analysing potential water problems.

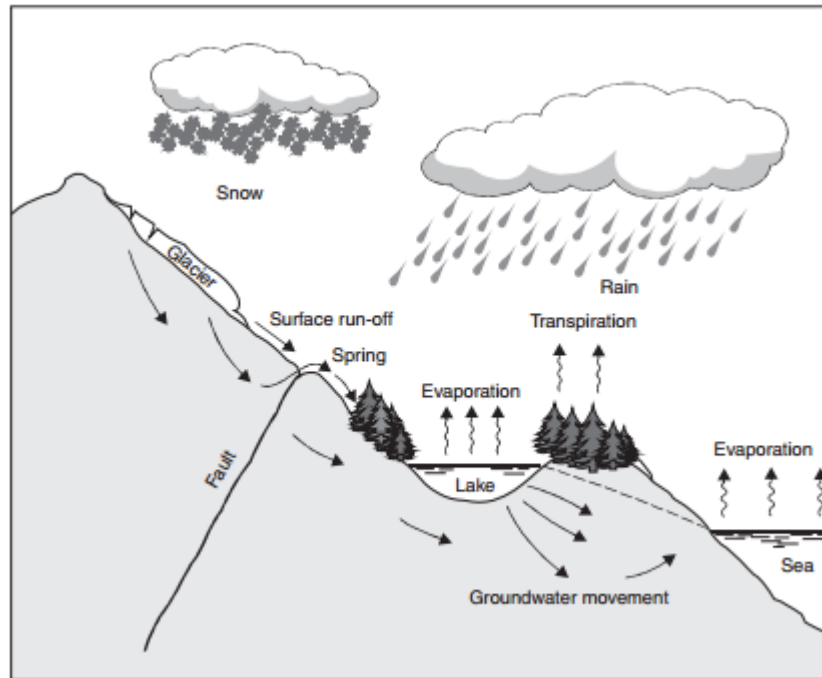


Figure 2. 5: The way ground water participate in the hydraulic circle (Palmström & Stille, 2000).

Significant groundwater pressure and flow may be encountered in practically any rock mass, but it will normally only cause serious stability issues in crushed or sand-like materials, or when associated with other forms of instability. Groundwater effects stability by reducing the strength of rock materials and the shear strength of discontinuities. In swelling clay, this reduction of friction and strength will be significant. Water leakage often occurs in areas close to the surface, because of more extensive jointing and open joints (Nilsen & Palmström, 2000).

In underground openings, failures related to joint water pressure is relatively rare. However, groundwater pressure may contribute to instability, particularly in weak rock masses. The impact of groundwater pressure should always be evaluated in cases where it is potentially significant (Nilsen & Palmström, 2000).

2.6 Considerations regarding large scale caverns

Several factors make excavation of large scale caverns specially challenging. Such as large span and pillar stability are important issues that needs to be considered with caution. To avoid, or at least reduce stability problems, a careful and systematic design approach is essential.

The general procedure recommended for the design of underground caverns can be divided in the following stages:

1. Select an optimal location from a stability point of view, and from the engineering geological conditions in the actual area.
2. Orient the length axes of the caverns to give minimal stability problems and overbreak.
3. Shape the caverns openings taking into account the mechanical properties and jointing of the rock masses as well as the local stress conditions.
4. Dimension the components of the complex to give an optimal economical arrangement.

(Edvardsson & Broch, 2002)

2.6.1 Large span

Large span will make demands to a favourable confining pressure. Low gripping tension will allow potential wedges to slide and destabilise the excavation. Increasing span will allow larger blocks to be relieved. Stability problems in caverns will in general be increasing with increasing span. It is often preferable to meet the need for increased volumes by extending the opening along its length axis rather than increasing the span (Nilsen & Thidemann, 1993).

2.6.2 Location

The site location is crucial to the stability of the cavern, since the location of an underground powerhouse is a combined site and construction material selection. It is important to avoid unfavourable types of rock. Weak, heavily jointed and porous rocks are not propitious. Aggregate quality should also be taken into account when selecting site location. This is to reduce the net costs of the project. However, the site location is often limited to a smaller area due to possibilities for access tunnels, hydraulic conditions in the waterway and other economically determined conditions (Edvardsson & Broch, 2002).

Assessment of the overburden is also decisive for the stability of the cavern. The cavern should be placed deep enough to give the normal stresses on joints and fissures which are necessary for a self-supporting roof. It is also important to leave a reasonable layer of unweathered rock above the cavern. For more deep-seated caverns it is important that the stresses don't exceed a level which can cause overstressed rock and stress-induced stability problems. Weakness zones and heavy jointing should also be avoided. Mapping and evaluation of jointing and weakness zones are important preconstruction phase investigations (Edvardsson & Broch, 2002).

2.6.3 Orientation

The caverns orientation is selected with respect to the orientation of local joint sets. It is preferably to orient the length axis of the caverns along the bi-section line of the maximum intersection angle between the two dominating joint, bedding or foliation directions (Figure 2.6). However, it should not be parallel to an eventual third or fourth joint set direction. In areas with high anisotropic stresses, the length axis of the caverns should be oriented in an angle of 15°-25° to the horizontal projection of the major principal stress to obtain the most stable situation regarding stress-induced instability (Edvardsson & Broch, 2002).

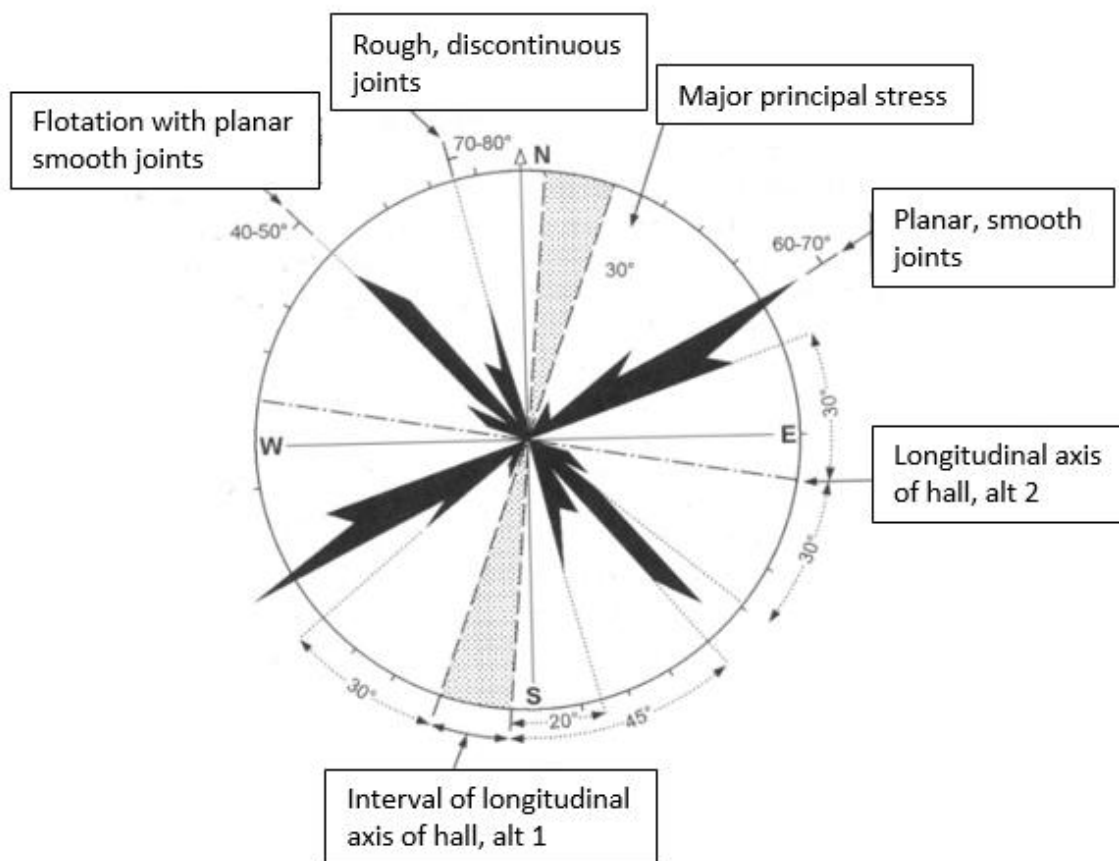


Figure 2. 6: Typical rosette plot and favourable orientation of caverns with respect to joints and stress directions. Modified from Edvardsson & Broch (2002).

2.6.4 Cavern shape

The conventional shape for a powerhouse cavern is shown in figure 2.7a. This shape is preferable in strong rock masses. The arched roof distributes the rock stresses and provides convenient headroom for an overhead crane. Practically, this cross section is favourable to excavate due to the straight walls. In weak rock masses, an elliptical shape (Figure 2.7b) will be favourable to prevent the walls to deflect inwards due to tensile failure. While this cavern shape is preferable from a stability point of view, it has some practical disadvantages. The construction has to be more carefully executed than the conventional straight-walled cavern and items such as the cranes and services must be design to fit into the elliptical shape (Hoek, 2000).

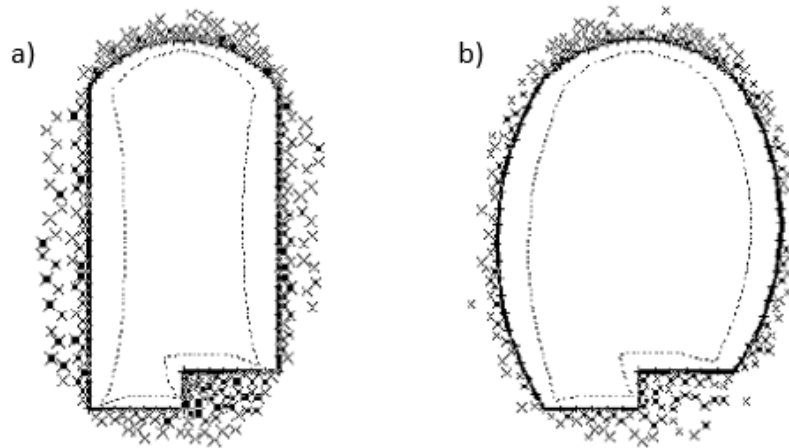


Figure 2. 7: Comparison of zones of failure for conventional straight-walled cavern (a) and elliptical shaped cavern (b) (Hoek, 2000).

Ideally, the shape of a cavern should relate directly to rock mechanical properties and stress conditions. In reality, the cavern shape is often not optimal regarding design parameters. Figure 2.8 show the most common cavern shapes, and their applicability according to rock mass properties (E_{int} , E_{rm} , UCS_{int} , UCS_{rm}) and stress conditions (h , K_0) (Marcher & Saurer, 2013).

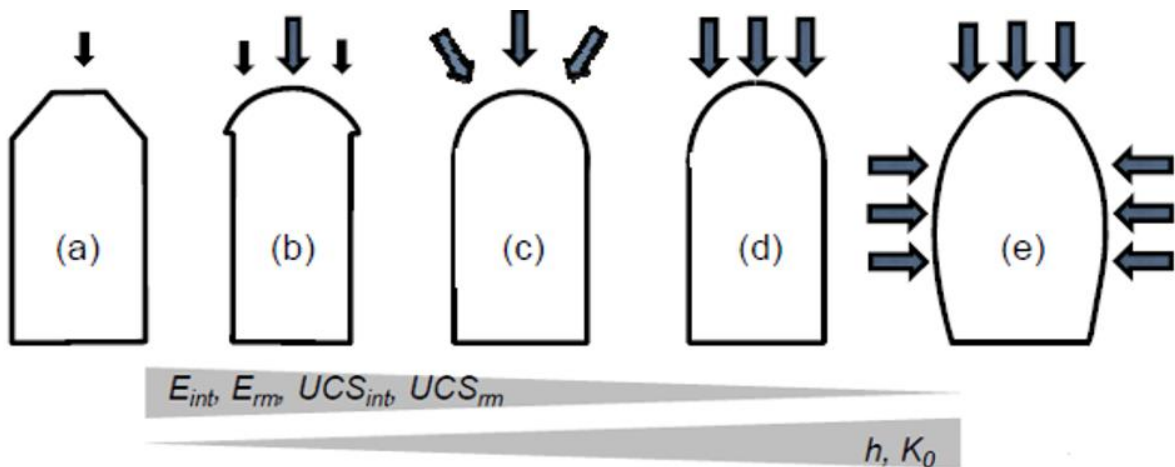


Figure 2. 8: Different cavern shapes and their applicability according to rock mass properties (E_{int} , E_{rm} , UCS_{int} , UCS_{rm}) and stress conditions (h , K_0): a) trapezoidal b) mushroom c) circular shape d) bullet shape e) horse shoe (Marcher & Saurer, 2013).

2.6.5 Pillar width

The transformer hall is often placed in a smaller cavern parallel to the powerhouse cavern. This has the advantage of reducing the dimensions of the powerhouse cavern and of isolating the transformers in case of fire. To minimize the length and cost of busbars that link the generators to the transformers, it is favourable to place the two caverns as close to each other as possible (Hoek, 2000).

If the caverns are placed too close, the pillar between them will be overstressed. Based on Kirsch's equations (discussed in Chapter 3), the stress distribution between two openings will be similar to what is shown in figure 2.9a. The maximum stress will be located at the surface of the caverns. The rock mass close to the openings will often be jointed due to blasting. This results in a lower capacity for obtaining stresses in the rock close to the openings, which leads to the stress distribution illustrated in figure 2.9b. If the jointing and stress concentration spread inwards in the pillar, the peak stress will eventually move to the middle as shown in figure 2.9c (Myrvang, 2001).

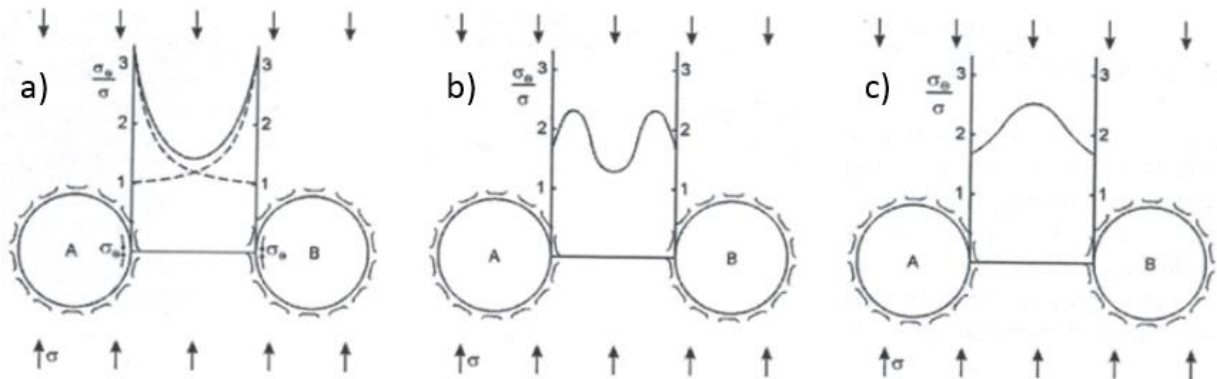


Figure 2. 9: Different stress situations in a pillar between two excavations. The different figures (a-c) shows an increasing level of failure. Modified from Myrvang (2001).

Figure 2.9a indicates that an increase of pillar width beyond the diameter of the opening will result in a small reduction in maximum pillar stress. If fracturing due to blasting is considered, increasing the pillar width to more than 1,5 times the diameter will have little significance to the pillar stress (Myrvang, 2001). This is applicable for circular excavations, but it can also give a rough estimate for powerhouses. In addition, the quality of the rock mass has to be taken into account. For caverns in weak rock masses, the distance between the two caverns should not be less than the height of the larger cavern to obtain satisfying stability (Hoek, 2000; Hoek, 2007).

3. Theory on stability assessment of underground caverns

Underground caverns are exposed to different kinds of failure modes depending on both rock mass quality and stress situation (Figure 3.1). Assessment of stability are executed by different methods depending of the type of failure. This thesis will be focusing on brittle failure under intermediate to high in situ stresses.

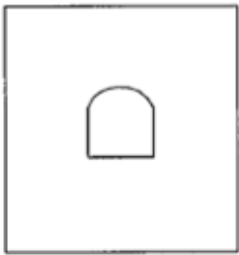

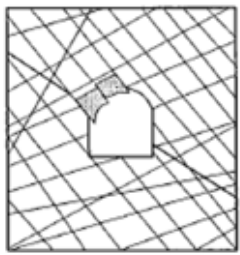

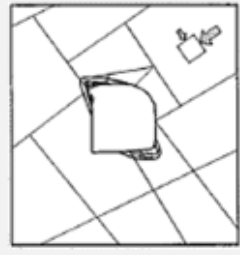
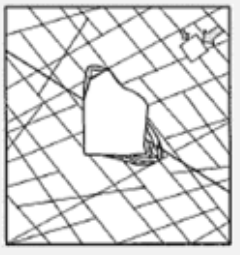

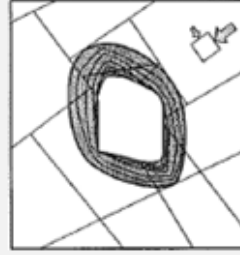
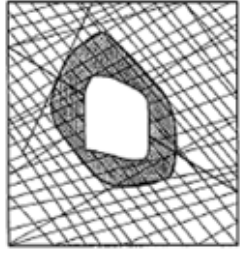
	<i>Massive</i> (RMR > 75)	<i>Moderately fractured</i> (50 > RMR < 75)	<i>Highly fractured</i> (RMR < 50)
<i>Low in-situ stresses</i> ($\sigma_1 / \sigma_c < 0,15$)	 Linear elastic response	 Falling or sliding of blocks and wedges.	 Unravelling of blocks from the excavation surface.
<i>Intermediate in-situ stresses</i> ($0,15 > \sigma_1 / \sigma_c < 0,4$)	 Brittle failure adjacent to excavation boundary.	 Localized brittle failure of intact rock and movement of blocks.	 Localized brittle failure of intact rock and unravelling along discontinuities.
<i>High in-situ stresses</i> ($\sigma_1 / \sigma_c > 0,4$)	 Brittle failure around the excavation.	 Brittle failure of intact rock around the excavation and movement of blocks.	 Squeezing and swelling rocks. Elastic/plastic continuum.

Figure 3. 1: Examples of instabilities and brittle failure (grey squares) as a function of Rock Mass Rating (RMR) and the ratio of the major principle stress and UCS. Modified after Martin et al. (1999).

3.1 Structurally controlled instability

In hard rock excavations at shallow depth, gravity controlled mobilisation of blocks or wedges defined by intersecting structural discontinuities is the most common type of failure (Figure 3.2). At least three structural planes needs to be present to define a block, with the excavation boundary as the fourth plane (Hammet & Hoek, 1981). The stability of the opening will

deteriorate rapidly if loose wedges are allowed to slide. Falling wedges will cause a reduction in the restraint and the interlocking of the rock mass. This will in turn allow other wedges to be destabilised (Hoek et al, 1995). Both orientation of the discontinuities in the rock mass, the cavern shape and the state of the structural features in terms of friction and weathering will affect the structurally controlled instabilities.



Figure 3. 2: Example of block downfall from structurally controlled instability. From the Hanekleiva tunnel, Norway (Beitnes et al., 2007).

Support of blocks and wedges requires a dynamic support design, where rock bolts or cables are installed to support the weight of possible loose wedges. The identification and support of wedges will not be the focus of this task, and will not be discussed further.

3.2 Tensile failure

A rock mass can resist little tensile stress, due to its discontinuous character. In most cases, tensile jointing will not have a great impact on the rock stability. The exception is high-pressure water tunnels, where tensile jointing will lead to leakage and loss of water pressure. This will again lead to economic losses (Nilsen & Thidemann, 1993).

To avoid tensile failure in an unlined pressure tunnel, certain properties regarding stability of the rock mass is required. In order to avoid leakage, it is crucial to avoid areas with high

permeability. The rock mass requirements can be divided into two categories: geological and topographical (Nilsen & Thidemann, 1993).

The geological properties required are in a high degree corresponding to general requirements for stability in underground openings. For unlined pressure shafts, the following conditions should be avoided:

- High porosity rocks
- Karstic areas
- Heavily jointed rock mass and inter-communicating joints
- Weakness zones with unfavourable orientation
- Impermeable layers between the shaft and the surface, which may cause high water pressure to build up in critical locations

(Nilsen & Thidemann, 1993)

The topographical requirements are based on sufficient overburden. If the water pressure in the shaft exceeds the minor principle stress, hydraulic fracturing will occur. Hydraulic fracturing is critical regarding loss of water pressure. Rules of thumb have been developed to provide an estimate for critical overburden. The rules of thumb represent simple limit equilibrium methods, where the basic principle is that the load of the overlaying rock mass must exceed the internal water pressure on the shaft. This is expressed through equation [3.2.1] and [3.2.2].

$$\gamma_r \times h \times \cos\alpha > H \times \gamma_w \quad [3.2.1]$$

$$\gamma_r \times L \times \cos\beta > H \times \gamma_w \quad [3.2.2]$$

γ_f = rock mass density [g/cm^3]

γ_w = density of water [g/cm^3]

h = vertical depth from the surface [m]

L = shortest distance from the surface to the shaft [m]

α = inclination of the pressure shaft [$^\circ$]

β = average inclination of the valley side [$^\circ$]

H = static water head [m]

(Nilsen & Broch, 2011)

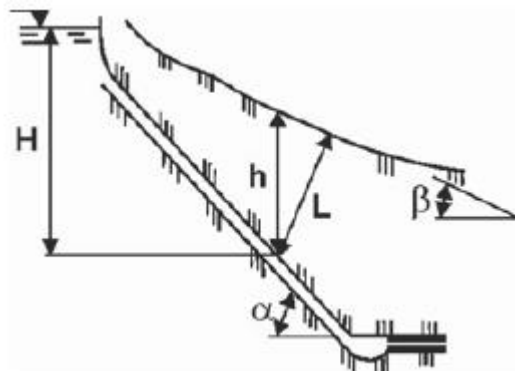


Figure 3. 3: Topographic requirements for placement of unlined pressure shaft from the rules of thumb described above (Panthi, 2014).

These rules of thumb only consider gravitational stresses. This is an inaccurate assumption since the valley sides where pressure shafts often are placed are highly influenced by topographical stresses (Nilsen & Thidemann, 1993). The area discussed in this task is also in great extent affected by tectonic stresses.

3.3 Compressive failure

If the tangential stresses in hard rocks exceeds the strength of the rock, it will result in fracturing parallel to the cavern contour (Nilsen & Palmström, 2000). The fracturing process will often result in loud noises from the rock, called rock bursts. At moderate stress levels, thin slabs will loosen due to fracturing. This is often referred to as rock slabbing or spalling. In cases of very high tangential stresses, large rock slabs may pop with considerable force and speed. Rock burst activity is most intense immediately after excavation. The area close to the working face is the most exposed (Nilsen & Thidemann, 1993).

The tangential stress around an excavation will act as an axial stress on rock slabs forming parallel to the excavation contour, illustrated in figure 3.4. The rock slab will buckle when the axial stress (σ_a) reach a certain level given by [3.3.1]:

$$\sigma_a = \frac{\pi^2 E}{12q^2(l/t)^2} \quad [3.3.1]$$

Where E is the Youngs modulus of the rock, l/t is the slenderness ratio of the slab and q is a constant, which depends upon the end conditions of the plate. The constant q has the following values:

Both ends pin-jointed	$q = 1$
Both ends clamped	$q = 0,5$
One end clamped, one free	$q = 2$
One end clamped, one pin-jointed	$q = \frac{1}{\sqrt{2}}$

(Hoek & Brown, 1980)

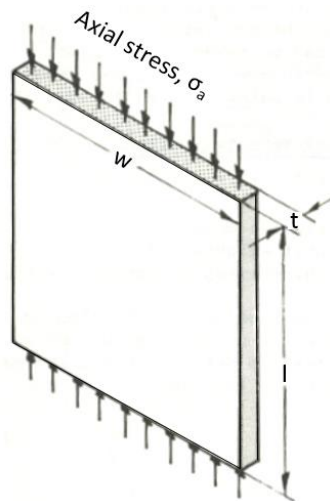


Figure 3. 4: Illustrating the parameters that define theoretical buckling. Modified after Hoek & Brown (1980).

Equation [3.3.1] shows that the critical axial stress is inversely proportional to the square of the slenderness ratio. Consequently, thin slabs buckle more easily than thick slabs. The equation is theoretical and of limited use in practical application, but it states that the critical axial stress is dependent of the stiffness of the rock. It also suggest that an effective way of reinforcing the excavation where buckling of rock slabs may occur is to pin the slabs together. This can be done by rock bolting.

In soft rock, the failure mechanism will have a plastic nature rather than brittle. This plastic deformation is called squeezing. Convergence due to squeezing can cause a reduction of an excavation diameter of several tens of centimetres (Nilsen & Palmström, 2000). The peridotite discussed in this thesis is a brittle material. Consequently the squeezing phenomenon will not be discussed further.

3.4 Failure criteria

A number of theoretical failure criteria for explaining or predicting failure in materials are developed over the years. Familiar examples are Mohr-Coulomb, Tresca-criterion and von Mises. These theories are based on an assumption where failure occurs due to a particular mechanism, which exceeds a particular mechanical property. They are also evaluating the combinations of principal stresses that can lead to such conditions (Myrvang, 2001).

Mohr-Coulomb is one of the most widely used theoretical failure criteria in rock engineering. The strength criterion is linear, and it suggests that the shear strength of a rock material is made up by a constant cohesion and a friction angle varying with normal stress. The shear strength (τ) is given by equation [3.4.1].

$$\tau = c + \sigma_n \tan \phi \quad [3.4.1]$$

Where, c is the cohesion, σ_n is the normal stress acting on the plan of failure and ϕ is the angle of internal friction (Zhao, 2000).

The Hoek-Brown criterion is on the other hand an empirical strength criterion, which is developed by the process of trial and error (Hoek & Brown, 1980). Based on test data, the empirical relationship between the principal stresses associated with rock failure can be described as in [3.4.2] for intact rock:

$$\sigma'_1 = \sigma'_3 + \sigma_{ci} \left(m_i \frac{\sigma'_3}{\sigma_{ci}} + 1 \right)^{0,5} \quad [3.4.2]$$

σ'_1 = maximum effective principal stress at failure

σ'_3 = minimum effective principal stress at failure

σ_{ci} = uniaxial compressive strength of the intact rock

m_i = Hoek-Brown constant for the intact rock

(Hoek, 2007)

In practical applications, a failure criterion for the entire rock mass is often more useful. For this purpose, it is appropriate to apply the generalised Hoek-Brown criterion:

$$\sigma'_1 = \sigma'_3 + \sigma_{ci} \left(m_b \frac{\sigma'_3}{\sigma_{ci}} + s \right)^a \quad [3.4.3]$$

Where, m_b is the value for the Hoek-Brown constant for the rock mass, s and a are constants depending on the rock mass characteristics. The rest of the parameters are similar to [3.4.2].

(Hoek, 2007)

The geological strength index (GSI) was introduced to convert strength of intact rock to the reduced strength of the rock mass for different geological conditions (Figure 3.8). In addition, the factor D is used to describe the influence of blast damage and stress relaxation (Appendix A). It varies from 0 for undisturbed in situ rock masses to 1 for very disturbed rock masses (Hoek, 2007). The relationships for m_b , s and a are given by:

$$m_b = m_i \exp\left(\frac{GSI-100}{28-14D}\right) \quad [3.4.4]$$

$$s = \exp\left(\frac{GSI-100}{9-3D}\right) \quad [3.4.5]$$

$$a = \frac{1}{2} + \frac{1}{6} \left(e^{-\frac{GSI}{15}} + e^{-\frac{20}{3}} \right) \quad [3.4.6]$$

(Hoek, 2007)

To analyse post peak behaviour of the rock mass, residual parameters must be conducted. Cai et al. (2007) proposes a set of equations ([3.4.7] to [3.4.10]) to determine residual Hoek-Brown parameters from a residual GSI value (GSI_r). The equations are especially applicable for rock masses with GSI values between 40 and 80, which is suitable for the particular case in this thesis.

$$GSI_r = GSI e^{-0,0134GSI} \quad [3.4.7]$$

$$m_r = m_i \exp\left(\frac{GSI_r-100}{28}\right) \quad [3.4.8]$$

$$s_r = \exp\left(\frac{GSI_r-100}{9}\right) \quad [3.4.9]$$

$$a_r = 0,5 + \frac{1}{6} \left(e^{-\frac{GSI_r}{15}} - e^{-\frac{20}{3}} \right) \quad [3.4.10]$$

The Hoek-Brown criterion has an advantage pursuant to the Mohr-Coulomb criterion by its non-linear form, which agrees with experimental data over a range of confining stresses. This particular difference is shown in figure 3.5. The Hoek-Brown criterion is developed through an extensive evaluation of laboratory test data covering a wide range of rock types. It also provides empirical means to estimate rock mass properties (Eberhardt, 2012).

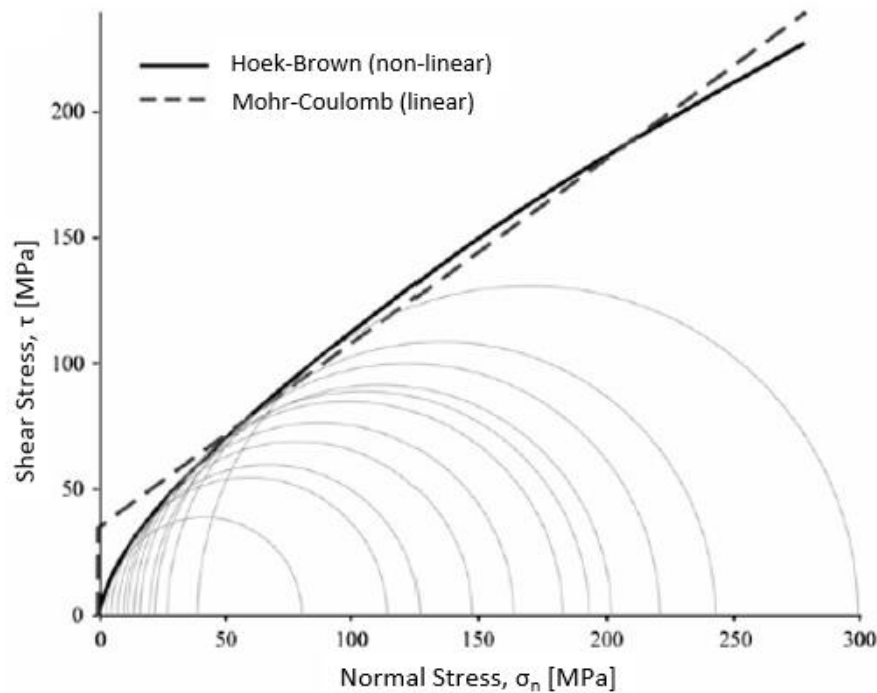


Figure 3. 5: Comparison of Mohr-Coulomb and Hoek-Brown failure envelopes plotted against triaxial test data for intact rock (Eberhardt, 2012).

3.5 Empirical and analytical methods to evaluate stability

3.5.1 Estimating stress distribution

To assess stability with analytical methods, predicting stress distribution is of main importance. Redistribution of in-situ stresses around underground openings is complex, and analytical solutions is in practice limited to simplified two-dimensional problems (Myrvang, 2001).

When analysing the effect of rock stresses, the stress situation close to the contour of the excavation is of particular interest. These stresses depend on in-situ stress field and excavation geometry (Palmström & Stille, 2010). The analytical equations presented in this chapter are idealised equations for homogeneous materials. In reality, joints and discontinuities will influence the stress distribution.

In an isostatic stress field, the stresses around a circular opening depend on the distance (r) from the circle centre. With no external forces on the excavation surface, the stress magnitude for radial stresses (σ_r) and tangential stresses (σ_θ) are given by [3.5.1] and [3.5.2] and are illustrated in figure 3.6:

$$\sigma_r = \sigma_0 \left(1 - \frac{r_i^2}{r^2}\right) \quad [3.5.1]$$

$$\sigma_\theta = \sigma_0 \left(1 + \frac{r_i^2}{r^2}\right) \quad [3.5.2]$$

r_i = radius of the circular opening

σ_0 = the virgin stresses

(Palmström & Stille, 2010)

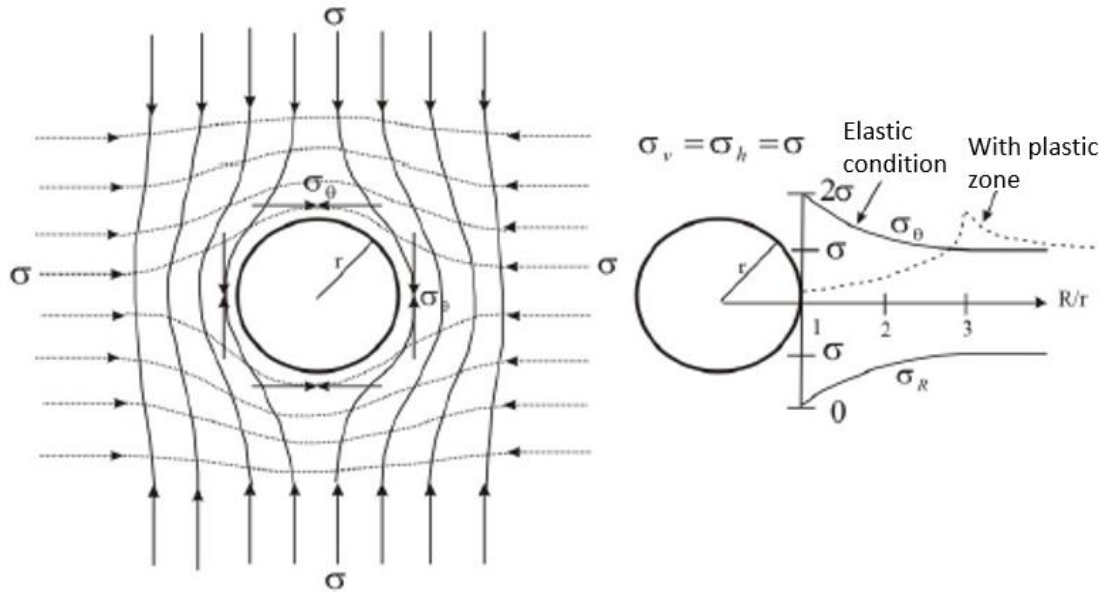


Figure 3. 6: Stress trajectories in surrounding a circular opening (left) and tangential and radial stress distribution in elastic and non-elastic conditions (Panthi, 2006).

The tangential stress will vary around the periphery of a circular opening in an anisotropic stress field. According to Kirsch's solution, the tangential stress will reach its maximum value ($\sigma_{\theta \max}$) where the direction of the largest principal stress (σ_1) is a tangent to the contour. The minimum value ($\sigma_{\theta \min}$) of the tangential stress appears where the direction of the smallest principal stress (σ_3) is a tangent to the contour. The relation between the extremal values of the tangential stress and the principal stresses are formulated in Kirsch's equations:

$$\sigma_{\theta \max} = 3\sigma_1 - \sigma_3 \quad [3.5.3]$$

$$\sigma_{\theta \min} = 3\sigma_3 - \sigma_1 \quad [3.5.4]$$

As seen from the equations, the tangential stress distribution is strongly influenced by the degree of stress anisotropy. Large stress anisotropy might lead to negative tangential stresses. This results in the possibility of tensional jointing. The stress magnitude depends in theory on the shape of the opening, and not on its size. However, the zone of influence will increase with larger openings (Palmström & Stille, 2010).

Kirsch's equations quantifies the extremal values of the tangential stresses. Equation [3.5.3] and [3.5.4] describes the stress situation in four points around a circular opening. To make the stress analysis applicable for a cavern, it is useful to calculate the tangential stresses around different shapes.

Magnitude of tangential stresses can be estimated for various types of openings through a more empirical approach. Hoek and Brown (1980) developed a method for calculating tangential stresses in roof ($\sigma_{\theta r}$) and walls ($\sigma_{\theta w}$) in massive rock based on a large number of boundary element analysis:

$$\sigma_{\theta r} = (A \times k - 1)\sigma_z \quad [3.5.5]$$

$$\sigma_{\theta w} = (B - k)\sigma_z \quad [3.5.6]$$

A and B are factors for the geometry of the opening (Figure 3.7), k is the horizontal/vertical stress ratio and σ_z is the vertical stress.

(Nilsen & Palmström, 2000)








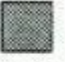

									
A	5.0	4.0	3.9	3.2	3.1	3.0	2.0	1.9	1.8
B	2.0	1.5	1.8	2.3	2.7	3.0	5.0	1.9	3.9

Figure 3. 7: Values for the factors A and B for various excavation shapes (Nilsen & Palmström, 2000).

3.5.2 Classifying rock mass quality

Potential stability problems are often difficult to quantify. Hence, the evaluation of stability and rock support are often based on more or less subjective judgement and practical experience. In such cases, classification systems can be a helpful tool. Classification systems helps the user to relate decisions to experience gained on other sites (Nilsen & Thidemann, 1993).

Classification systems has the purpose of identifying features or parameters of importance to a project and the assessments to be performed. Such systems should also describe the properties of these parameters, giving values according to their structure, composition and properties (Palström & Stille, 2010). In general, classification systems have the following aims:

- identify zones of material of similar geomechanical characteristics
- provide an indication of the predicted stability for excavations of a given size
- aid in the selection of an appropriate support strategy
- provide an indication of in situ rock mass strength, modulus of deformability etc.

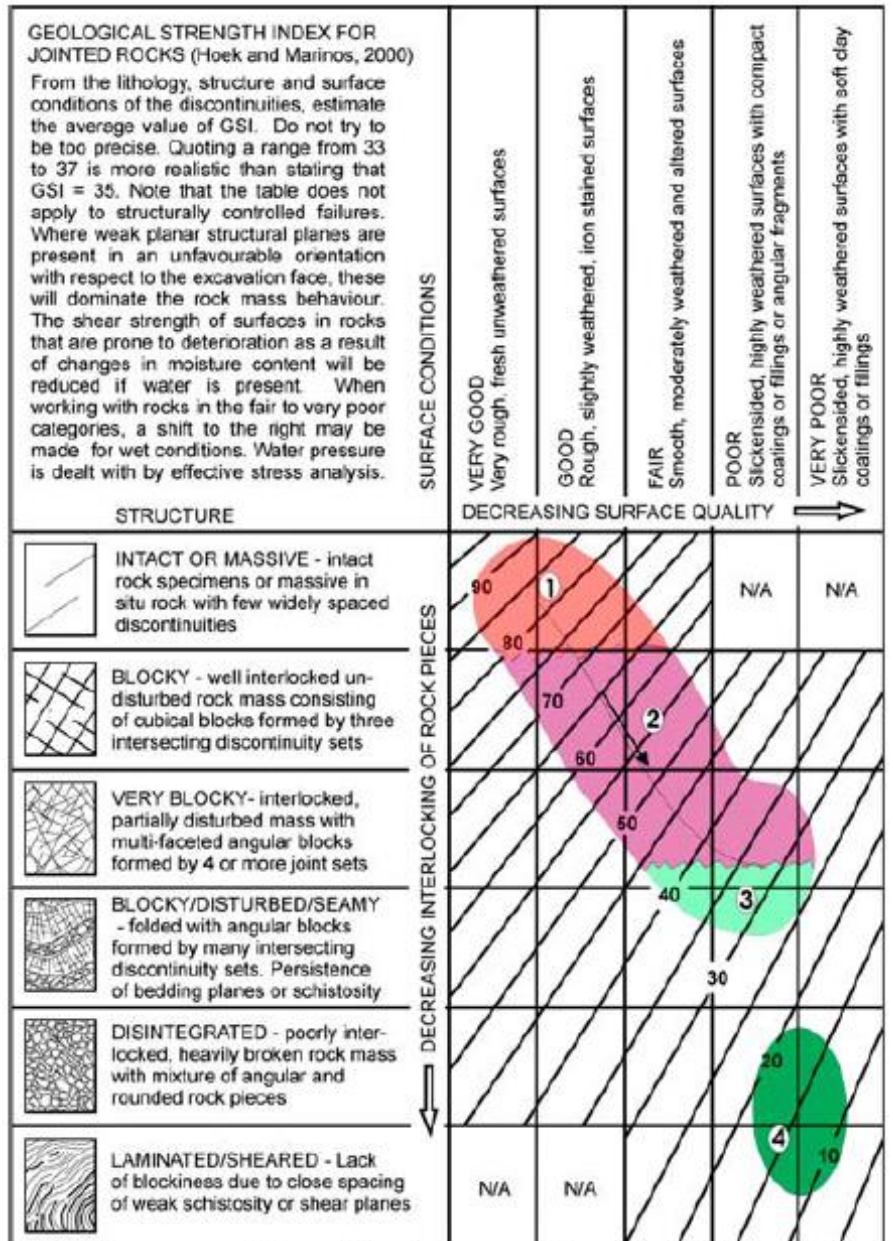
(Palmström & Stille, 2010)

Over the years, several classification systems has been developed. The most relevant systems in the context of a stability assessment are those involving rock support estimates. Among these are the Terzaghi, RMR, RMi and Q classification system. In the following, the GSI, RMR and Q system will be discussed further, since these systems are widely used in rock engineering today.

Geological strength index (GSI)

The GSI system estimates the strength of jointed rock masses, based upon an assessment of the interlocking of rock blocks and the condition of the surfaces between these blocks (Marinos & Hoek, 2000). GSI was introduced by Hoek (1994) and Hoek, Kaiser and Bawden (1995) and provides a value which, when combined with intact rock properties, can be used for estimating the reduction in rock mass strength for different geological conditions (Hoek, 2007).

The geological character of the rock material and the rock mass it forms is used as input parameters. This approach enables the rock mass to be considered as a mechanical continuum where the influence of geology on the mechanical properties is still taken into account (Marinos et al., 2005). Figure 3.8 shows the general GSI chart, with coloured areas for the typical range of ophiolites, which are relevant for the further analysis in this thesis.



1. Massive strong peridotite with widely spaced discontinuities. The conditions of discontinuities are poorly only affected by serpentinisation
2. Good to fair quality peridotite or compact serpentinite with discontinuities which may be severely affected from alteration.
3. Schistose serpentinite. Schistosity may be more or less pronounced and their planes altered.
4. Poor to very poor quality sheared serpentinite. The fragments consisting of weak materials

Figure 3. 8: GSI chart with coloured areas for typical ranges of ophiolites (Marinos et al., 2006).

Rock Mass Rating (RMR)

The RMR system was developed by Bieniawski (1976) and has been refined as more case records have been examined (Hoek, 2007). In this thesis, the 1989 version of the RMR system has been the basis. The following parameters are used to classify the rock mass using the RMR systems:

- Uniaxial compressive strength of rock material
- Rock Quality Designation (RQD)
- Spacing of discontinuities
- Condition of discontinuities
- Groundwater conditions
- Orientation of discontinuities

This system divides the rock mass into a number of structural regions. Each region is classified separately. The boundaries of the regions will coincide with major structural features. The RMR system with recommendation for rock support is given in appendix B. The recommendation for excavation and rock support is only given for horseshoe-shaped drill and blast tunnels with a span of 10 meters which are subjected to a vertical stress <25 MPa (Palmström & Stille, 2010).

The RMR value can be linked to the GSI value with the relationship given by [3.5.7]:

$$RMR = GSI + 5 \quad [3.5.7]$$

Here the RMR value has a groundwater rating set to 15 and the adjustment for joint orientation is set to zero (Appendix B) (Hoek & Brown, 1997).

Q-system

The Q system was developed by Barton et al. (1974) of the Norwegian Geotechnical Institute. The numerical value of the index Q varies on a logarithmic scale from 0,001 to a maximum of 1000 and is defined by:

$$Q = \frac{RQD}{J_n} \times \frac{J_r}{J_a} \times \frac{J_w}{SRF} \quad [3.5.8]$$

Where

RQD – Rock Quality designation, describes the joint density of the rock mass

J_n – Describes the number of joint sets

J_r – Describes the joint roughness

J_a – Describes the joint alteration

J_w – Describes the water conditions in the rock mass

SRF – Describes the stress conditions in the rock mass

(Hoek, 2007)

These parameters are measures of:

1. Block size (RQD/J_n)
2. Inter-block shear strength (J_r/J_a)
3. Active stress (J_w/SRF)

(Palmström & Broch, 2006)

The block size factor is representing the structure of the rock mass, differing the extreme values (100/0,5 and 10/20) by a factor of 400. The inter-block shear strength factor represents the friction characteristics of joint walls or filling materials. Clay mineral coatings and fillings will reduce this factor significantly (Hoek, 2007).

The active stress factor consists of two stress parameters. The J_w parameter is a measure of water pressure, which has a reducing effect on the shear strength of joints due to a reduction in effective normal stress. Water will also act destabilising by softening eventually clay fillings in joints. SRF is a measure of: 1) Loads during excavation through weakness zones, 2) squeezing loads in plastic, incompetent rock, and 3) rock stress in competent rock, which is the most relevant for this assignment. SRF is regarded as a total stress parameter.

It is difficult to combine J_w and SRF to a consistent parameter for inter-block effective stress. This is because paradoxically a high value of effective normal stress can result in less stable conditions than a low value, despite the higher shear strength (Hoek, 2007).

By combining the estimated Q-value, the span (or wall height) of the excavation and an excavation support ratio (ESR), a recommended amount of support can be found in the Q-value chart (Appendix C). The Q-values can also be obtained from RMR values by formulas published by Bieniawski (1989) [3.5.9] and Barton (1995) [3.5.10]:

$$RMR = 9 \times \ln Q + 44 \quad [3.5.9]$$

$$RMR = 15 \times \log Q + 50 \quad [3.5.10]$$

(Panthi, 2006)

Limitations

Empirical methods in the form of rock mass classification systems suffer from several limitations. The classification systems are significant tools in order to describe the stability characteristics of the rock mass and their best applications are in jointed rock masses where instability is caused by block falls (Palmström & Stille, 2010).

Today's classification systems are simplified to cover a wide spectrum of conditions. These simplifications may result in overlooking local geometrical and structural features. Classification systems give averaged values. There might be a significant variation between the highest and the lowest values. The support charts are derived from cases where the installed support are based on varying contractual conditions. The different excavation and rock support practices in various countries will also contribute to uncertainties (Palmström & Stille, 2010). There are a lot of uncertainties and variations between rock mass classification and actual support and between different classification systems (Figure 3.9 and Figure 3.10).

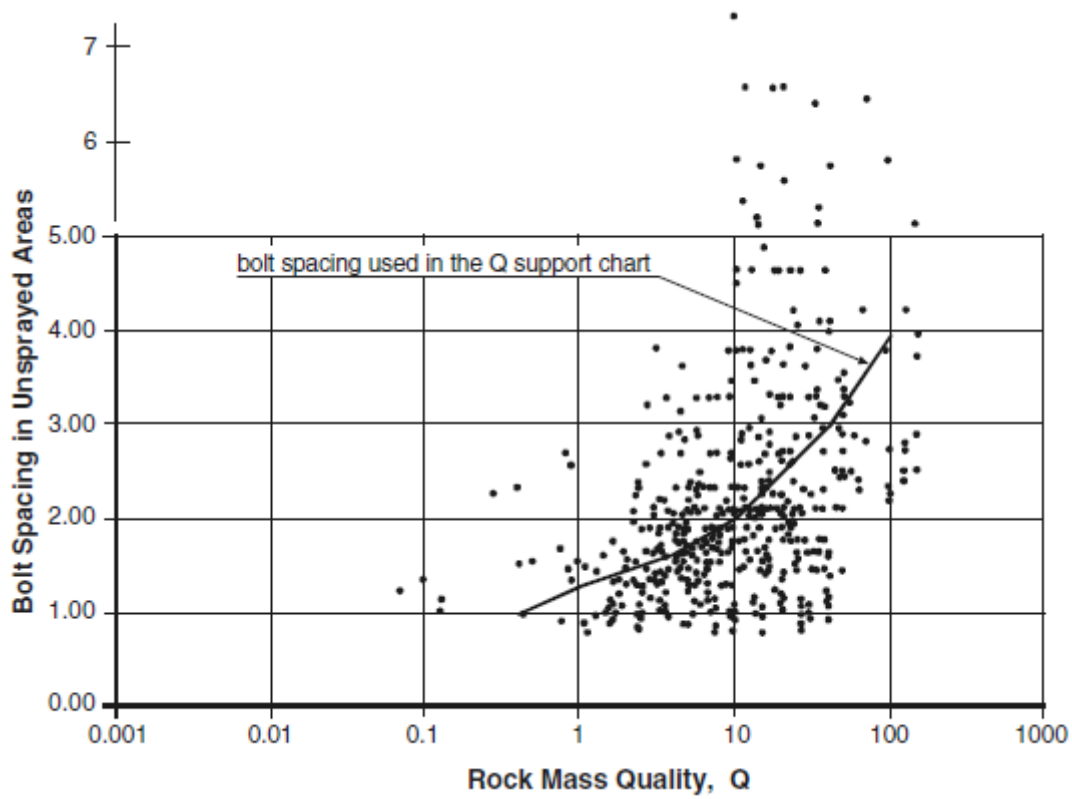


Figure 3. 9: Bolt spacing related to Q-value in unsprayed areas. The line indicates the bolt spacing used in the Q support chart (Palmström & Broch, 2006).

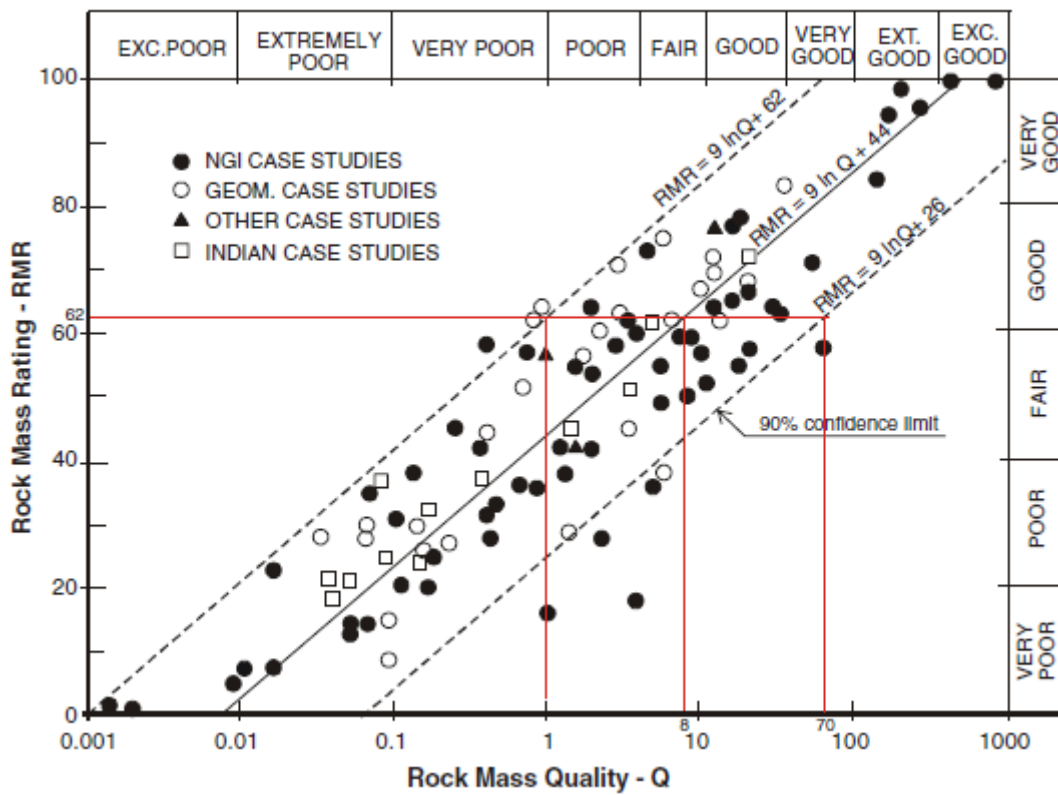


Figure 3. 10: Correlation between RMR and Q. Example: for RMR = 62, Q varies from 1 to 70 (Palmström & Broch, 2006).

The limitation in shape and size of the excavation when using the support chart for the RMR system is unfavourable when proposing rock support for underground caverns with significant larger span than 10 meters. The RMR system is not optimal when dealing with stress related stability issues, because rock stresses are not an input parameter to the system. Rock stresses are included in the Q-system by the SRF. Palmström & Broch (2006) describes the SRF as a sort of “correction factor” or “fine tuning factor”, rather than a factor expressing active stress aiming at arriving at a Q-value that estimates appropriate rock support.

However, as optimisation of rock support is a complex task, the assistance from empirical systems is valuable in such assessments. The support estimates should not be done from rock classification systems alone, but combined with assessments more accurate for the specific project. When the rock engineering and design are based on empirical tools, Palmström & Stille (2010) advises that at least two classification systems are being used.

“little-q”, classification in the ophiolite complex in the Moglicë area

For all rock types of the ophiolite complex, the “little q” system was used (Table 3.1). The basis of this classification system is a modification of the Q-system and RMR-system. The “little q” system was developed in Norway as a easy to handle system, appropriate for sound rock mass providing fair to excellent conditions (JCG, 2011).

Table 3. 1: Classification of rock mass quality with respect to stability. Modified from (Norconsult/Multicosult, 2011).

Rock mass quality	Description
<i>q1: Very Good</i>	Massive - low joint frequency, $J_v < 5$ joints/m ³ . Tight joints, unaltered strong rock and insignificant stress slabbing.
<i>q2: Good</i>	Low - moderate degree of jointing, $5 < J_v < 10$ joints/m ³ . Strong rock with none or insignificant alteration and with coating on some joints. Low to moderate stress slabbing.
<i>q3: Fair</i>	Moderate - high joint frequency, $10 < J_v < 20$ joints/m ³ . Moderately strong - strong rock generally with coated joints and with some seams and some minor weakness zones. The rock mass may be slightly weathered. Also applies to q1 and q2 rockmass qualities with moderate to high intensity stress slabbing, and to medium - low strength rock subjected to low - medium stresses causing plastic deformations.
<i>q4: Poor</i>	High joint frequency, $J_v > 20$ joints/m ³ , clay seams (fault zones, swelling clays) in moderately strong rock. Also applies to moderately weathered strong rock and to high - very high intensity stress slabbing in q1 and q2 rockmass qualities; and to medium - low strength rock subjected to swelling and/or slaking and/or medium - high stresses causing plastic deformation.
<i>q5: Very - Extremely Poor</i>	Completely crushed rock containing a significant amount of secondary clay minerals as in major fault zones. Smectite gouge clays may lead to significant swelling. Also applies to highly weathered rock and to low strength rock mass subjected to swelling and/or slaking and/or high stresses causing plastic deformation.

In correlation with the classification system “little q”, different rock support classes with appropriate rock support have been developed. Each rock mass quality class are linked to a rock support class, which is presented in table 3.2.

Table 3. 2: Appropriate rock support as a function of rock mass quality (q), according to the “little q” system (Norconsult/Multiconsult, 2011).

Rock mass quality (q) vs Rock support (RS)	Appropriate rock support
$q1 \rightarrow RS 1$	Scaling and spot bolts.
$q2 \rightarrow RS 2$	Scaling. Spot bolting for smaller cross-sections. Systematic bolting and spot applied fibre reinforced sprayed concrete for larger cross-sections.
$q3 \rightarrow RS 3$	Scaling. Systematic bolting and minimum one layer of fibre reinforced sprayed concrete in crown and walls. Numbers and lengths of bolts and thickness of sprayed concrete depend on the cross-section.
$q4 \rightarrow RS 4$	Systematic bolting and a minimum of two layers of fibre reinforced sprayed concrete in crown and walls. Occasionally (10 - 20%) spiling bolting and reinforced ribs of lattice girders and sprayed concrete or concrete lining. Occasionally concreting of the invert at face. Number/length of bolts and thickness of sprayed concrete depend on the cross-section. Also applies to occasionally short blasting rounds and subdivision of rounds depending on cross-section.
$q5 \rightarrow RS 5$	Systematic bolting and spiling bolts. Fibre reinforced sprayed concrete when short stand up time and application of rebar reinforced sprayed concrete or concrete ribs, or lattice girders and sprayed concrete at the face and concrete lining behind the face. Reinforced ribs may be deleted if concrete lined at the face. Concreting of the invert at face may be required. Number and length of bolts and the thickness of sprayed concrete as well as the distance between the lattice girders depend on the cross-section. Also applies to systematic short rounds for small cross-sections and subdivided rounds for larger cross-sections.

3.5.3 Predicting failure and extent

Failure of underground openings in hard rocks is a function of the in-situ stress magnitudes and the characteristics of the rock mass. At low in-situ stress magnitudes, the failure process is controlled by continuity, density and orientation of joints in the rock mass. As the in-situ stress magnitudes increase, the failure process is dominated by stress induced fracturing, propagating parallel to the excavation boundary (Martin et al., 1999).

Due to practical difficulties, it is impossible to conduct excavation scale tests to determine the rock mass strength in-situ. Therefore, in-situ rock mass strength is often estimated using empirical approaches based on back-analyses, using case histories where failure is highly documented (Cai & Kaiser, 2014). This has been done in South African mining tunnels, where the far field stress (K_0) is equal to 0,5, and the tunnels were square shaped. Figure 3.11 shows an empirical stability classification, developed by Hoek and Brown (1980), based on the South African cases. The classification can briefly be described as follows:

- $\sigma_1 / \sigma_c \leq 0,1$: a stable unsupported opening
- $\sigma_1 / \sigma_c = 0,2$: minor spalling can be observed, requiring light support
- $\sigma_1 / \sigma_c = 0,3$: severe spalling, requiring moderate support
- $\sigma_1 / \sigma_c = 0,4$: heavy support required to stabilize the opening
- $\sigma_1 / \sigma_c = 0,5$: extreme support required, stability of the opening may be very difficult to achieve

(Martin et al., 1999)

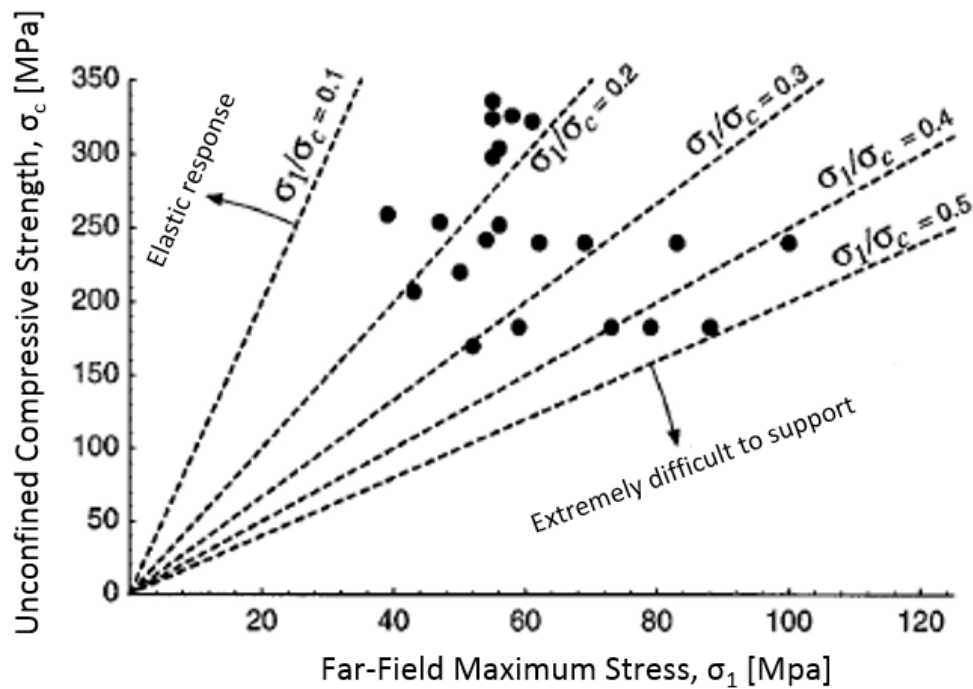


Figure 3. 11: Empirical stability classification developed for square tunnels in South Africa ($K_0 = 0,5$) (Martin et al., 1999).

It is important to note that before applying the South African classification to other sites, the effect of the excavation geometry and varying stress ratios on the maximum tangential stress at the boundary of the excavation must be evaluated (Martin et al. 1999).

Potential of spalling and rock burst based on intact rock properties is illustrated in figure 3.12. It is likely that shear processes will dominate where the spalling potential is low, resulting in squeezing rather than bursting at depth (Diederichs, 2007). Spalling potential is dependent on the brittleness of the rock, while rock bursting requires higher energy and hence stronger rocks.

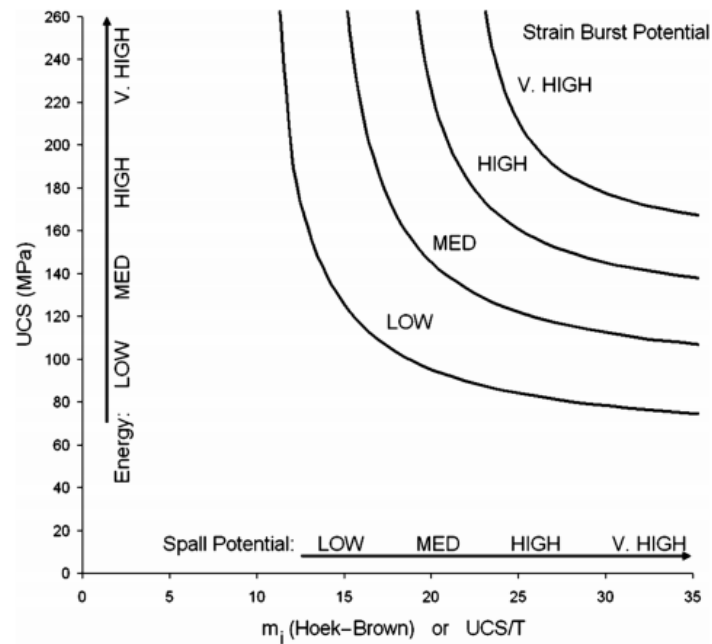


Figure 3. 12: Spall potential and strain burst potential as a function of UCS and m_i or UCS/T (Diederichs, 2007).

The relation between the maximum tangential stress on the excavation boundary and the uniaxial compressive strength of the intact rock has been widely examined. It has been recognized through empirical observation that rock failure in massive to moderately jointed hard rock in an excavation starts when the tangential stress at the excavation boundary exceeds 0,3 to 0,5 times the rock's UCS (Cai & Kaiser, 2014). In crystalline rocks, the spalling strength frequently occur between 0,4 and 0,6 of the UCS (Martin & Christainsson, 2009).

Several factors contribute to the low spalling strength compared to the UCS of the intact rock. These factors include pre-existing damage, surface interaction effects, loading path, stress rotations and loss of effective confinement into the excavation due to progressive slabbing. In addition, the geometry difference between laboratory tests and in-situ conditions is contributing to the low spalling strength (Cai & Kaiser, 2014).

Cai & Kaiser (2014) argues that a spalling strength of $0,4 \pm 0,1$ UCS is underestimating the actual strength of the rock mass. The reason is that this result is based on studies of a smooth excavation contour, and it does not consider excavation boundary irregularities. These irregularities will lead to local stress concentrations, which yields a higher tangential stress than the theoretical maximum for a smooth contour.

Spalling strength of 0,3 to 0,5 UCS can only be used to describe field rock strength when simplified model geometries are used (Cai & Kaiser, 2014). For the analysis obtained in this task, simplified model geometries will be the case. In-situ spalling strength of $0,4 \pm 0,1$ UCS can therefore be used as a reasonable estimation.

As discussed earlier in this section, there are several failure modes, dependant on stress situation and rock mass properties. Figure 3.13 illustrates the different failure modes for brittle rock. CI

indicates the crack initiation threshold (typically 35-50% of UCS) and CD defines the yield or crack damage threshold (typically 70-90% of UCS) (Diederichs et al., 2010).

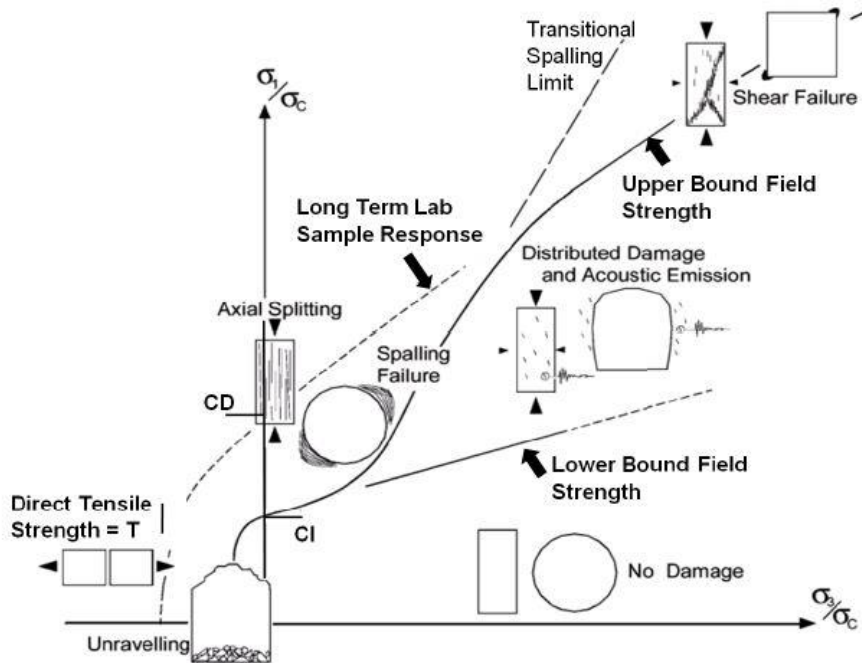


Figure 3. 13: Different failure modes for brittle rock (Diederichs et al., 2010).

Predicting potential spalling and rock bursting is important, but not sufficient for a stability analysis. Information about the depth-impact of the rock burst is of great importance, regarding optimization of support design. Particularly pursuant to determining length of rock bolts. Martin (1997) postulated the deviatoric stress criterion (equation [3.5.11]). This provides an adequate estimate of the radial extent of brittle failure. The criterion is recognized to be somewhat conservative, still it provides simple means for estimating the depth of failure. The deviatoric stress criterion assumes that at low confining stresses, such as around an underground excavation, the brittle failure process is dominated by cohesion loss.

$$\sigma_1 - \sigma_3 = \frac{1}{3} \sigma_c \quad [3.5.11]$$

(Martin, 1997)

Several empirical formulas are developed in order to predict the depth-impact of brittle failure. In this chapter, three formulas are presented. The input parameters are opening radius (r), maximum tangential stress on the excavation boundary ($\sigma_{\theta max}$) and strength intact rock (UCS) or spalling strength (σ_{sm}).

Martin and Christiansson (2009) proposed a relationship to calculate rock burst depth-impact (d_f) by using spalling strength as an input parameter (equation [3.5.12]). As discussed previously, spalling strength can be related to strength of intact rock by $\sigma_{sm} = 0,4 \pm 0,1$ UCS for hard rocks.

$$d_f = r \times \left(0,5 \times \frac{\sigma_{\theta max}}{\sigma_{sm}} - 0,52 \right) \quad [3.5.12]$$

(Panthi, 2012)

Similarly, Kaiser et al. (1996) proposed an estimate for determining the depth of brittle failure based on field observations of brittle failure in massive rocks:

$$\frac{d_f}{r} = 1,34 \frac{\sigma_{\theta max}}{UCS} - 0,57(\pm 0,05) \quad [3.5.13]$$

(Cai & Kaiser, 2014)

Based on eight different case histories where the depth and shape of failure around individual excavations had been measured, Martin et al. (1999) approximated a linear relationship given by [3.5.14].

$$\frac{R_f}{a} = 0,49(\pm 0,1) + 1,25 \frac{\sigma_{\theta max}}{UCS} \quad [3.5.14]$$

The excavations that made the basis for the equation were either circular or D-shaped (Martin et al., 1999). Figure 3.14 illustrates [3.5.14] and the variation in the case histories.

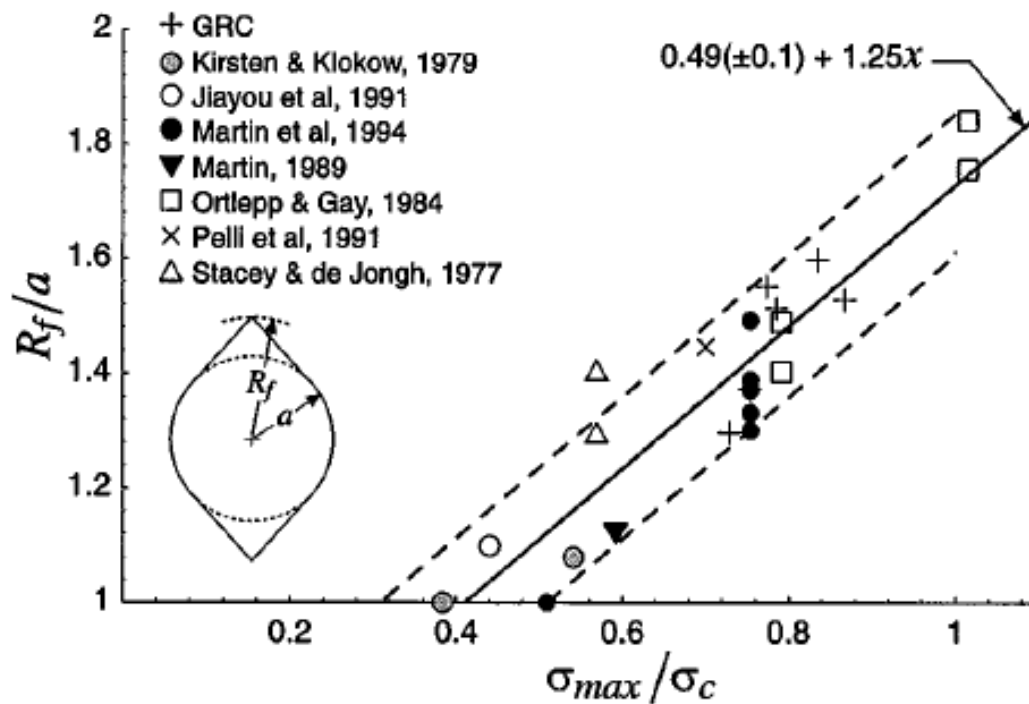


Figure 3. 14: Relationship between depth of failure and the maximum tangential stress at the boundary of the opening (Martin et al., 1999).

As figure 3.14 illustrates, a great deal of uncertainties are connected to the empirical equations estimating depth of failure in brittle rock mass. However, these relationships are useful tools in order to design a reasonable support system.

3.5.4 Proposing support

There are several empirical rules of thumb to determine the anchor length of rock bolts together with support spacing. Empirical relations found in literature are presented in table 3.3 and 3.4. Rules of thumb for support design have been developed for blocky and fractured ground. These are based on data from tunnels, caverns and mine openings and they summarize support practice. It should be noted that such guidelines should be used in conjunction with other design tools (Hutchinson & Diederichs, 1996).

Table 3. 3: Empirical formulas, estimating necessary length of rock bolts as a function of cavern span/height. S = span, H = height, Sp = Spacing of primary bolting.

Bolt length	Reference	Comment
$L = 0,67 \times S^{0,67}$	Lang & Bischoff, 1984	
$L = 0,3 \times S$	Farmer & Shelton, 1980	Span > 15m, alternate with secondary bolting
$L = 0,3 \times Sp$	Farmer & Shelton, 1980	Secondary bolting
$L = 2 + 0,15 \times S$	Hoek, 2000	Suited for weak rock masses (roof)
$L = 2 + 0,15 \times H$	Hoek, 2000	Suited for weak rock masses (walls)
$L = 1,40 + 0,184 \times S$	Myrvang, 2001	Norwegian approach

Table 3. 4: Empirical formulas for determining spacing between rock bolts.

Spacing	Reference	Comment
$Spacing = \sqrt{T/P}$	Hoek, 2000	T=working load of bolt or cable P=support pressure
$Spacing = 0,5 \times L$	Farmer & Shelton, 1980; U.S.C.E., 1980	Primary bolting
$Spacing = 0,5 \times L(\text{secondary})$	Farmer & Shelton, 1980	Secondary bolting
$Spacing = 0,5 \times L$	Myrvang, 2001	Applicable to jointed rock mass

3.6 Numerical methods

Analytical methods are best suited for simple geometries in a homogeneous medium. Most underground excavations have a complex shape, and are located in an inhomogeneous rock mass. In addition, openings are frequently grouped close to other excavations. The equations for such cases will be too complex to be solved analytically. Over the past few decades, a number of computer-based numerical methods have been developed to provide means for obtaining approximate solutions to these problems. These methods for analysing stress driven problems in rock mechanics can be divided into two classes:

- *Boundary discretization methods*, where only the excavation boundary is divided into elements. The interior of the rock mass is represented as an infinite continuum. This division will normally restrict the methods to cover elastic analysis.
- *Domain discretization methods*, in which the interior of the rock mass is divided into elements with assumed properties. The collective behaviour and interaction of these simplified elements yields a model for the complex and inhomogeneous rock mass. This means that the domain methods allow analysis of more complex material models than boundary methods. Within the domain discretization methods, finite element and finite difference methods techniques that treat the rock mass as a continuum. The distinct element method models each individual block of rock as an unique element.

The two classes can be combined in the form of hybrid models to maximise the advantages of each method (Hoek, 2007).

3.6.1 *Finite element methods*

The finite element divides the domain into finite elements. Each element contains a material with certain properties. The method is connecting many simple elements to approximate a more complex state over a larger domain. The problem contains differential equations, which can be solved numerically by minimizing an associated error function.

The finite element method is suited for solving problems involving heterogeneous or non-linear material properties, since each element explicitly models the response of its contained material (Hoek, 2007).

3.6.2 *Phase²*

Phase² is a versatile two-dimensional finite element program for designing underground or surface excavations and their support systems, provided by Rocscience Inc. (Rocscience, 2014a). The program consists of three modules: modelling, computing and interpreting. Phase² offer a wide variety of options when it comes to modelling, meshing, material properties and behaviour, support, far-field stress, loads, joints and data interpretation.

3.6.3 *RocLab*

RocLab is a software program for determining rock mass strength parameters, based on the generalized Hoek-Brown failure criterion (Rocscience, 2014b). From the input parameters: UCS, GSI, intact rock property m_i and disturbance factor (D), RocLab calculates the Hoek-Brown parameters m_b , s and a (these parameters are described in section 3.4).

4. Moglicë Hydropower Project

4.1 Project Description

Devoll hydropower (DHP) project is located in southeast Albania, approximately 70 km southeast of the capital Tirana (Figure 1.1). In total, the Devoll project consists of three hydropower plants in the valley of Devoll. The plants will have a total installed capacity of 278 MW, with an average production of about 800 GWh annually. This will increase the Albanian electricity production by almost 20 per cent (Statkraft, 2015)

Initially, it's decided to build the two hydropower plants Banjë and Moglicë with a combined capacity of 243 MW and an annual production of about 700 GWh. When the two plants are completed, the investment decision for the third plant, Kokël, will be considered.

Devoll hydropower project was awarded to Devoll Hydropower Sh.A. by the Albanian government through an open international tender. The concession entitles Devoll hydropower Sh.A. to build, own, operate and transfer the project. Devoll Hydropower Sh.A. is an Albanian registered company, owned and operated by the Norwegian power company Statkraft AS (DHP, 2013).

Moglicë HPP is the upper and largest power plant of the DHP project. It utilizes a head of 300 meters between 650 and 350 m.a.s.l. The dam is an asphalt-core, rock filled structure that will be the highest in the world of its kind with its 150 meters. The reservoir has a storage capacity of approximately 360 million m³ and a surface area of about 7,2 km², which is an area comparable to about 1000 football fields. There will be a 10,8 km long headrace tunnel between the Moglicë reservoir and Moglicë power plant. The power plant is dimensioned with two Francis turbine units and will have an installed capacity of about 175 MW. Moglicë HPP will generate an average of approximately 450 GWh, yearly. (iC consulente, 2014).

4.1.1 Project layout features

The features presented in this section is the current layout, which will be evaluated in later sections of this task. Table 4.1 presents an overview of the tunnel sections related to Moglicë HPP.

Table 4. 1: Overview over different tunnel sections connected to the Moglicë powerhouse complex. Modified from Norconsult/Multiconsult (2011).

Tunnel section		Excavation method	Cross section	Length (m)
<i>Tunnel sections near Moglicë Dam</i>	Diversion tunnel, shafts and grouting galleries	Drill and blast	Various	Various
	Headrace tunnel from intake and adit to headrace, including assembly chamber	Drill and blast	Various	400 + 600
<i>Headrace tunnel</i>	Headrace tunnel Moglicë-Shemshit	TBM	Ø = 6,1 m	7000
	Adit Shemshit	Drill and blast	20 m ²	775
	Shemshit right face tunnel (towards TBM meeting)	Drill and blast	31 m ²	500 - 1000
	Shemshit surge tunnel	Drill and blast	20 m ²	690
	Shemshit left face tunnel (towards power station)	Drill and blast	37 m ²	860
<i>Tunnels in power station area</i>	Access tunnel to power station	Drill and blast	40 m ²	479*
	Various tunnels in power station area	Drill and blast	20 – 80 m ²	400
	Tailrace tunnel	Drill and blast	37 m ²	835
	Headrace tunnel	Drill and blast	37 m ²	1759

* Updated from table 4.3 (original placement)

4.1.2 Powerhouse complex design

The general design of the powerhouse cavern and the transformer cavern are shown in figure 4.1. The transformer cavern and the power station caverns are respectively 45 m and 61 m long. Busbar tunnels are connecting the 14 m high and 20 m wide transformer hall to the 28 m high and 17 m wide powerhouse cavern (Multiconsult, 2011).

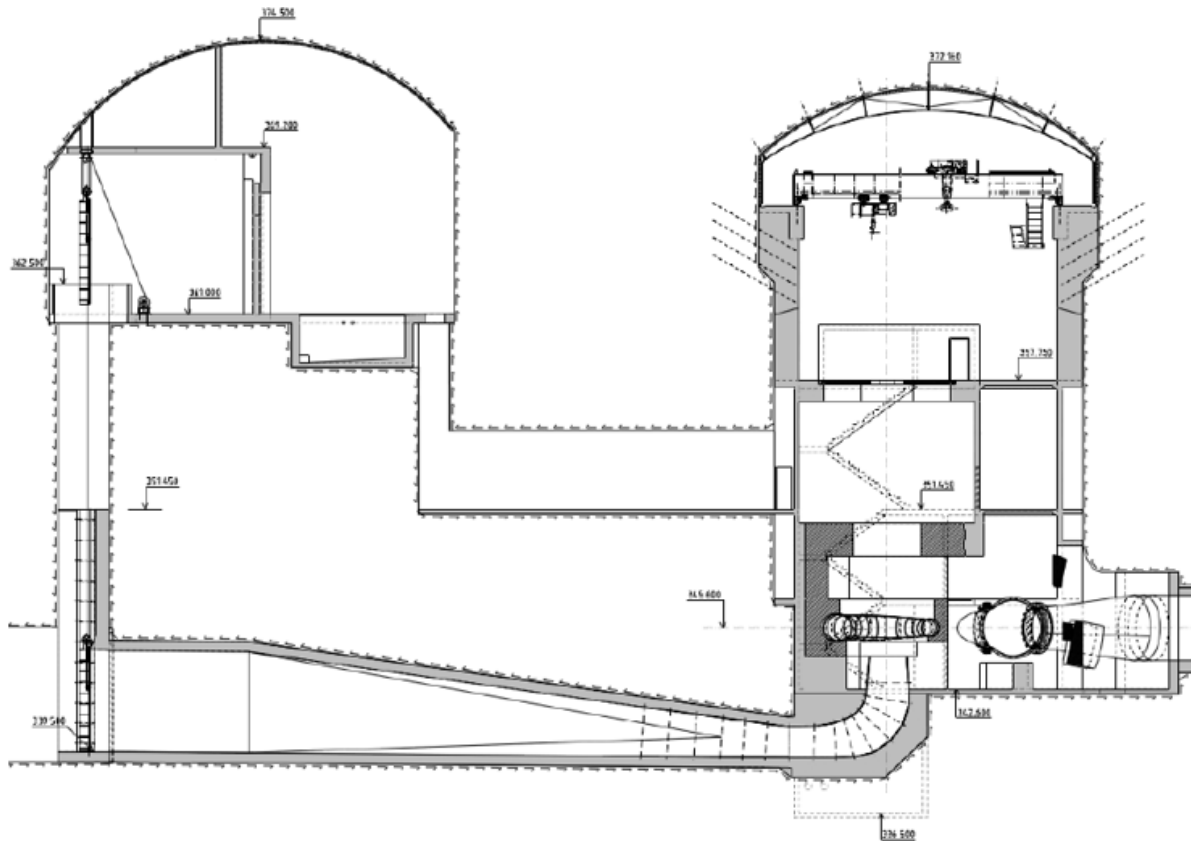


Figure 4. 1: Cross section of the powerhouse cavern and transformer hall in the Moglicë power plant (Multiconsult, 2011).

In addition to the caverns, the complex consists of an extensive tunnel system including:

- Adit and surge tunnel
- Access tunnel
- Escape and cable tunnel
- Tailrace tunnel

Information about proposed support are given in figure 4.2. Rock bolts and fiber/mesh reinforced shotcrete will be installed. Heavier support, including spiling bolts, lattice girder and steel ribs are taken consideration of.

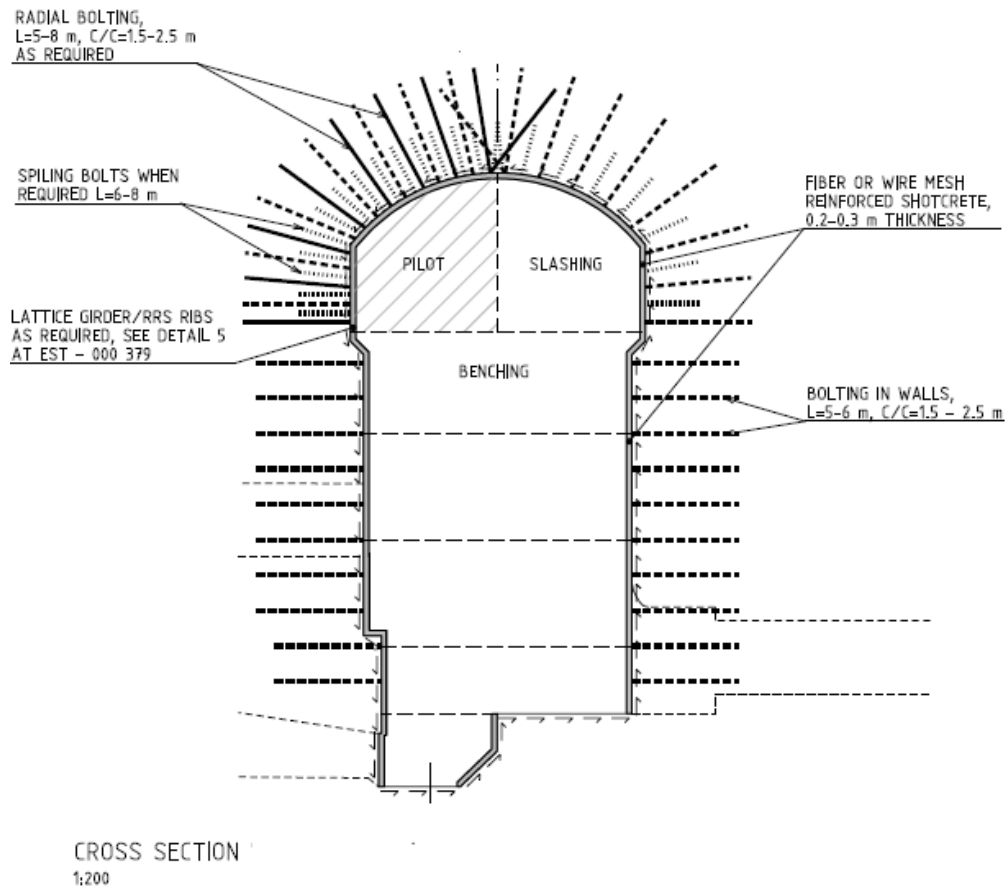


Figure 4. 2: Proposed support in a cross section of the powerhouse cavern (Norconsult, 2011).

4.2 Engineering Geological Conditions

4.2.1 Regional geology

Albania is located where the south-westernmost part of the Eurasian plate is convergent with the Adriatic plate (Figure 4.3). This convergent motion creates a tectonic regime, which is divided into two domains. The external domain of compression regime, comprising the western part of the country, and the internal domain of extensional regime, located in the interior of the country, creating horst-graben structures. Structural zones and regional faults are shown in appendix D. Moglicë is located in the internal domain. Nappe structures of tectonic zones are visible in the Moglicë area. Among them are the Moglicë ophiolite massif over-thrusting a zone of flysch (Allkja, 2013).

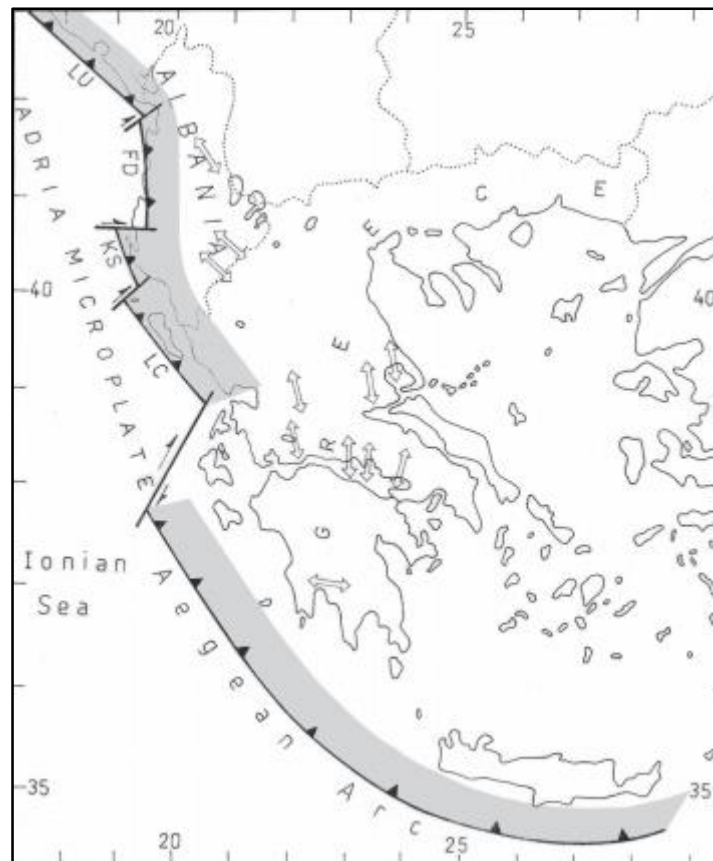


Figure 4. 3: Convergent margin between the Eurasia plate and the Adriatic plate (Aliaj, 2006).

Ophiolites are considered as pieces of the oceanic crust generated at an oceanic ridge and the upper mantle of an ancient ocean. This geologic feature can also be formed by thrusting on the continental crust during orogeny. An ophiolitic complex is characterised by underlying peridotitic rock, which are covered by gabbro/peridotite, which again are covered by basalts or spilites. The overlaying basalts are either massive or in the form of pillow lavas (Marinos et al., 2006).

As ophiolitic sequences mainly occur in tectonic zones, this structure can be highly disturbed. The original nature of the minerals are often changed due to metamorphism. A special case is the transformation of ferromagnesian minerals, olivine in particular, to serpentine (Marinos et al., 2006). This transformation is called serpentinisation and is unfavourable regarding stability because serpentine minerals have a fibrous or laminar form. The mentioned tectonic influence and serpentinisation are reported in the outcrop overview from Devoll Hydropower (2011).

4.2.2 Ground investigations

Besides field mapping and desk studies, the ground investigations for the headrace tunnel and the powerhouse complex mainly consists of rotary core drilling and refraction seismic measurements. A total of six core drillings were performed for the headrace tunnel. 860 m core material was gathered for geological mapping and laboratory testing. Monitoring of groundwater level and field testing of rock mass permeability were executed in all investigation boreholes (Aasen et al., 2013).

Laboratory tests have been carried out to obtain information about the mechanical properties of the intact rock. Besides standard index tests, such as density and porosity, the following tests were considered necessary:

- Uniaxial compressive strength, UCS
- E-modulus, E
- Point load, Is50
- Brazilian tensile strength, BTS
- Sound velocity, v_p
- Petrographic analysis/thin sections
- Drilling rate index/Cutter life index (DRI/CLI)
- Cerchar scratch test
- Slake durability

(Aasen et al., 2013)

4.2.3 Geology along headrace tunnel

The geology of the headrace tunnel is illustrated in figure 5.4 and in appendix E. The first 7,5 km of the 10,8 km long headrace tunnel will be excavated in tectonic flysch. The flysch typically consist of alternating layers of claystone, siltstone, sandstone and conglomerates. The sandstones are more rigid and strong than the silt- and claystones (Aasen et al., 2013). Further downstream, the tunnel encounters an approximately 250 m wide ophiolitic fault breccia, before entering the ophiolite massif.

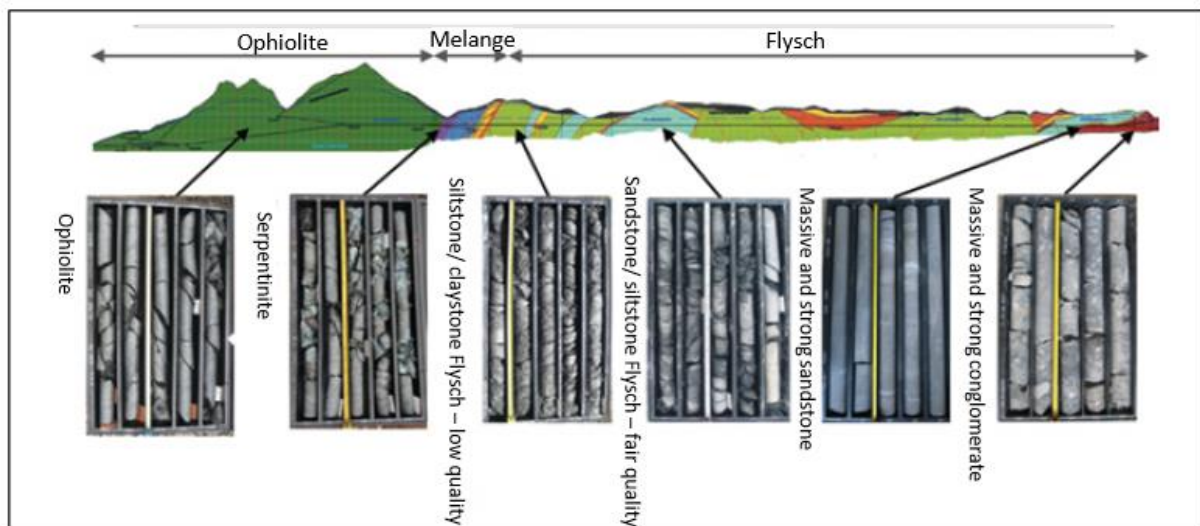


Figure 4. 4: Longitudinal profile of the Moglicë headrace tunnel, with examples from the core drilling (Aasen et al., 2013).

The ophiolitic rocks along the headrace tunnel are in general homogeneous and sound. Localized serpentinization of peridotite and fault zones are the main concern regarding rock mass quality. On the other hand, the flysch can be extremely heterogeneous, and locally of very poor rock mass quality. The ophiolitic fault breccia in the melange zone are also weak and tectonically disturbed (Aasen et al., 2013).

The faults appurtenant the horst-graben structures mentioned in section 4.2.1 are mapped and visible in the longitudinal section of the headrace tunnel (Appendix E and Figure 4.4). From lineaments in the terrain, these faults seem to have a NE-SW strike direction, which yields a favourable angle to the alignment of the headrace tunnel.

4.2.4 Geology in the area of the Powerhouse complex

Rock type

The main rock type in the area of the powerhouse complex are peridotite (Harzburgite)(Appendix E). Peridotite (Figure 5.5) is a ultramafic rock with high density ($3,2 - 3,4 \text{ g/cm}^3$), consisting mainly of olivine and orthopyroxene minerals (Multiconsult, 2011).

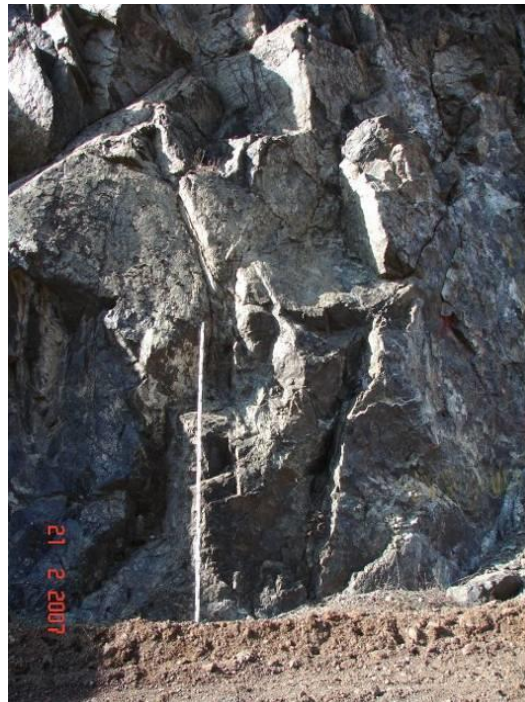


Figure 4. 5: Example of peridotite from the ophiolite massif (DHP, 2011).

The engineering geological mapping is executed by investigating outcrops mainly along the road following the Devoll river (Figure 4.6). The outcrops in figure 4.6 are in the ophiolite part of the alignment. In addition, core drilling has been performed in several locations (Figure 4.6). Hydraulic fracturing has been carried out in the bore hole GR-1 in the black rectangle in figure 4.6.

In the bore hole logs for GR-1 (DHP, 2011), the bedrock is referred to as generally very strong in areas without joints and medium strong to strong in jointed areas. It is also reported that many joints are showing serpentine mineralisation. Serpentine mineralisation will reduce an initial rough joint condition to smooth and slippery (Marinos et al., 2006).

Peridotites (harzburgites) are strong with a range of unconfined strength for the intact mass from many tens of MPa to more than 100 MPa at which stage they behave as typical brittle materials (Marinos et al., 2006). Laboratory tests results for the intact peridotite in the area of the cavern location are listed below. According to table 2.1, the rock strength is regarded as

high. The high E-modulus support the assumption that the peridotite will behave as a brittle material.

- UCS = 84,0 MPa
- E-modulus = 111,8 GPa
- Poisson's ratio = 0,18

(Multiconsult, 2011)

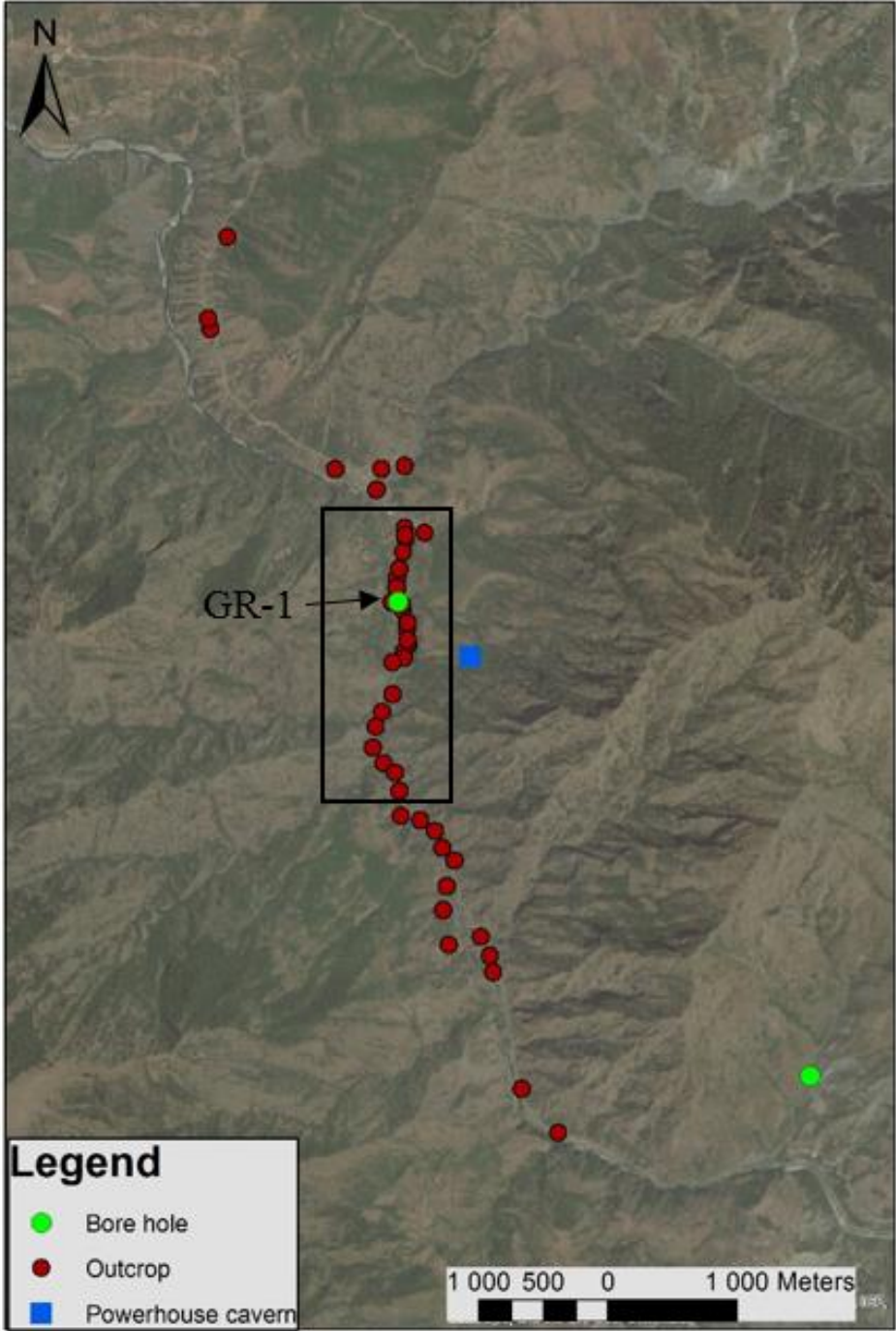


Figure 4. 6: Overview of mapped outcrops and bore holes in the ophiolite massif.

Jointing

Rosettes are plotted based on values from an outcrop database. Figure 4.7a shows a rosette plot of all the joint measurements from the outcrops in the ophiolite complex, and figure 4.7b contains the joint measurements from the outcrops near the powerhouse cavern, which are assumed to be the most relevant for the situation near the powerhouse complex. These outcrops are located in the black rectangle in figure 4.6. As the rockmass is homogeneous, the joints appear in all directions. It is difficult to point out distinct joint sets from figure 4.7a. Figure 4.7b shows more defined joint sets. The two most significant directions are marked with dip values, even though these values varies a lot. The most propagating joint direction has an average dip of 60° , but the dip values varies from 20° - 85° . Stereo plots in Appendix F illustrate the dip variation.

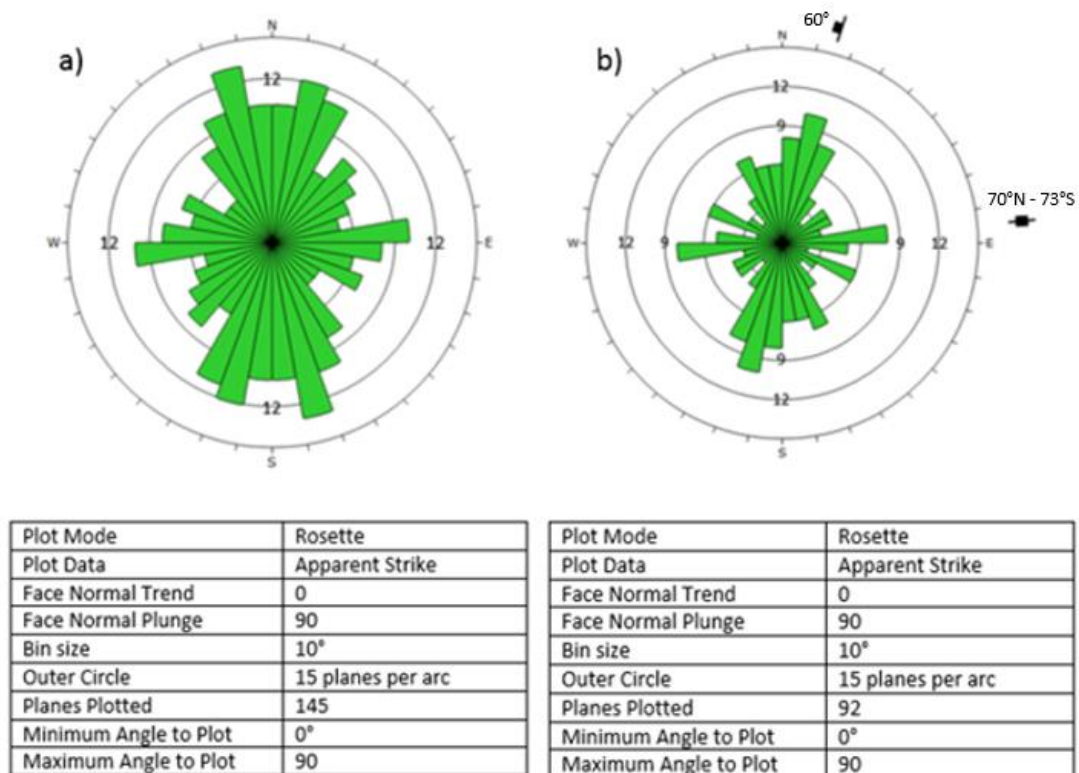


Figure 4. 7: Rosette plots of the joint measurements from the ophiolite massif (a) and outcrops near the powerhouse caverns (b).

Analysis of the outcrop database gives the following joint characteristics:

- Joint spacing is in general moderate (10-30 cm spacing)
- 59 % of the joints have a stepped surface. The rest are planar or slightly undulating
- Joint surfaces are mostly smooth (37%)
- Joint alteration is slightly-moderately weathered
- The dominant joint filling is serpentine
- 78% of the joints have a joint aperture of less than 1 mm

Weakness zones

Weakness zones in the ophiolite complex vary in thickness from decimetre to tens of meters. These zones show a significantly higher joint density than the surrounding rocks. The surfaces are often undulated to plain and polished to slickensided showing moderate to high alteration. Fillings of serpentine are common (JCG, 2011).

The longitudinal profile of the headrace tunnel (Appendix E) predicts that the area of the powerhouse cavern will avoid conflicts with weakness zones. There are visible lineaments and depressions in the terrain, both north and south of the planned location of the powerhouse complex (Figure 4.10). These possible weakness zones will be referred to as zone 1 and zone 2. The dip of these zones will decide whether they will interfere with the powerhouse caverns. Zone 1 looks rather steep from the outcrop in the map sheet, while zone 2 can be assumed to have a southerly dip direction due to the curvature of the outcrop.



Figure 4. 8: Weakness zone within the rocks of the Devoll ophiolite massif along the state road, dm-scale, filled with serpentine minerals (DHP, 2011)

4.2.5 Stress situation and executed measurements

The stress situation in the area of Moglicë is influenced by the tectonic activity between the Adriatic plate and the Eurasian plate (as discussed in section 4.2.1). The tectonic development results in relatively high horizontal stresses.

Along the Albanian coast line, the major principle stresses are mainly in an approximate E-W direction, perpendicular to the plate boundary (Figure 4.9). In the internal part of the country, the major principle stresses are oriented more in a N-S direction. Moglicë HPP are located close to the boundary of the two zones, but it is regarded as a part of the internal domain (Section 5.2.1). Hence, the major principle stress is likely to be of an N-S character.

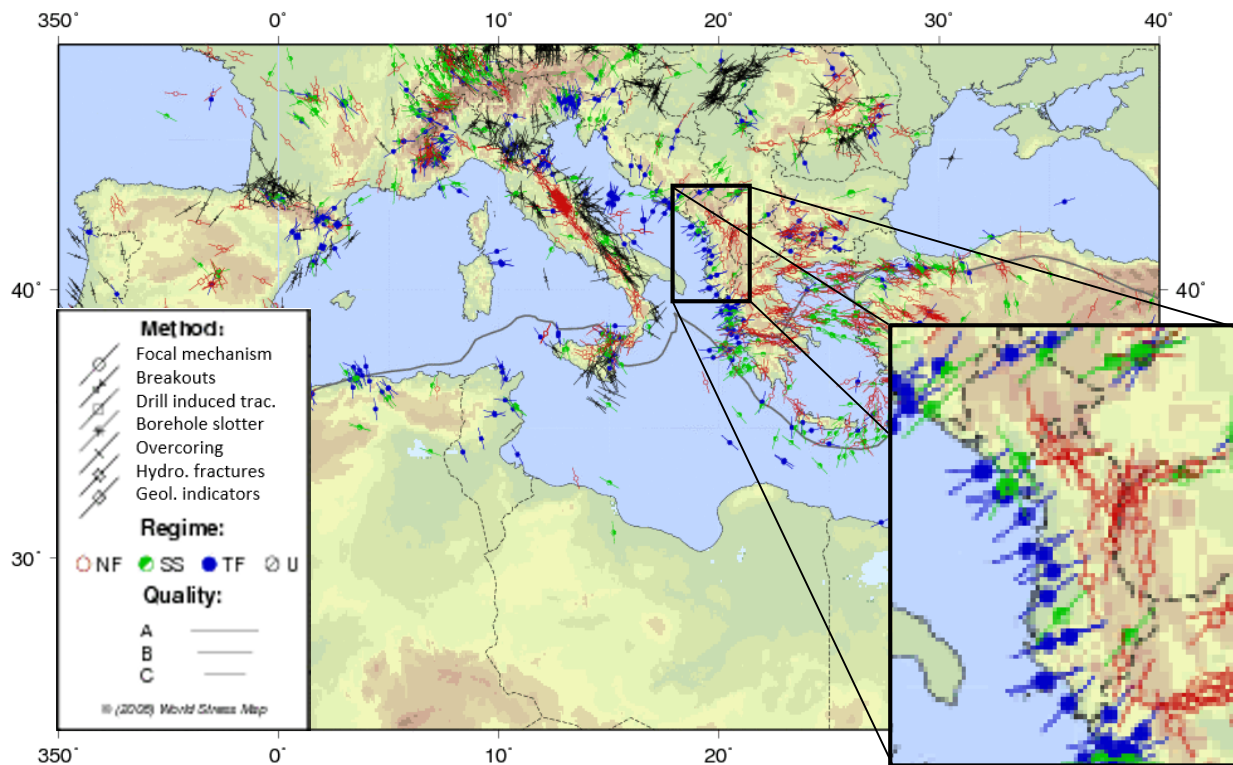


Figure 4. 9 Stress measurements in the Mediterranean region with special emphasis on the measurements conducted in Albania (World stress map, 2008).

In-situ stress measurements in the area of the powerhouse caverns are limited to hydraulic fracturing measurements in one vertical borehole (GR-1, Figure 4.6). The test was performed by SINTEF and the report SINTEF (2010) states that the quality of the tests seems to be quite good. The borehole (GR-1) is located adjacent to the bottom of the valley, about 500 m away from the planned location of the power station (original placement). The measurements were performed in the lower parts of the boreholes. Six successful measurements were executed at a depth between 81 m and 105,3 m in the borehole (SINTEF, 2010). From the impression packers, the orientation of the minor principle stress are measured to N125°E (Ødegaard, 2015).

The test procedure is carried out by sealing an interval of the borehole with packers, and pressurising the interval until tensile failure occurs, which determines the fracture initiation pressure (P_f). By reducing the pressure, the shut-in pressure (P_s) yields the pressure where the fracture is sealed. Re-pressurisation cycles are used to determine fracture reopening pressure (P_r) and repeated measurements of the shut-in pressure (SINTEF, 2010).

The average value of the shut-in pressure are anticipated to be equal to the minor principal rock stress, σ_{\min} , in the current part of the rock mass. On basis of the recorded data and the tensile strength of the rock (σ_t), determined from laboratory tests, it is possible to calculate an estimate of the maximum principal rock stress, σ_{\max} . Based on Kirch's equations, the following expressions may be used:

$$\sigma_{\max} = \sigma_t + 3P_s - P_f - P_0 \quad (\text{for the fracture initiation cycle}) \quad [4.2.1]$$

P_0 = initial pore water pressure

$$\sigma_{\max} = 3P_s - P_r - P_0 \quad (\text{for subsequent re-pressurisation cycles}) \quad [4.2.2]$$

The calculation of maximum principal stress contains a relatively large uncertainty, and should be verified by other stress measurements, such as the overcoring method (SINTEF, 2010). Overcoring measurements will be executed as the access tunnel progresses towards the planned location of the powerhouse caverns (Aagaard, 2015).

Table 5.2 contains the results from the hydraulic fracturing measurements. The average value for the shut in pressure will be equivalent to σ_h for the rest of the analysis, while σ_H are the average values of the maximum stress. According to the SINTEF (2010), the stress levels must be corrected for the hydrostatic pressure in the water filled bore hole. This means a reduction of about 0,5 MPa for an approximate depth of 90 m.

Table 4. 2: Results from the hydraulic fracturing measurements. Modified from SINTEF (2010).

Depth [m]	Fracturing pressure, P_f [MPa]	Reopening pressure, P_r [MPa]	Shut in pressure, Pisi [MPa]			Maximum stress [MPa]	Stress ratio
			1. cycle	2. cycle	3. cycle		
105,3	22,9	19,8	16,5	13,7	13,2	23,6	1,6
100,6	26,1	16,1	11,7	11	10,7	17,3	1,6
92,5	22,3	13,7	10,7	10,3	10	17,3	1,7
83,8	21,5	17,5	15,1	15,1	15,8	28,5	1,9
81	21,7	16,4	13,2	12,7	12,5	22	1,7

The following average values are calculated (corrected for 0,5 MPa water pressure):

$$\sigma_h = 12,3 \text{ MPa} \quad \sigma_H = 21,2 \text{ MPa}$$

σ_h is expected to remain the same underneath the valley side at the planned location of the caverns. However, the stress anisotropy is expected to cease deeper into the valley side. This equalization of anisotropy is then likely to be due to a reduction of the major stress component (SINTEF, 2010). The stress ratio of the average values are 1,73. Taking the prediction from the stress measurement report into account, it seems likely that the stress ratio might be reduced to 1,6 at the planned location of the caverns. Hence, the major principle stress will be $\sigma_H = 19,7$ MPa.

4.3 Placement and orientations of Underground Caverns

4.3.1 Original placement and orientation

The planned location of the powerhouse complex are shown in figure 4.10. There are approximately 235 m overlaying rock above the caverns. Depressions and lineaments in the terrain are found both north and south of the cavern location (Figure 4.10). In the longitudinal section (Appendix E), no faults or weakness zones are predicted to inflict the caverns.

The length axis of the caverns are oriented N120°Ø. From the hydraulic fracturing tests, the orientation of the major principle stress is N35°Ø. This means that the length axis of the caverns are almost perpendicular to the major principle stress. Figure 4.11 illustrates the cavern orientation with respect to the measured joint orientations in the area of the powerhouse complex.

4.3.2 Alternative placement and orientation

An alternative placement and orientation of the caverns are proposed as a part of this thesis. The adjustment in location involves moving the cavern 150 meters horizontally towards the valley side, in the direction of the access tunnel. Figure 4.12 illustrates the different options in a longitudinal section aligned with the original access tunnel. The vertical overburden to the caverns will be approximately 180 m, and the situation regarding faults and weakness zones are considered almost unaltered to the original placement.

The length axis of the caverns are proposed in a direction of $N48^{\circ}E$. This orientation is shown in the rosette plot in figure 4.11 together with the original orientation and the major horizontal stress. Length of the penstock can remain unaltered, as the overburden is considered adequate. Associated calculations will be presented in section 4.4.

The tunnel system is proposed to match the original complex in a high degree. Portals will stay unaltered, except for the portal for the escape/cable tunnel, which is suggested to be moved approximately 130 m north. This is to obtain a practical feasible inclination of the tunnel.

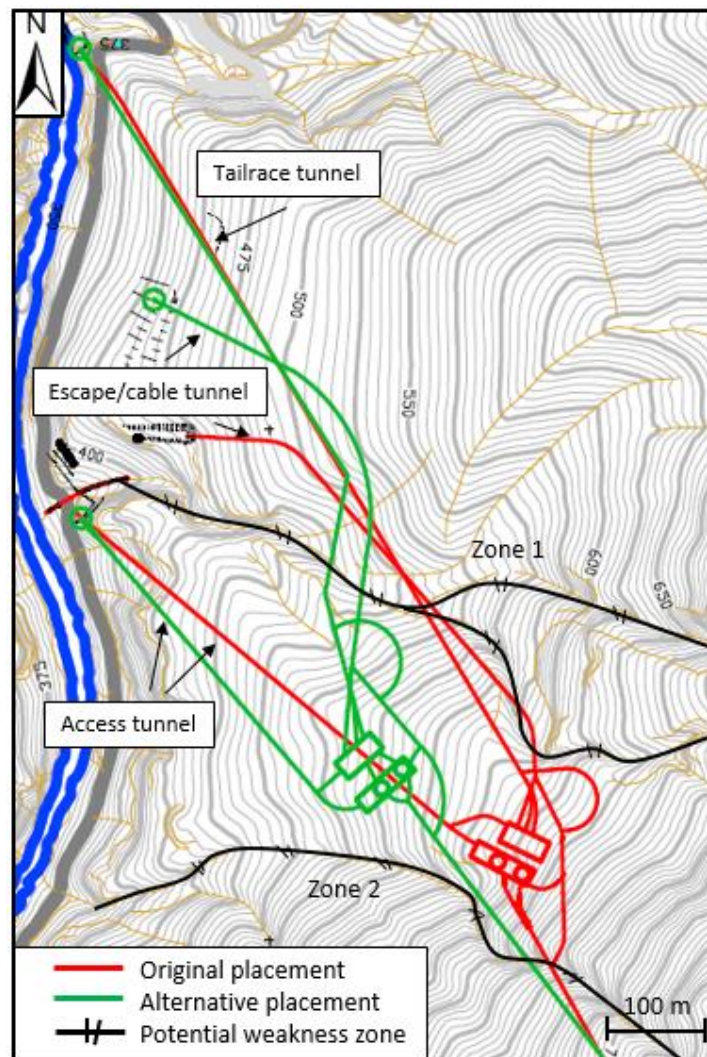


Figure 4. 10: Layout for the original and alternative placement of the powerhouse complex. Possible weakness zones that might inflict with the tunnel system are indicated.

By changing the location of the caverns, the length of the appurtenant tunnels will change accordingly (Table 4.3). The waterway is assumed to have the same length for both alternatives. The escape and cable tunnel will have an inclination of about $6,7^\circ$. It should be noted that the design for the alternative placement in figure 4.10 is a sketch. Hence, the tunnel system is not designed in detail.

Table 4. 3: Length of access tunnel and escape/cable tunnel for the original and alternative placement.

Tunnel section	Length [m] Original placement	Length [m] Alternative placement	Difference [m]
Access tunnel	479	353	-150
Escape and cable tunnel	570	557	-13

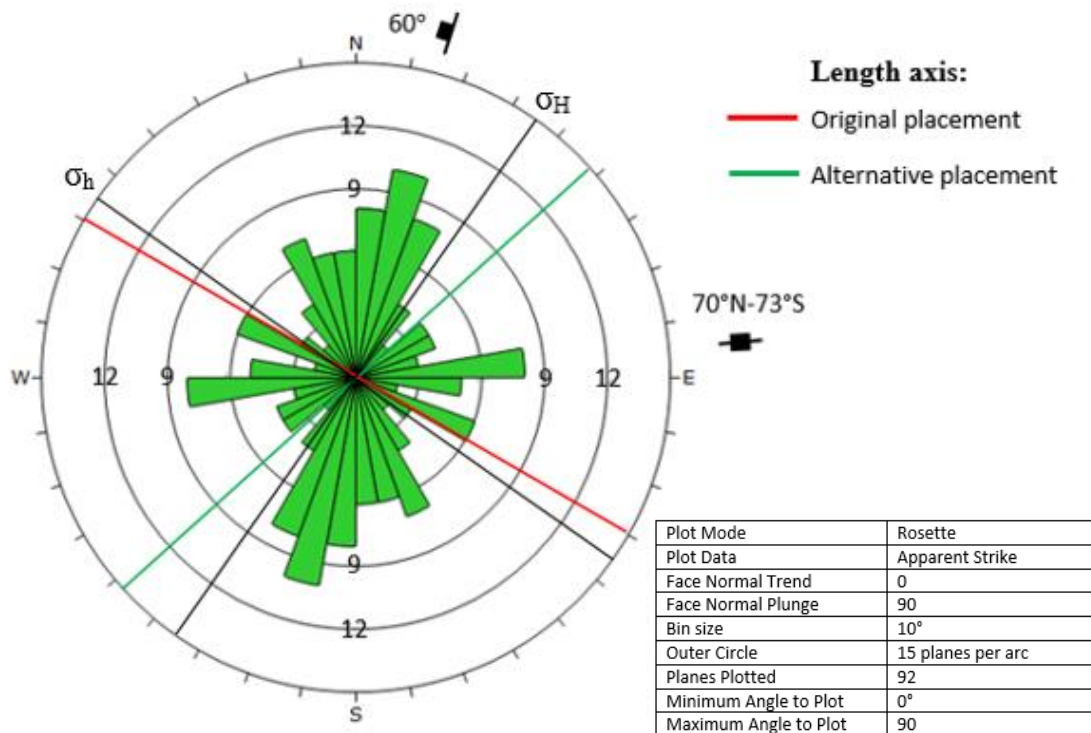


Figure 4. 11: Rosette plot of the joint measurements close to the powerhouse complex (black rectangle figure 4.6). Length axis for the caverns for both alternatives are indicated together with directions for major and minor horizontal stresses from the hydraulic fracturing measurements.

4.4 Location of unlined pressure shaft

From the rules of thumb discussed in section 3.2 (equation [3.2.1] and [3.2.2]), the required overburden for the pressure shaft is calculated. Hence, also the safety factor for placement of the cone.

$$\gamma_r = 33 \text{ kPa/m}$$

$$\gamma_w = 10 \text{ kPa/m}$$

$$H = 650 - 352 \text{ m} = 298 \text{ m}$$

$$\alpha = 7^\circ$$

$$\beta = 28^\circ$$

In consultation with supervisor, it is decided to deduct a zone of 20 meters from the measured overburden due to weathering of the rock mass (Panthi, 2015).

Table 4. 4: Calculation of factor of safety for required overburden of the cone from empirical rules of thumb.

Description	Necessary overburden [m]		Measured overburden [m]		Corrected overburden [m]		Factor of safety
	h	L	h	L	h	L	
<i>Original placement</i>	91	102	312	269	292	249	2,44
<i>Alternative placement</i>	91	102	228	209	272	189	1,85

The overburden used in the calculations in table 4.4 is estimated from a longitudinal section along the original access tunnel (Figure 4.12).

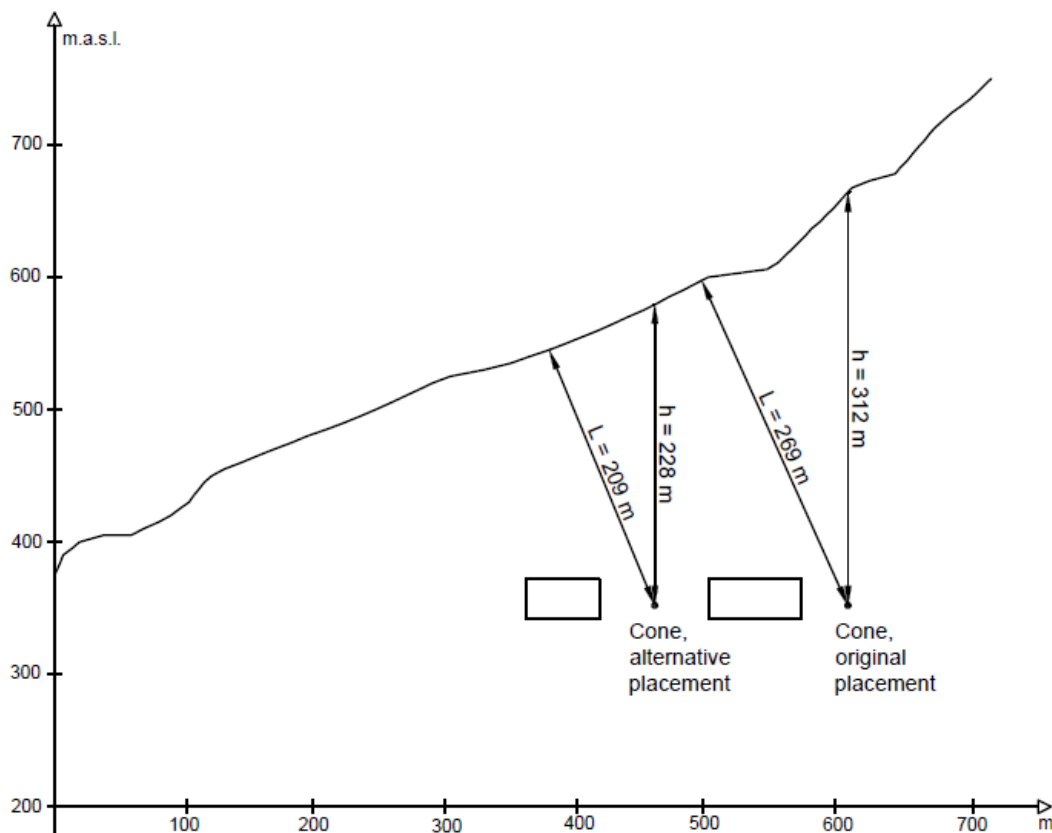


Figure 4. 12: Longitudinal section along the access tunnel for the original placement. Overburden used in the calculation of the factor of safety are indicated. The black rectangles are the approximate location of the powerhouse caverns. (Alternative placement is closest to the valley side.)

5. Empirical and analytical analysis

5.1 Stress distribution

To estimate the stress distribution around a cross section of the caverns, the directions of the principal stresses must be evaluated. For the original placement and orientation, the length axis of the caverns are oriented nearly perpendicular to the elongation of the valley. The out of plane stress component for the cross section will be dipping with an angle of approximately 45° . This angle is obtained from modelling in situ stresses in the valley side, and will be further documented in section 6.1.3. The maximum tangential stress is expected to occur in the cavern roof and floor (Figure 5.1).

The orientation proposed in the alternative placement has the length axis of the caverns oriented parallel to the valley elongation. This means that the in plane principal stress for the cross section will have a dipping angle. The angle is estimated to 30° (section 6.1.3), which means that the maximum tangential stress most likely will appear in the part of the cavern roof facing the valley side (Figure 5.1).

Kirsch's equations ([3.5.3] and [3.5.4]) are applicable to estimate the magnitude of the tangential stresses. The cavern geometry allows the Kirsch's equations only to be applied to the roof, due to its arched shape. Possible tension in the walls are difficult to calculate analytically.

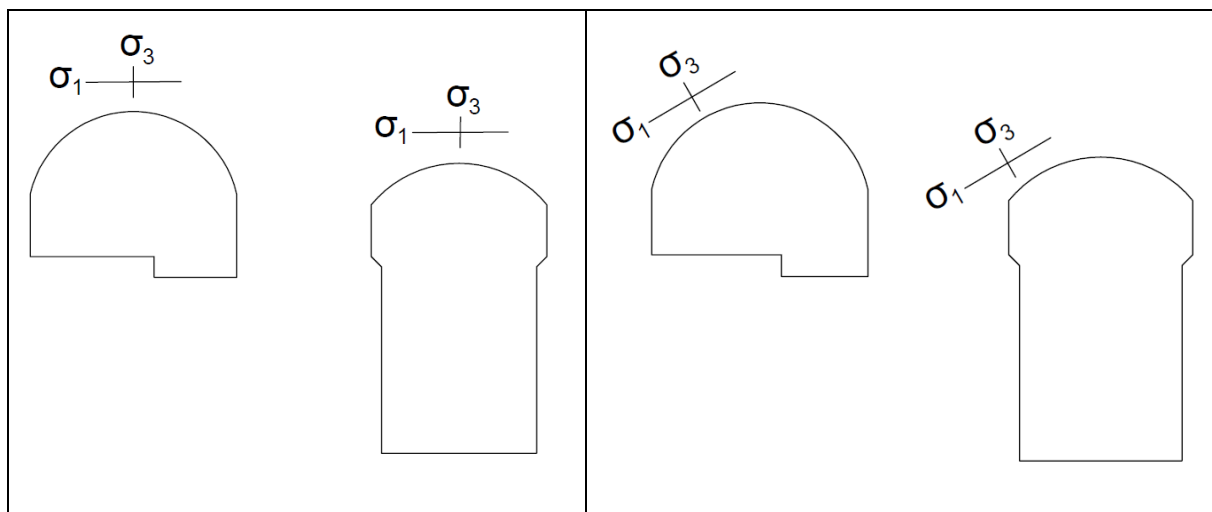


Figure 5. 1: Illustration of the in-situ stresses and the direction they act on the caverns in the original placement (left) and the alternative placement (right).

Table 5.1 presents the maximum values of the tangential stresses for both the original and the alternative placement. Calculation and assessment of σ_1 and σ_3 are documented in section 6.1.3. These tangential stress values are most applicable when the caverns are excavated to a level where the height and width are approximately the same. Especially for the powerhouse cavern, the tangential stress will in reality increase a bit after benching down to full height.

Table 5. 1: Maximum tangential stress on the cavern contour based on Kirch's equations.

Description		σ_1 [MPa]	σ_3 [MPa]	$\sigma_{\theta_{max}}$ [MPa]
<i>Original placement</i>	<i>Transformer hall</i>	19,7	7,8	51,3
	<i>Powerhouse</i>	19,7	7,8	51,3
<i>Alternative placement</i>	<i>Transformer hall</i>	12,7	5,9	32,2
	<i>Powerhouse</i>	12,7	5,9	32,2

Table 5.2 contains the results for tangential stresses in the roof (σ_{θ_r}) and walls (σ_{θ_w}) of the caverns. Equation [3.5.5] and [3.5.6] are the basis for the calculations together with figure 3.7. In these calculations, the principle stresses are assumed to be oriented along the horizontal and vertical axis also for the alternative placement.

Table 5. 2: Tangential stress in roof and walls calculated from the empirical method from Hoek & Brown (1980).

Description		A	B	k	σ_z [MPa]	σ_{θ_r} [MPa]	σ_{θ_w} [MPa]
<i>Original placement</i>	<i>Transformer hall</i>	3,2	2,3	2,5	7,8	54,6	-1,6
	<i>Powerhouse</i>	4,0	1,5	2,5	7,8	70,2	-7,8
<i>Alternative placement</i>	<i>Transformer hall</i>	3,2	2,3	2,1	5,9	33,7	1,2
	<i>Powerhouse</i>	4,0	1,5	2,1	5,9	43,7	-3,5

5.2 Rock mass quality

The Engineering geological summary report HPP3 (Norconsult/Multiconsult, 2011) presents the following distribution of rock mass quality for the area of the powerhouse caverns:

Table 5. 3: Rock mass quality in the area of the powerhouse complex from the "little q" system (Norconsult/Multiconsult, 2011).

Rock mass quality	<i>q1</i>	<i>q2</i>	<i>q3</i>	<i>q4</i>	<i>q5</i>
Share [%]	0-5	30-50	40-70	5-15	0-5

The classification is based on observation made in the terrain surface often several hundred meters from the actual cavern locations. Hence, the observations should be used as an indication of the statistical distribution of rock mass qualities. The distribution in table 5.3 is based on a great deal of assumptions (Norconsult/Multiconsult, 2011). More details on the rock mass quality in the relevant area are presented in section 4.2.

From the GSI value presented in Multiconsult (2011), equation [3.5.7], [3.5.9] and [3.5.10] are applicable to obtain roughly estimates of the RMR and Q-value (Table 5.4). Calculation of the Q-value is done with equation [3.5.10] due to its applicability to fair quality rock masses (Panthi, 2015).

Table 5. 4: Rock mass quality including RMR- and Q-values obtained from the GSI-value. $Q = 3$ from [3.5.9] which is in the same rock class as $Q = 1$

System	Value	Rock class	Description
<i>GSI</i>	45	-	-
<i>RMR</i>	50	III	Fair
<i>Q</i>	1	D	Poor

5.3 Failure and extent

It is possible to roughly estimate the degree of failure by the classification developed by Hoek and Brown (1980) (discussed in section 3.5.3). The results of this analysis is presented in table 5.5.

Table 5. 5: Predicted failure and extent from the empirical classification developed by Hoek & Brown (1980).

Description	σ_1 [MPa]	σ_1/σ_c	K_0	Predicted extent of failure
Original placement	19,7	0,23	0,40	Minor to severe spalling. Requiring light to moderate support.
Alternative placement	12,7	0,15	0,46	Minor spalling can be observed. Light support.

This classification is developed from square mining tunnels in South Africa, with a far field stress ratio (K_0) of 0,5. The far field stress factor is fairly similar in the case of the Moglicë caverns. Still the excavation shape and material properties deviates, which relates a great deal of uncertainty to this method.

From figure 3.11 section 3.5.3, the spalling and rock burst potential can be estimated based on the UCS and Hoek-Brown parameter (m_i). UCS = 84 MPa and $m_i = 25$ yields a high spalling potential, but low rock burst potential due to the limited UCS.

As a conservative assumption, the spalling strength for crystalline rocks such as peridotite/harzburgite can be set to 0,4 times the UCS (section 3.5.3). Table 5.6 gives an estimate of the spalling hazard for the caverns in both the original and the alternative placement.

Table 5. 6: Calculation of spalling hazard. Values for $\sigma_{\theta}/\text{UCS}$ over 0,4 indicates spalling.

Description		$\sigma_{\theta\max}$ (Kirsch's equations)	$\sigma_{\theta\max}/\text{UCS}$ (Kirsch's equations)	$\sigma_{\theta\max}$ (Hoek & Brown, 1980)	$\sigma_{\theta\max}/\text{UCS}$ (Hoek & Brown, 1980)
Original placement	Transformer hall	51,3	0,61	54,6	0,65
	Powerhouse	51,3	0,61	70,2	0,84
Alternative placement	Transformer hall	32,2	0,38	33,7	0,40
	Powerhouse	32,2	0,38	43,7	0,52

Spalling can be expected in both the powerhouse cavern and the transformer hall in the original and alternative placement. Especially in the original placement of the powerhouse, the

tangential stresses are high compared to the strength of the intact rock. The transformer hall in the alternative placement has values close to the spalling strength, and might not be exposed to spalling.

Predicted depth impact of brittle failure are calculated from [3.5.12], [3.5.13] and [3.5.14]. Results from these equations coincide well with each other. Table 5.7 contains the results from the calculations with stress values from both Kirsch's equations and the empirical method from Hoek & Brown (1980).

Table 5. 7: Depth of failure calculated from three different equation with stress values from Kirsch's equation and Hoek & Brown (1980) as input parameters.

		Radius [m]	Depth of failure in the roof [m]					
			Kirsch's equations			Hoek & Brown (1980)		
Description			[3.5.12]	[3.5.13]	[3.5.14]	[3.5.12]	[3.5.13]	[3.5.14]
<i>Original placement</i>	<i>Transformer hall</i>	10	2,43	2,48	2,53	2,93	3,01	3,03
	<i>Powerhouse</i>	8,5	2,07	2,11	2,15	4,46	4,67	4,54
<i>Alternative placement</i>	<i>Transformer hall</i>	10	-	-	-	-	-	-
	<i>Powerhouse</i>	8,5	-	-	-	1,11	1,08	1,19

Depth of failure is as expected corresponding to the magnitude of maximum tangential stresses. Spalling is less widespread for the alternative orientation due to the reduced principal stresses. No values were obtained for the situations where $\sigma_{\theta\max}/UCS < 0,4$ because the equations yields negative output. In other words, no spalling is expected to occur.

5.4 Support

Table 3.2 (section 3.5.2) proposes rock support based on the mapped "little q" values. As stated in table 5.3, most of the rock mass in the relevant area are in the classes q2 and q3. Appropriate rock support for the class q3 can be recommended as a conservative estimation. The suggested support is described in table 3.2 as follows: "Scaling. Systematic bolting and minimum one layer of fibre reinforced sprayed concrete in crown and walls. Numbers and lengths of bolts and thickness of sprayed concrete depend on the cross-section. It should be noted that rock mass of class q4 and even q5 may occur, which will call for heavier support.

Length of rock bolts are illustrated from the empirical relations presented in table 3.3 (Figure 5.2).

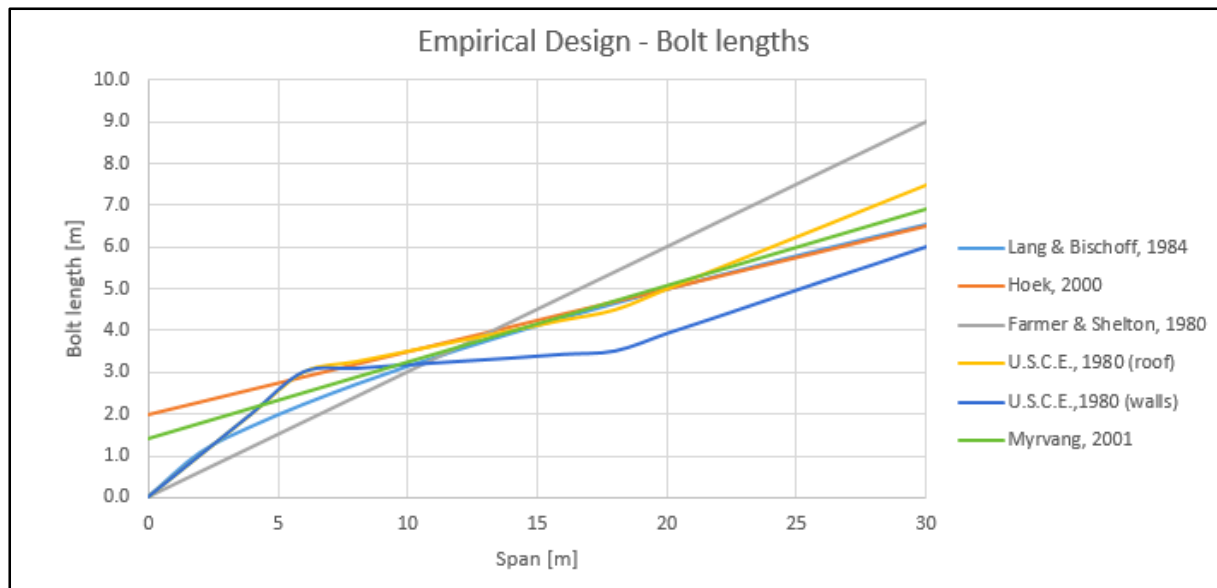


Figure 5. 2: Illustration of the formulas in table 3.3 over a span from 0 to 30 m.

By reading the graph in figure 5.2, bolt lengths can be estimated for the caverns (Table 5.2). Bolt spacing can be approximated to about half of the lengths (Table 3.4).

Table 5. 8: Estimation of required bolt length based on empirical formulas illustrated in figure 5.2.

Description		Span [m]	Bolt length [m]
<i>Transformer hall</i>	<i>Roof</i>	20	5
	<i>Wall</i>	16	4
<i>Powerhouse</i>	<i>Roof</i>	17	4,5
	<i>Wall</i>	28	6

The bolt lengths in table 5.8 are estimated with cavern span as input parameter. Parameters such as rock mass quality and stress situation should be evaluated before the lengths are determined.

Depth of failure predicted in table 5.7 is a valid basis for estimating length of rock bolts in the cavern roof. Myrvang (2001) recommends that rock bolts are placed at least one meter into competent rock. This criterion suggests the bolt lengths presented in table 5.9.

Table 5. 9: Recommended bolt length in the cavern roof based on the results presented in table 5.7. The most conservative values from the three equations are applied.

Description		Bolt lengths in the cavern roof [m]	
		Kirsch's equations	Hoek & Brown (1980)
<i>Original placement</i>	<i>Transformer hall</i>	3,4	4,0
	<i>Powerhouse</i>	3,2	5,7
<i>Alternative placement</i>	<i>Transformer hall</i>	-	-
	<i>Powerhouse</i>	-	2,2

Chapter 5

The RMR and Q system provides guidelines for support (Appendix B and C). From the converted values in table 5.4, the following support is recommended:

Table 5. 10: Recommended support from the RMR system (appendix B).

System	Value	Support
<i>RMR</i>	50	Systematic bolts, 4 m long; spaced 1,5-2 m in crown and walls with wire mesh in crown. 50-100 mm shotcrete in crown and 30 mm in sides.

Table 5. 11: Recommended support from the Q system (Appendix C).

Description		Span/ ESR	Correction for wall support	Support
<i>Transformer hall</i>	<i>Roof</i>	20	-	5 m bolts, c/c 1,7 m. E=700J shotcrete: 12 cm
	<i>Wall</i>	16	2,5	4 m bolts, c/c 2 m. E=500J shotcrete: 9 cm
<i>Powerhouse</i>	<i>Roof</i>	17	-	5 m bolts, c/c 1,7 m. E=700J shotcrete: 11 cm
	<i>Wall</i>	28	2,5	6 m bolts, c/c 2 m. E=700J shotcrete: 11 cm

6. Numerical modelling

Numerical modelling using Phase2 is carried out as a plane strain analysis, with Gaussian elimination as solver type. In the analysis, both elastic and plastic material properties are applied. Elastic material is used to analyse the redistribution of stresses and strength factor for the material. Plastic material allows the material to yield, and is useful to examine displacements and rock mass failure.

The numerical modelling for this case is carried out with two different set of rock mass parameters. In most of the analysis, frictional Hoek Brown parameters ($m > 0$) are being used. These parameters are calculated from rock mass properties with the generalized Hoek Brown failure criterion. Martin et al. (1999) states that use of rock mass failure criteria with frictional parameters significantly underpredicts the depth of brittle failure. Instead a set of brittle parameters are being proposed ($m = 0$ and $s = 0,11$). The brittle parameters are in addition modelled to get a better estimation of the depth of brittle failure.

6.1 Model set up and input data

6.1.1 Geometry and excavation stages

The cross section of the caverns are a slight simplification of the original geometry in order to ease the modelling. This excludes the busbar tunnels and draft tube. The global stability effects of these features are considered insignificant within the scope on this analysis. Figure 6.1 illustrates the simplified geometry used in the modelling, while the original geometry is presented in figure 4.1 (section 4.1.2). The transformer cavern and the powerhouse cavern are 45 m and 61 m long, respectively.

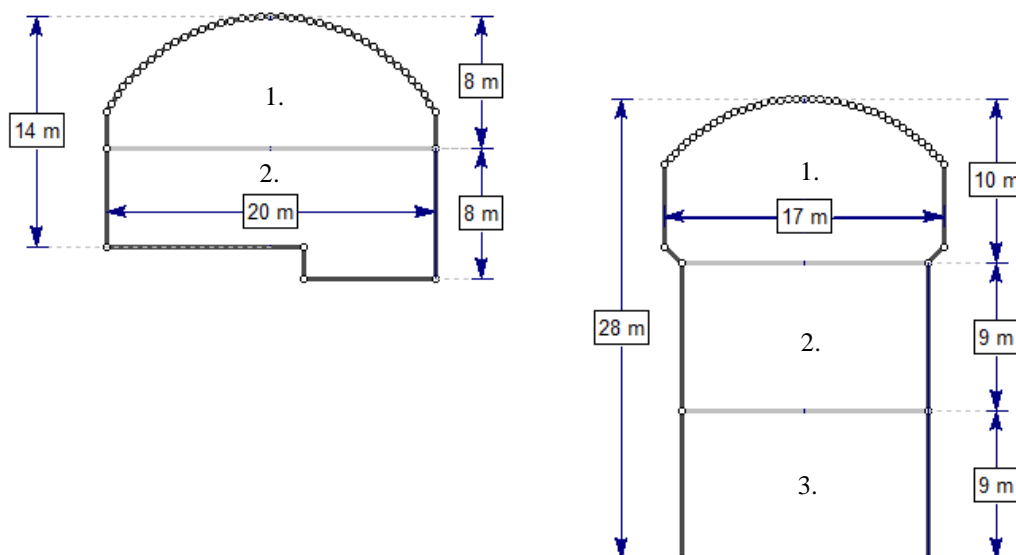


Figure 6. 1: Simplified cavern geometry applied in the numerical model. Numbers indicate excavation stages used in the model.

Large scale caverns will normally be excavated in several stages. The scope of this task is the overall stability. Hence, the number of excavation stages are reduced pursuant to the original excavation plan. Number and order of model stages are illustrated in figure 6.1

6.1.2 Mesh and displacement

A graded mesh type with 3 noded triangles are used in the model, with a gradation factor of 0,1 and the number of excavation nodes are 75. The number of excavation nodes determines the discretisation of the excavation boundaries directly, while the gradient factor determines the discretisation of all other boundaries in the model (in conjunction with the number of excavation nodes) (Rocscience, 2015).

The external boundary is rectangular with an expansion factor of 3, which is considered sufficient in order to avoid end effects. Displacements are handled by restraining the upper and lower external boundary in the vertical direction (y-direction) and the side boundaries in the horizontal direction (x-direction). The corners are restrained in both x- and y-direction. Due to a tilted stress situation, the boundaries in the model for the alternative placement is restrained in both x- and y-direction.

6.1.3 In-situ stresses

Due to relatively high stresses, where the horizontal stress is dominant, a constant field stress is chosen for the modelling. For the level of accuracy in this analysis, a constant field stress is applicable. A constant field stress allows the dip angle of the stresses to be adjusted manually, which is favourable for this analysis. The stress situation is discussed in detail in section 5.2.5. The minor principal stress is calculated from the approximate overburden from section 5.3.1 and 5.3.2 with a rock density of 3,3 g/cm³. Magnitude and direction of the principle stresses in the area of the powerhouse caverns are approximated in table 6.1.

Table 6. 1: Magnitude and principle stresses in the area of the powerhouse caverns. OP: Original placement, AP: Alternative placement.

Principal stress	Magnitude [MPa]		Direction
σ_1	19,7		N35°E
σ_2	12,3		N125°E
σ_3	7,8 (OP)	5,9 (AP)	

Since Phase 2 is a two-dimensional program, the horizontal stresses must be projected into the relevant cross-section for the model. This can be done from equation [6.1.1] derived from an equilibrium state in a two dimensional stress plane (Figure 6.2).

$$\sigma_{\alpha} = \sigma_H \cos^2 \alpha + \sigma_h \sin^2 \alpha \quad [6.1.1]$$

(Emdal, 2013)

σ_{α} is the normal stress on a plane, which in this case will be the excavation contour.

σ_H and σ_h are the horizontal principle stresses.

α is the angle between σ_h and the length axis of the excavation.

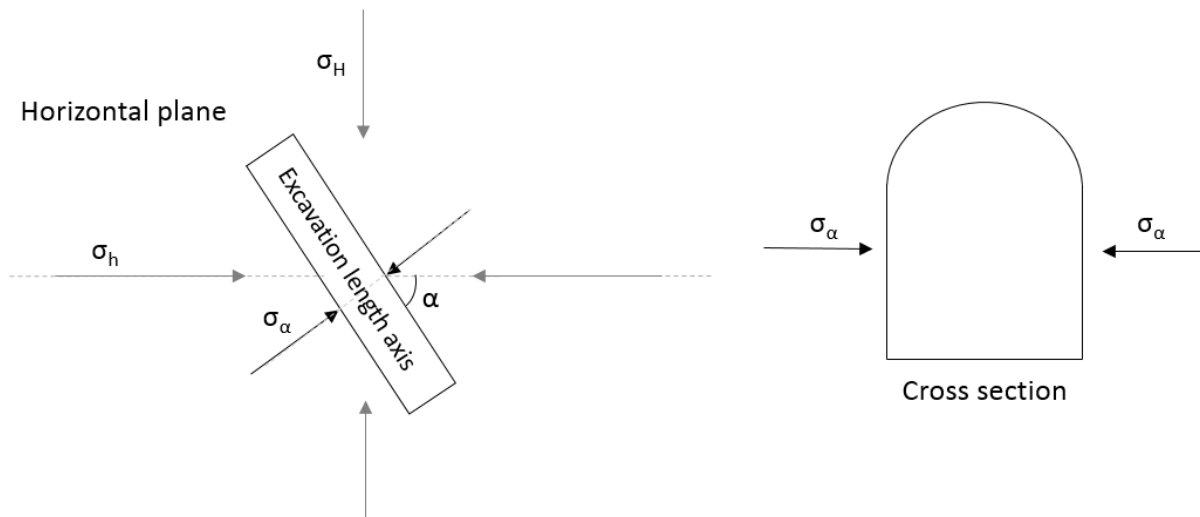


Figure 6. 2: Illustration of the use of equation [6.1.1]. This analysis disregards shear stresses along with the excavation contour in the out of plane direction.

The original orientation is aligned approximately parallel to σ_2 , hence the principal stress can be applied to the modelling of the cavern cross section. As the cavern orientation in the alternative placement deviates from the principal stresses by 13° , equation [6.1.1] is applicable to calculate the stresses in the cavern cross section (Table 6.2).

Since the location of the hydraulic fracture measurement is several hundred meters from the possible locations of the caverns, it is adequate to model a section (Figure 6.3) of the valley to obtain information about the in-situ stress at the relevant location of the caverns. To set the stress parameters, it is necessary to isolate the tectonic stress, which will be locked-in stresses in the model. This is done by the [6.1.2]:

$$\sigma_{tec} = \sigma_h - \frac{\nu}{1-\nu} \times \sigma_v \quad [6.1.2]$$

(Panthi, 2012)

By applying the stresses in table 6.1 to equation [6.1.2] the locked-in stresses will be 11,6 MPa in the in plane direction and 20,5 MPa in the out of plane direction. The modelled section is oriented along a straight line between the power house caverns and the borehole GR-1 (Figure 6.3). This is in the direction of the original access tunnel and approximately parallel to the σ_3 -direction.

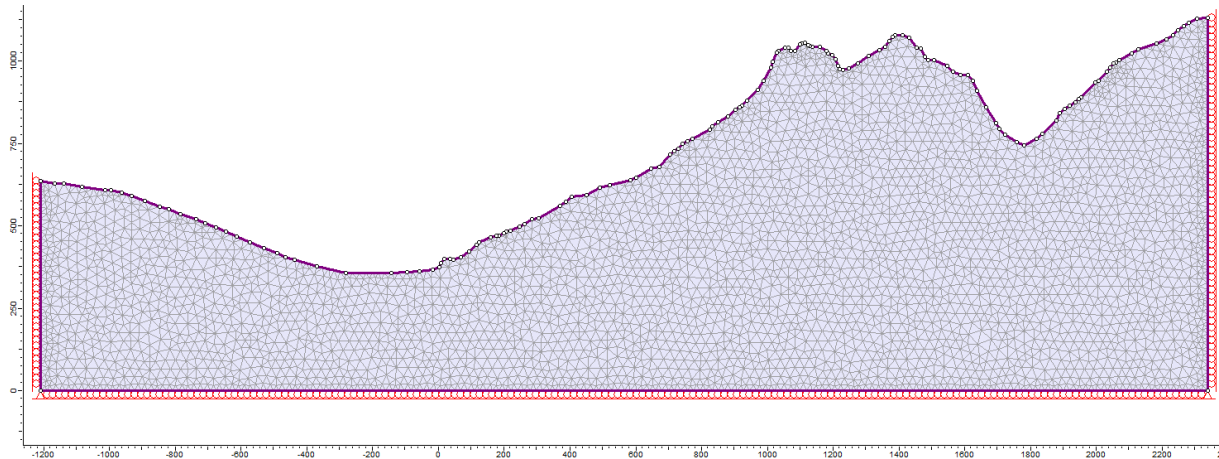


Figure 6. 3: Cross section of the valley in a straight line between the powerhouse caverns and GR-1 to model in-situ stresses.

The results are shown in figure 6.4, with a horizontal/vertical stress ratio of 2/1. This ratio is set to calibrate the stress to match the results from the hydraulic fracturing measurements. Sigma 1 in the model is matching the minor horizontal stress from the hydraulic fracturing measurements at a depth of approximately 90 m at the location of GR-1.

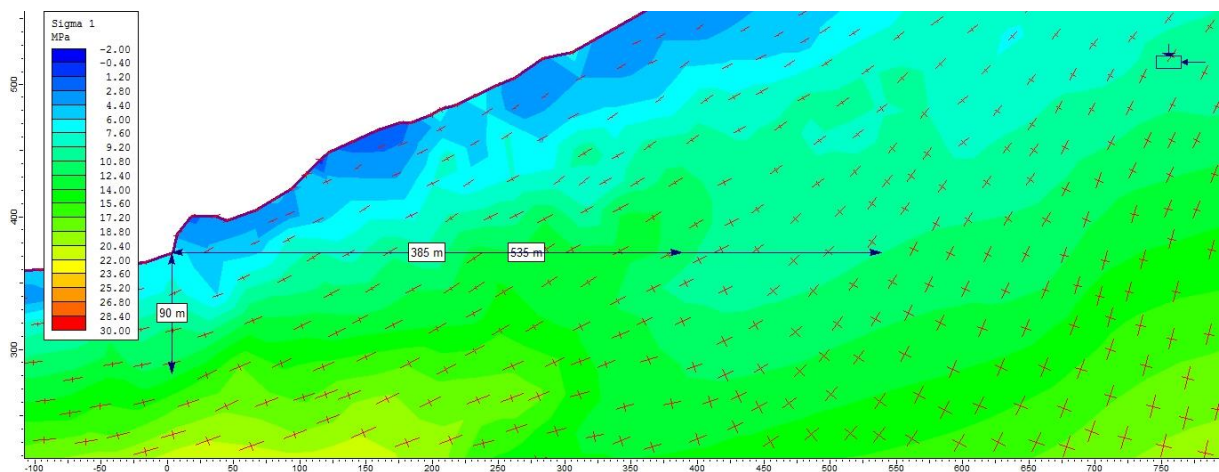


Figure 6. 4: Results from the modelling of in-situ stresses between GR-1 and the powerhouse caverns.

It should be noted that this model contains uncertainties regarding mesh width and calibration of the stress ratio. The main objective with this terrain model is to check if the stresses in the location of the caverns will be approximately in the same magnitude as the measurements in GR-1. Hence, the exact values should not be emphasised.

The results shows that the values are in the same order. The values from the hydraulic fracturing is adequate to use further in the stability analysis (Trinh, 2015). It is also worth noticing that the dipping of the principle stress is increasing further into the valley side, and the angle is quite steep in the original placement of the caverns. The dipping angle of σ_1 (Figure 6.4) in the original placement is measured to approximately 45° . This will be the out of plane component in the numerical analysis. In the alternative placement, the dipping angle of σ_1 (Figure 6.4) is

measured to about 30°. This in the in-plane stress component in the numerical analysis. The following stress situation is applied in the model (Table 6.2):

Table 6. 2: Stress situation applied in the numerical model in Phase².

Description	σ_1 [MPa]	σ_2 [MPa]	σ_3 [MPa]	Angle with horizontal stress (in plane) [°]
<i>Original placement</i>	19,7 (in plane)	12,3 (out of plane)	7,8 (in plane)	0
<i>Alternative placement</i>	19,3 (out of plane)	12,7 (in plane)	5,9 (in plane)	30

6.1.4 Material properties

The material input parameters are obtained from laboratory test result and field mapping and are presented in table 6.3:

Table 6. 3: Material properties obtained from laboratory tests and field mapping (DHP, 2011).

Parameter	Value
<i>UCS</i>	84 MPa
<i>E-modulus</i>	111,8 GPa
<i>Poisson's ratio</i>	0,18
<i>GSI</i>	45

The Hoek-Brown failure criterion is found suitable for the analysis. This criterion is often preferable in rock masses with several joint sets (Figure 6.5)(Hoek, 2007). It is also found applicable to the dynamic strength properties of brittle rock materials (Zaoh, 2000).

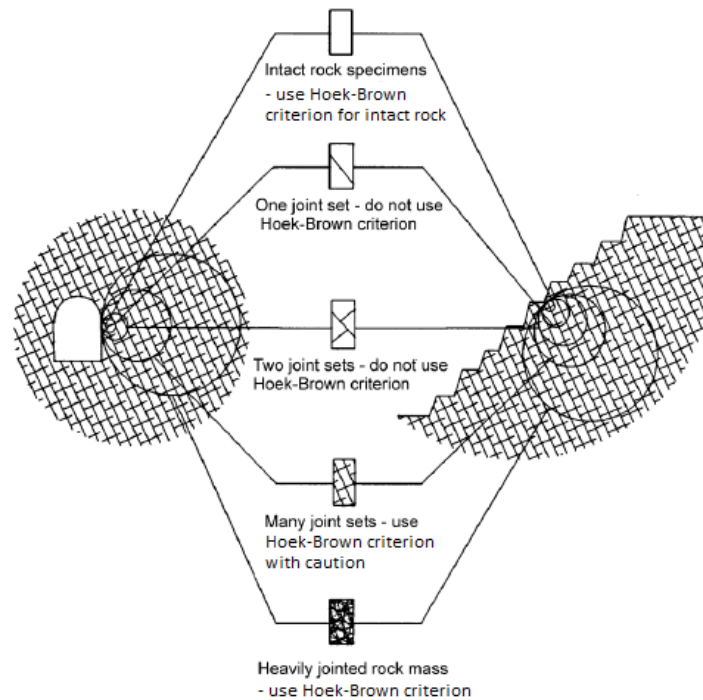


Figure 6. 5: Illustration of the area of application for the Hoek-Brown criterion. Modified after Hoek (2007).

RocLab calculates the Hoek-Brown parameters from the UCS, GSI, m_i and D . m_i is set to 25 from an internal overview in RocLab (Appendix G). The disturbance factor (D) is set to zero in most of the rock mass. In a 2 m radial zone around the excavations, the disturbance factor is set to 0,5 to account for blasting damage (Appendix A). Extension of the zone is determined in consultation with supervisor (Panthi, 2015). The Hoek-Brown parameters are given in table 6.4. In addition, the rock mass E-modulus (E_{rm}) is calculated from RocLab (Table 6.4).

A dilation parameter can be defined for plastic materials. Dilatancy is a measure of volume increase in succession to shearing of the material (Rocscinece, 2015). Dilation is set to zero in the rock mass, except for the disturbed zone. In this zone, the dilation is set to 0,05 due to plastic failure (Panthi, 2015). This is later substantiated by examining the area where the strength factor is less than one in the elastic model.

Table 6. 4: Rock mass properties applied in the numerical model.

Parameter	Peridotite	Disturbed zone
m_b	3,506	1,822
s	0,0022	0,00065
a	0,508	0,508
<i>Dilation</i>	0	0,05
E_{rm}	25,05 GPa	11,84 GPa

To model the post peak behaviour of the rock, the residual parameters are estimated. These are calculated from [3.4.7] to [3.4.10] and are listed in table 6.5. Since there are no GSI value available for the disturbed zone, the residual parameters (m_r and s_r) are determined from the

peak/residual strength ratio from the undisturbed zone. The parameter, a_r , will remain the same as for the undisturbed zone, due to its independence from the blast damage factor (D) (Hoek et al., 2002).

Table 6. 5: Residual rock mass parameters applied in the numerical modell.

Parameter	Peridotite	Disturbed zone
m_r	1,69	0,874
s_r	0,00023	0,000068
a_r	0,532	0,532

6.1.5 Support

The cavern support consists of rock bolts and shotcrete, and are customized from the results of the numerical modelling. Fully bonded CT bolts are used in the analysis. Rebar bolts are favourable due to high strength and resistance to corrosion. The bolt diameter is set to 33 mm to obtain a sufficient tensile capacity (0,38 MN) (VIKØrsta, 2012). 6 m bolts are chosen for roof support in the powerhouse for the alternative placement, and 8 m bolts for the original placement together with the transformer hall roof in the alternative placement. Centre/centre distance is 1,5 m for the bolts in the roof.

The cavern walls are supported with 8 m bolts, except for the wall of the transformer hall facing the valley side, which is supported with 6 m bolts. Centre/centre distance is 2,0 m for the bolts in the wall. High horizontal virgin stresses might lead to negative secondary stresses and horizontal tensional cracks for the original placement. Hence, the bolts should be installed with a 15 degree upward angle. Further details on the bolts are given in table 6.6.

Table 6. 6: Rock bolt properties applied in the model.

Properties	Values
<i>Bolt type</i>	Fully bonded (CT-bolt)
<i>Length [m]</i>	6-8
<i>Spacing [m*m]</i>	1,5*1,5 – 2*2
<i>Diameter [mm]</i>	33 ¹
<i>Bolt modulus [GPa]</i>	200 ²
<i>Tensile capacity [MN]</i>	0,38 ¹
<i>Residual tensile capacity [MN]</i>	0,01 ²
<i>Pre-tension</i>	No

¹ Values from VIKØrsta (2012)

² Standard values in Phase²

A standard beam liner is used to simulate the shotcrete. This liner has flexural rigidity, i.e. resistance to bending (Rocscience, 2015). The Timoshenko beam formulation are used for the beam elements to take into account transverse shear deformation effects (Rocscience, 2015). Total shotcrete thickness is 30 cm for the alternative placement and 40 cm for the original placement. The liner properties are staged, due to practical limitations in applying 30-40 cm shotcrete in one layer. Two stages are applied, where the first stage applies 10 cm, and the

second stage adds another 20-30 cm. The second stage represents several layers in practice. Further details on the shotcrete is given in table 6.7.

Table 6. 7: Liner properties applied in the model. Standard values from Phase² have been used. Strength values and modulus are corresponding to values used by Multiconsult (2011).

Properties	Values
Shotcrete modulus [GPa]	30
Thickness [cm]	30-40
Poisson's ratio	0,2
Material type	Plastic
Peak compressive strength [MPa]	35
Residual compressive strength [MPa]	5
Peak tensile strength [MPa]	5
Residual tensile strength [MPa]	0
Beam element formulation	Timoshenko

6.3 Numerical modelling results

6.3.1 Spacing between caverns

To evaluate spacing between the caverns, different pillar widths are modelled. In figure 6.6 and figure 6.7 the strength factor is illustrated in an elastic model. In the white area, the strength factor is higher than one, and this indicates that the rock mass strength exceeds the redistributed pressure. For the original placement, pillar widths over 18 m are needed to avoid strength factors less than one, in the middle of the pillar. For the same reason, pillar widths over 24 m are required for the alternative placement.

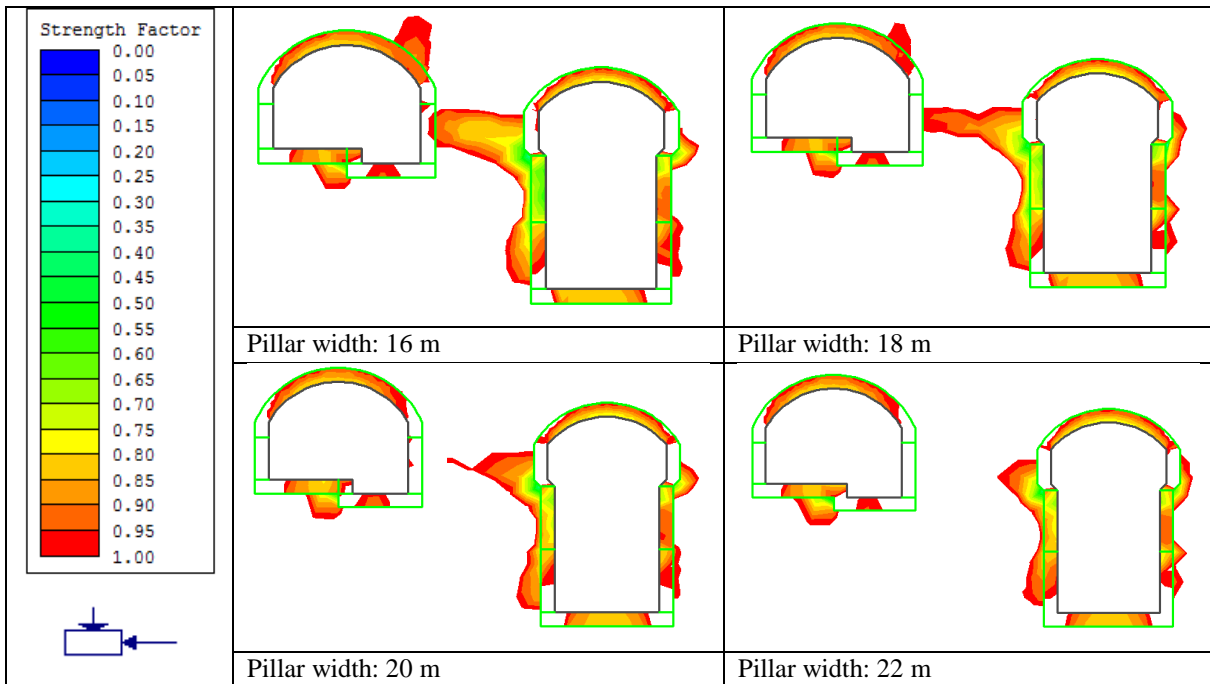


Figure 6. 6: Illustration of areas with strength factor less than one for the original placement (elastic)

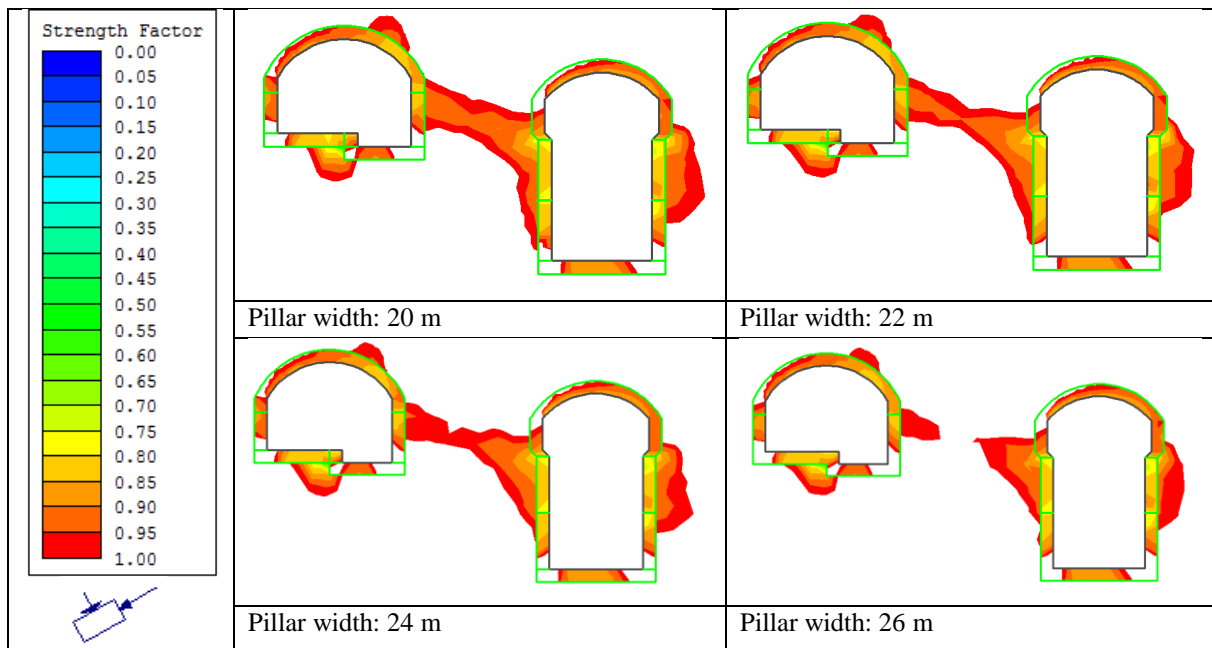


Figure 6. 7: Illustration of areas with strength factor less than one for the alternative placement (elastic)

From the strength factor, it would be recommended to use a pillar width of 22 m for the original placement, and 26 m for the alternative placement. Before setting the definite pillar width, a plastic model is run to get information about the extension of the yielded zone (Figure 6.8).

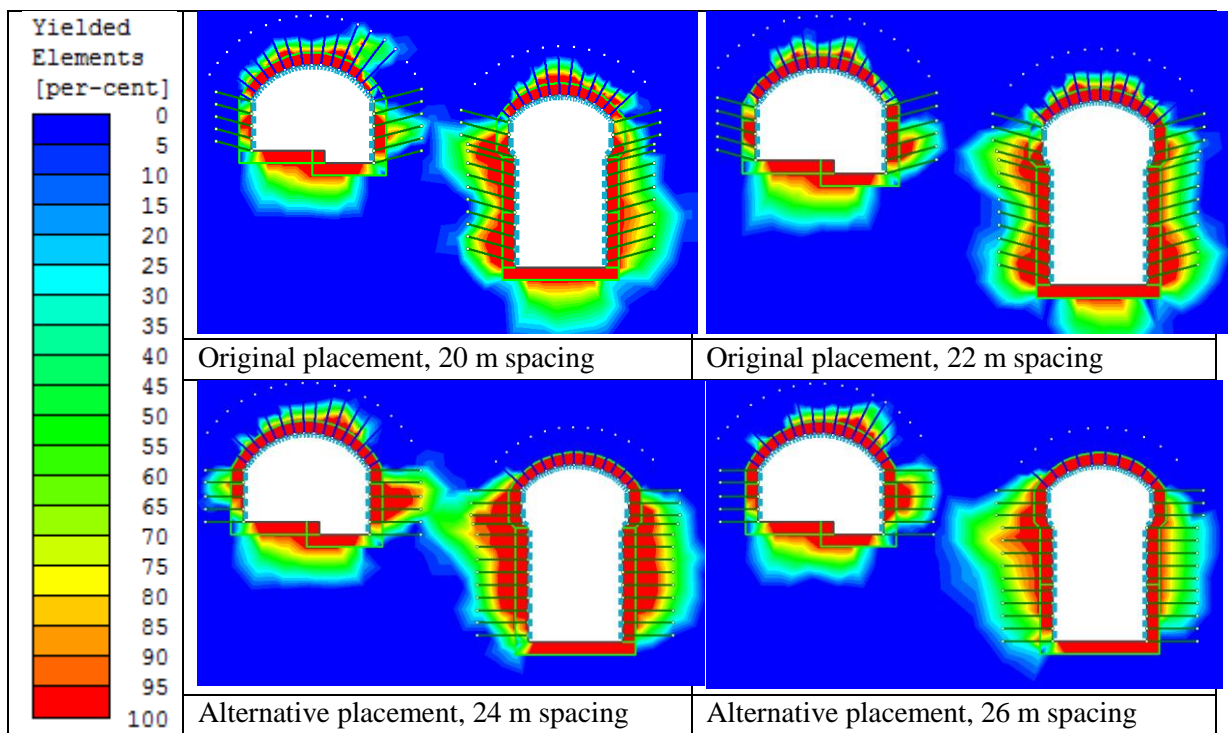


Figure 6. 8: Yielded elements for different pillar widths for both the original and alternative placement (plastic model).

To achieve an unyielded pillar centre, 22 m spacing will be applied for the original placement and 26 m spacing will be applied for the alternative placement. Maximum stress through the pillar for the 22 m spacing and 26 m spacing are shown in figure 6.9. Related to figure 2.9 chapter 2.6, the stress concentration has moved further into the pillar centre for the pillar in the original placement than the pillar in the alternative placement. That being said, the differences are rather small.

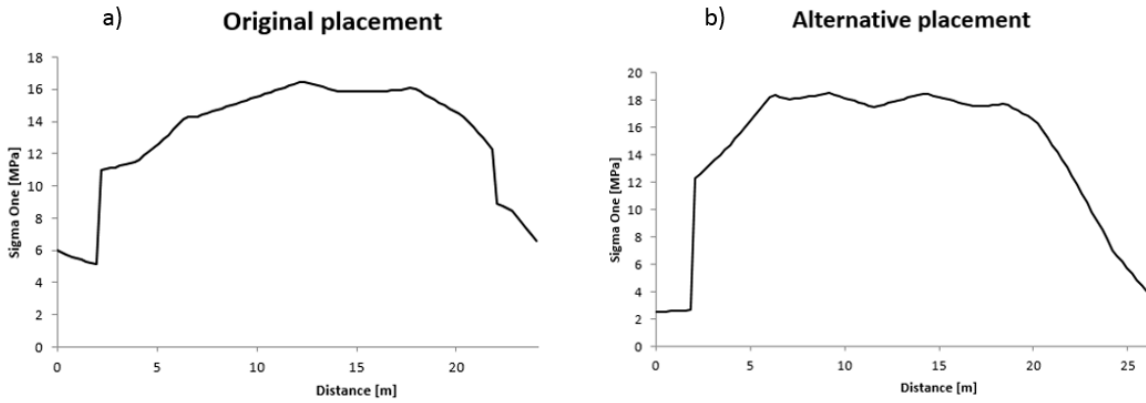


Figure 6. 9: Maximum stress through the pillar for the original placement (22 m pillar) and the alternative placement (26 m pillar).

6.3.2 Stress distribution

The stress distribution around the openings are modelled with elastic material properties (Figure 6.10 and 6.11). The maximum values in roof are labelled and rendered in table 6.8. Since the disturbed zone has a lower E_{rm} than the rest of the rock mass, the stresses are distributed to the transition between the disturbed zone and the rest of the rock mass.

Table 6. 8: Maximum tangential stress in the cavern roofs and their ratio with UCS. Values over 0.4 indicates spalling.

Description		$\sigma_{\theta_{max}}$ (roof) [MPa]	$\sigma_{\theta_{max}}/UCS$
Original placement	Transformer hall	32,5	0,38
	Powerhouse	40,0	0,48
Alternative placement	Transformer hall	24,0	0,29
	Powerhouse	32,0	0,38

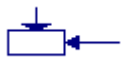
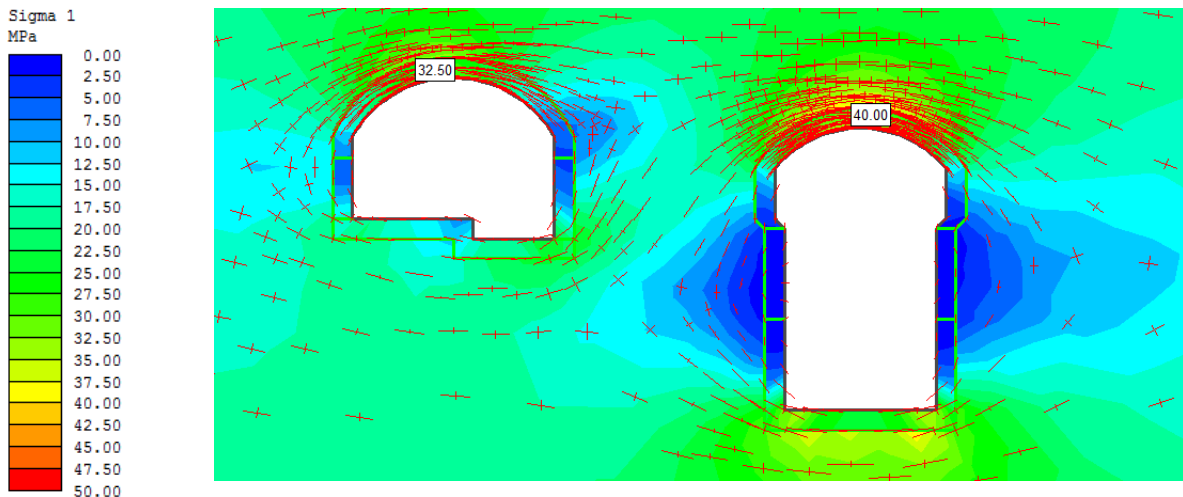


Figure 6. 10: Stress distribution (Sigma 1) with trajectories for the original placement. Maximum stress in the roof is labelled [MPa] (elastic model).

In the alternative placement, figure 6.10 displays low stresses in the right side of the roof. This leads to lack of gripping tension, which in turn can result in downfall of blocks.

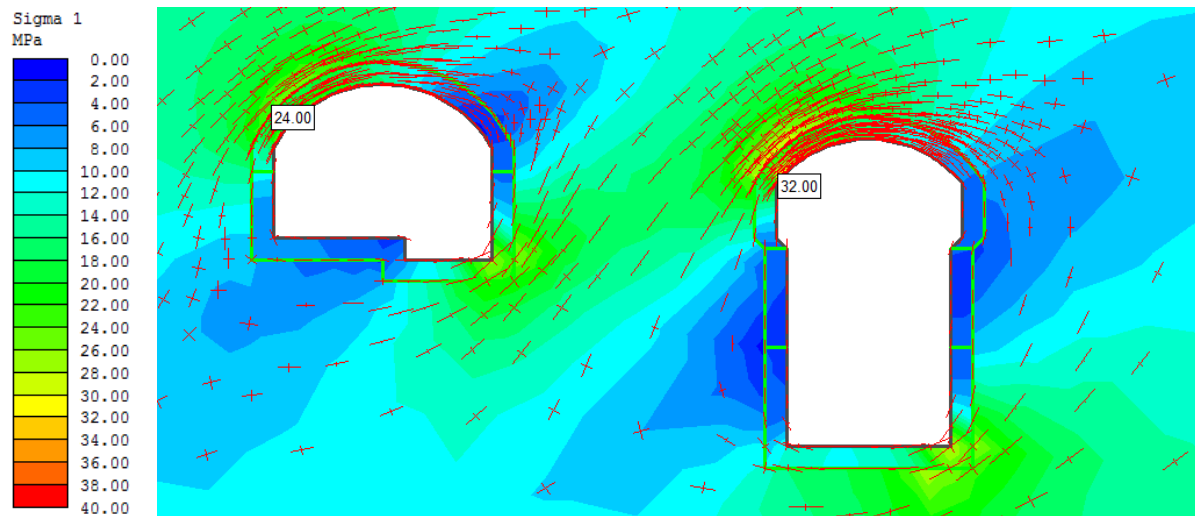


Figure 6. 11: Stress distribution (Sigma 1) with trajectories for the alternative placement. Maximum stress in the roof is labelled [MPa] (elastic model).

Negative stress might cause stability problems due to tension. The zones with negative stress are modelled in figure 6.12. It is primarily in the walls of the powerhouse cavern that this could be a problem. This is due to the geometry of the cavern and the direction and magnitude of the stresses. The critical zone is more extensive in the original placement than in the alternative placement because of a larger in-situ stress anisotropy in the cross section.

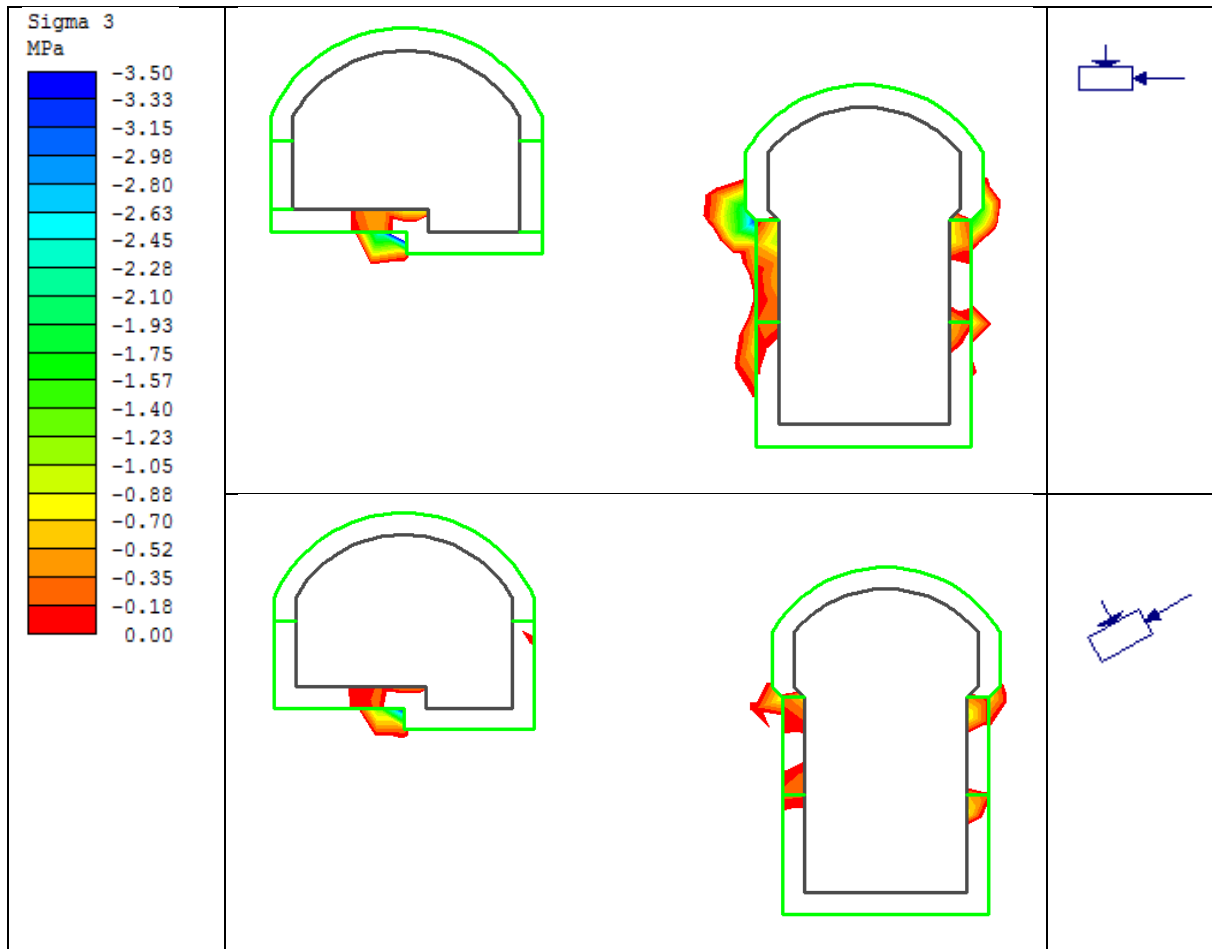


Figure 6. 12: Areas with negative stresses for the original placement (over) and the alternative placement (under).

6.3.3 Failure and extent

As discussed in section 3.5.3, depth of brittle failure can be modelled by the constant deviatoric-stress-criterion or by examining the strength factor using Hoek-Brown brittle parameters. These two methods coincide well (as shown in figure 6.13-6.16). Due to the stress situation, the roof and floor will be subjected to the largest compressive stress. Figure 6.13-6.16 displays depth of failure in the roof since this is the most crucial regarding stability. The disturbed zone is not implemented in these models, because the purpose is to examine the potential of brittle failure in the rock mass. Disturbed zones will transfer more stress due to its lower E-modulus. This will lead to a discontinuous failure zone with one brittle fracturing zone on the excavation contour and one additional zone on the transition between the disturbed zone and the rest of the rock mass.

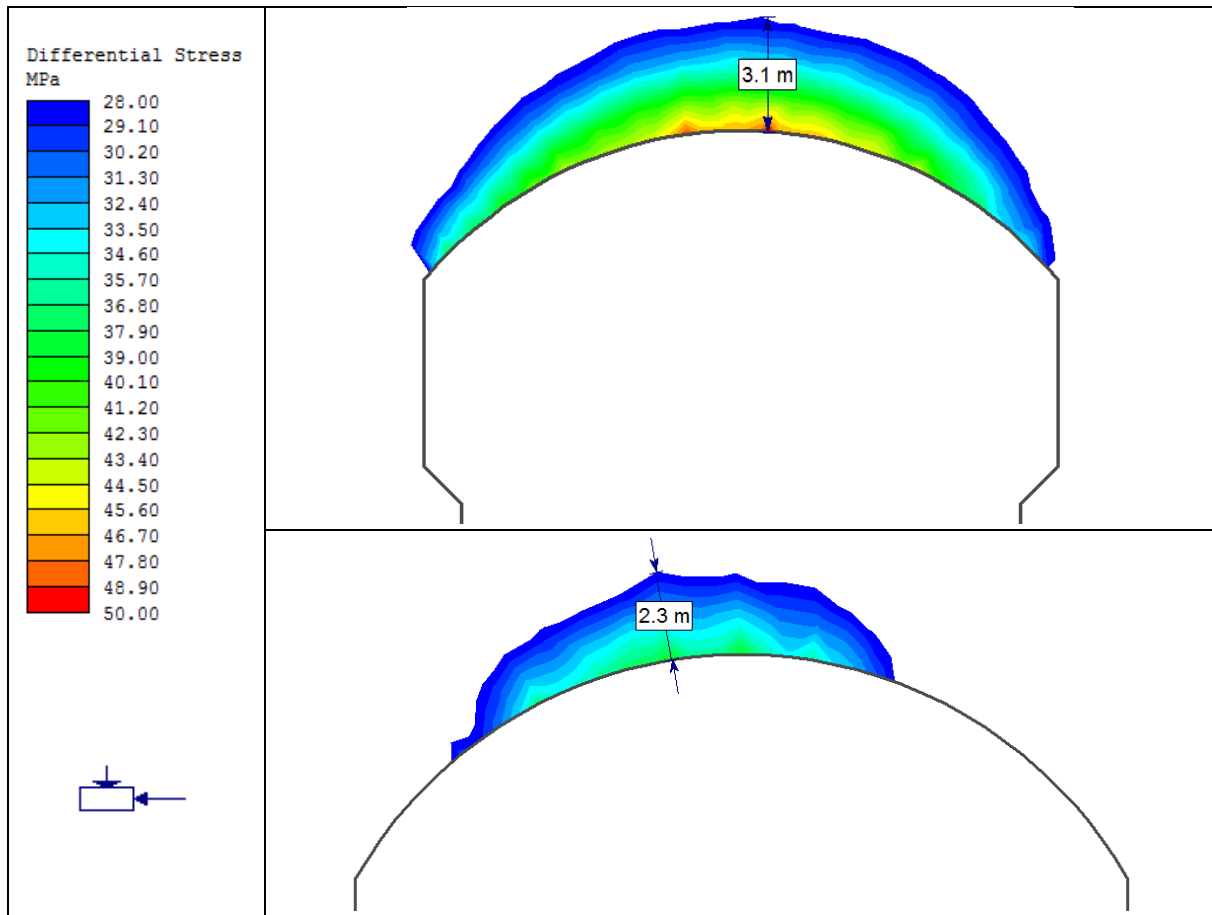


Figure 6. 13: Depth of potential brittle failure from the deviatoric stress criterion for the powerhouse (over) and the transformer hall (under) in the original placement.

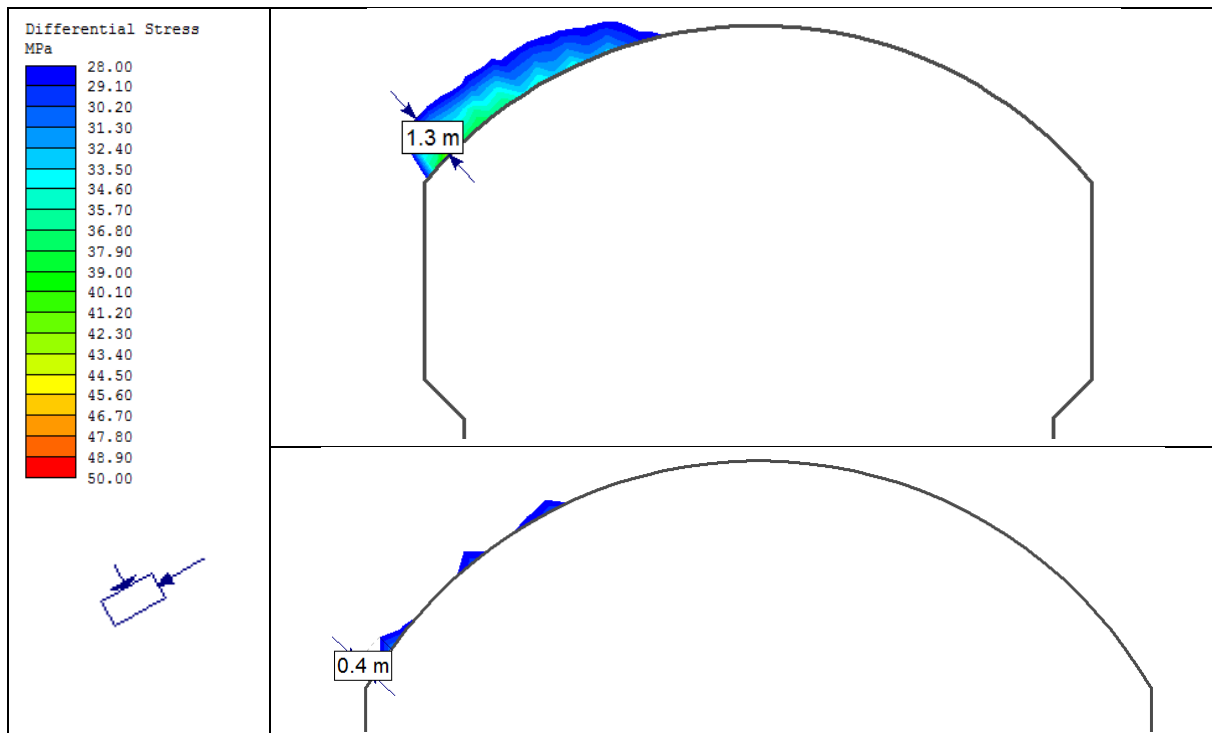


Figure 6. 14: Depth of brittle potential failure from the deviatoric stress criterion for the powerhouse (over) and the transformer hall (under) in the alternative placement.

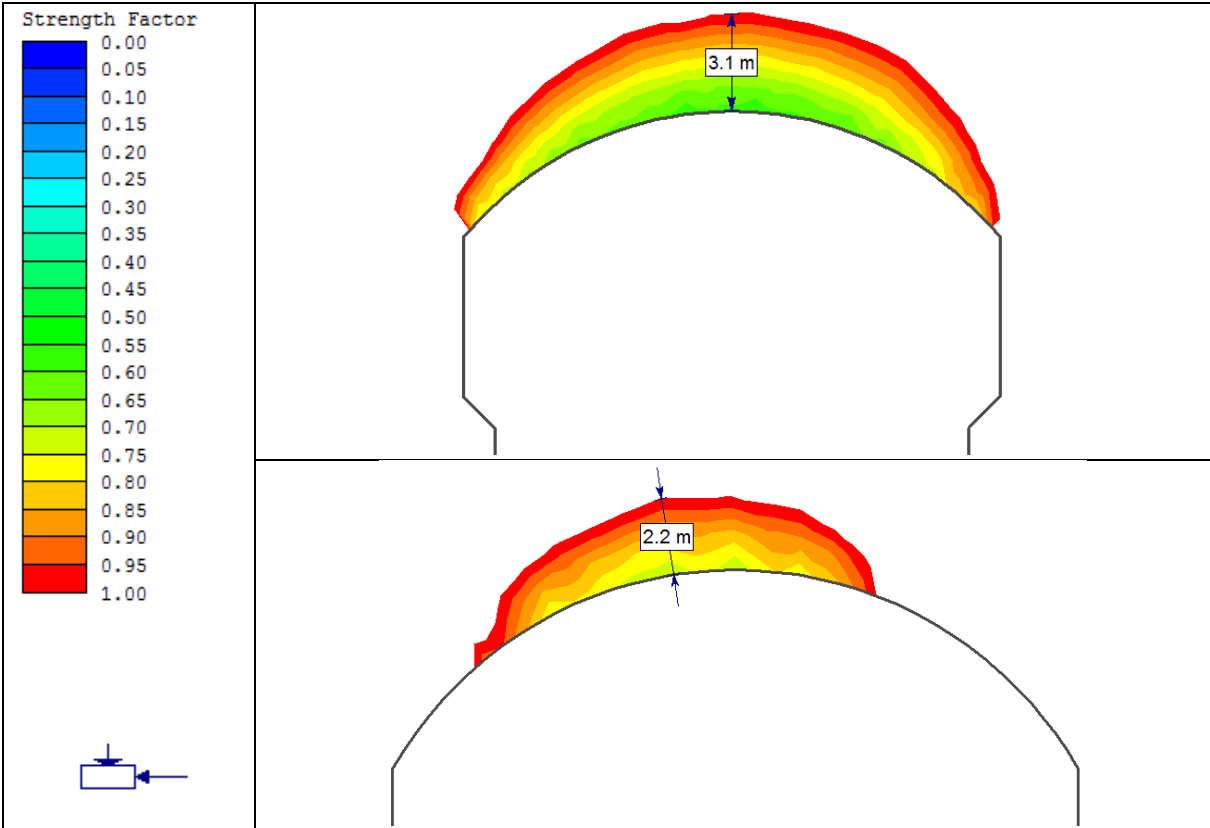


Figure 6. 15: Depth of potential brittle failure with Hoek-Brown brittle parameters for the powerhouse (over) and the transformer hall (under) in the original placement.

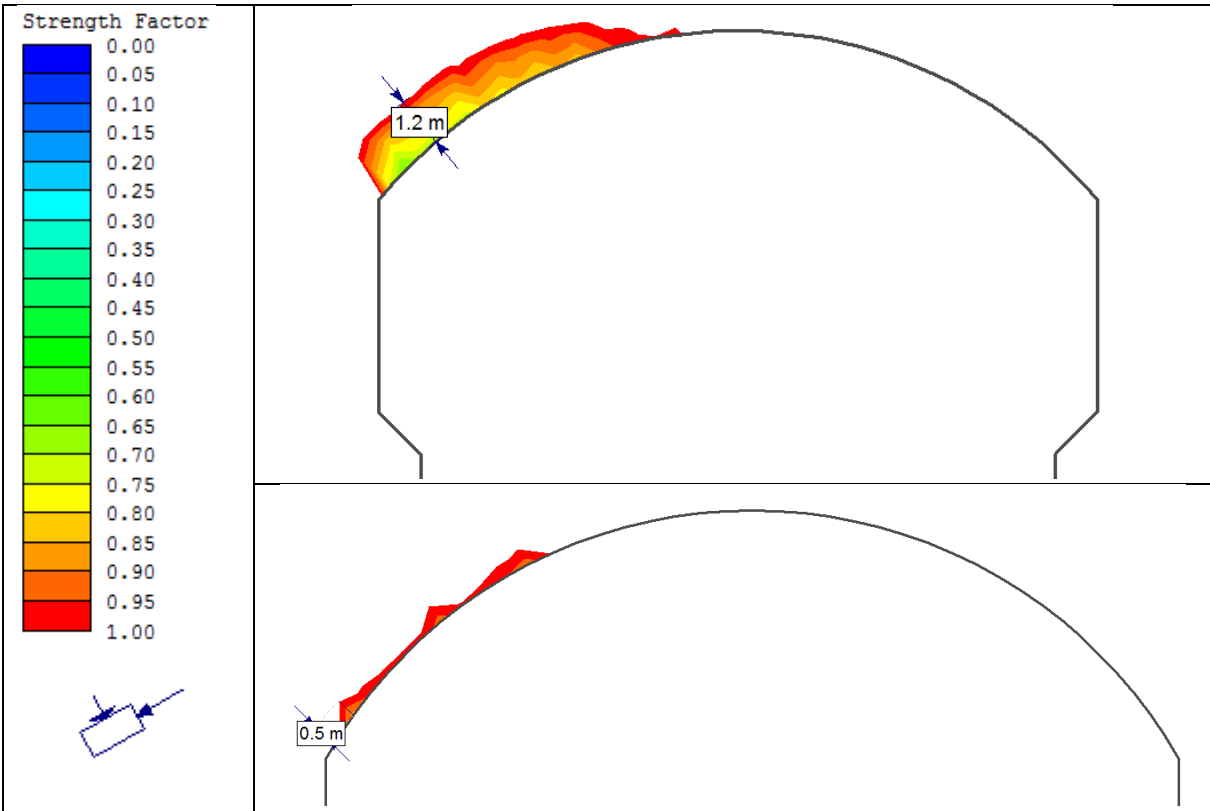


Figure 6. 16: Depth of potential brittle failure with Hoek-Brown brittle parameters for the powerhouse (over) and the transformer hall (under) in the alternative placement.

A plastic model is analysed to evaluate the extent of damage when the material is allowed to yield. The yielded zone is more extensive in the cavern roof for the original placement than the alternative placement, while in the pillar and walls, there is not much difference in the extent of the yielded zone for the two alternatives (Figure 6.17). Yielded elements in the cavern walls indicates tensile fracture initiation.

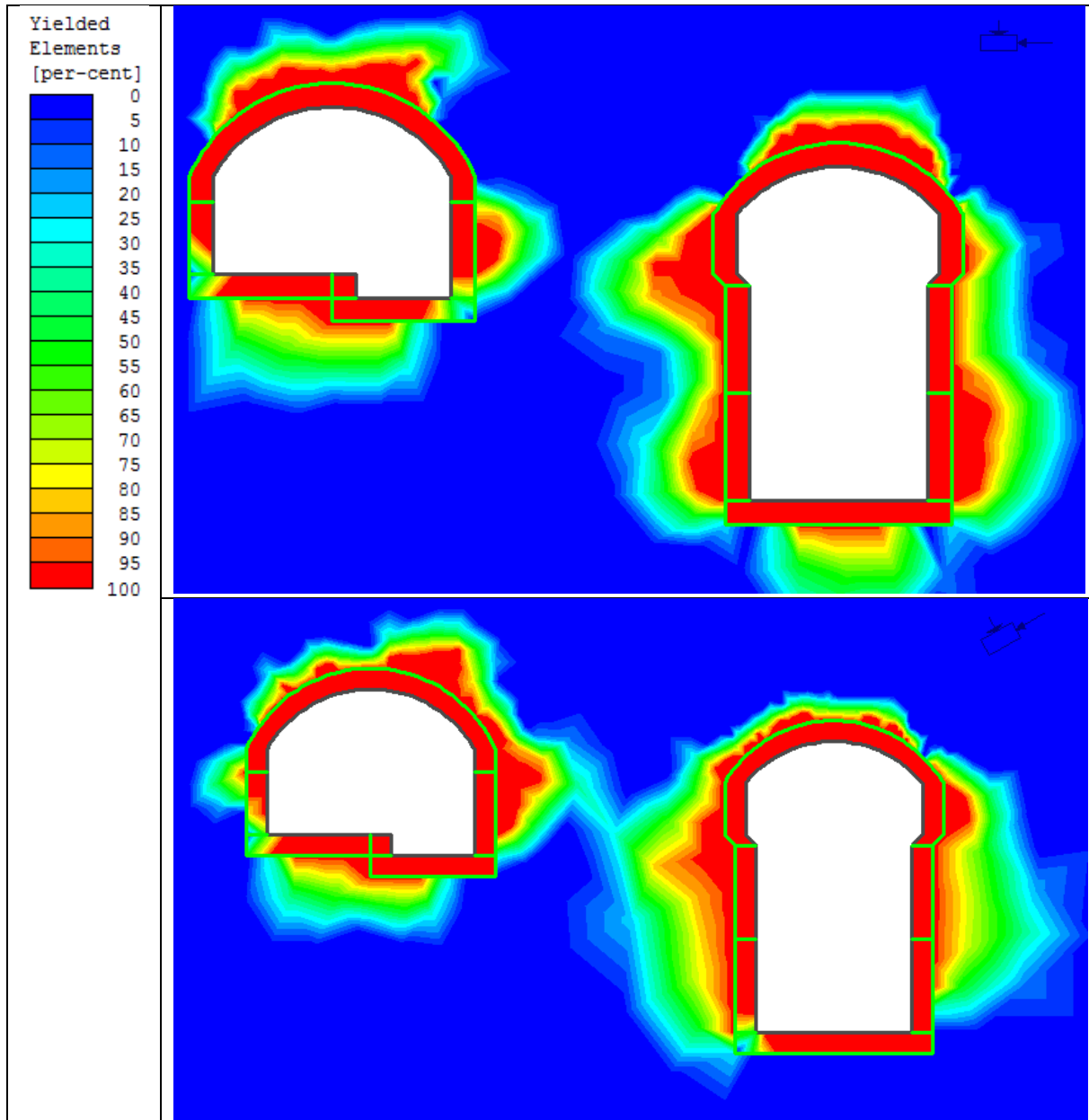


Figure 6. 17: Yielded elements in an unsupported state for the original placement (over) and the alternative placement (under) (plastic model).

Total deformation is plotted in figure 6.18, with some critical areas labelled. In the alternative placement, the deformation is more concentrated in the left side of the roof (Figure 6.18), due to the tilted stress situation. In total, the total displacement is more favourable in the alternative placement than in the original.

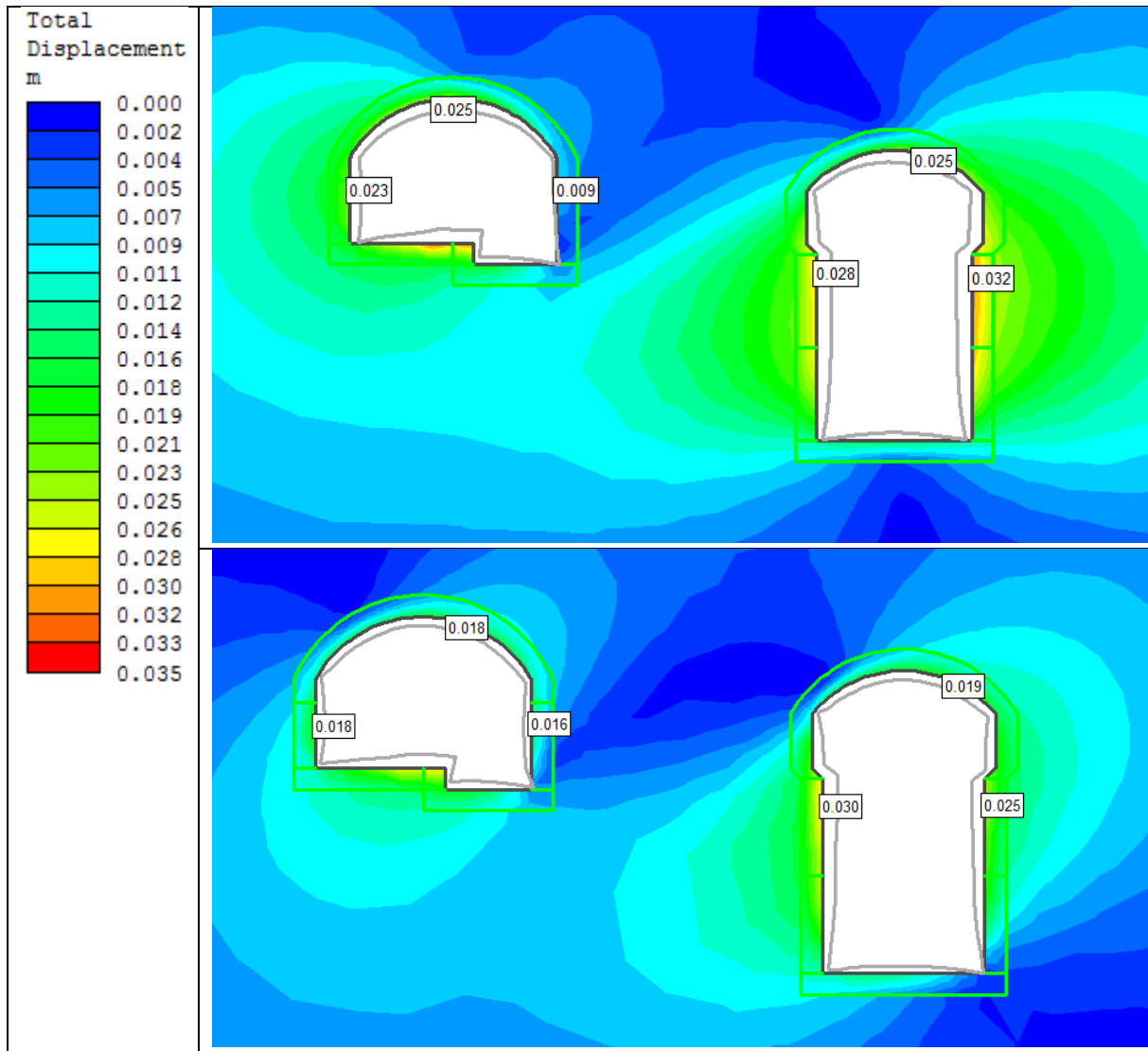


Figure 6. 18: Total displacement in an unsupported state for the original placement (over) and alternative placement (under). Values in the roof and walls are labelled [m]. Deformation boundary is scaled 50:1.

6.3.4 Support

Many bolts are yielding in the disturbed zone. This is affected by the deformation applied by the dilation parameter in this area. The increased deformation leads to tensile yielding in the support.

Liner elements are yielded in the cavern roofs for the original placement, due to large span and high horizontal stress. In the alternative placement, there are also some yielded liner elements in the roof of the caverns (Figure 6.19). These appear in the left side of the roof due to the concentration of compressive stress from the tilted stress situation. Both the original and the alternative placement shows some yielded liner elements in the walls of the powerhouse cavern due to displacement.

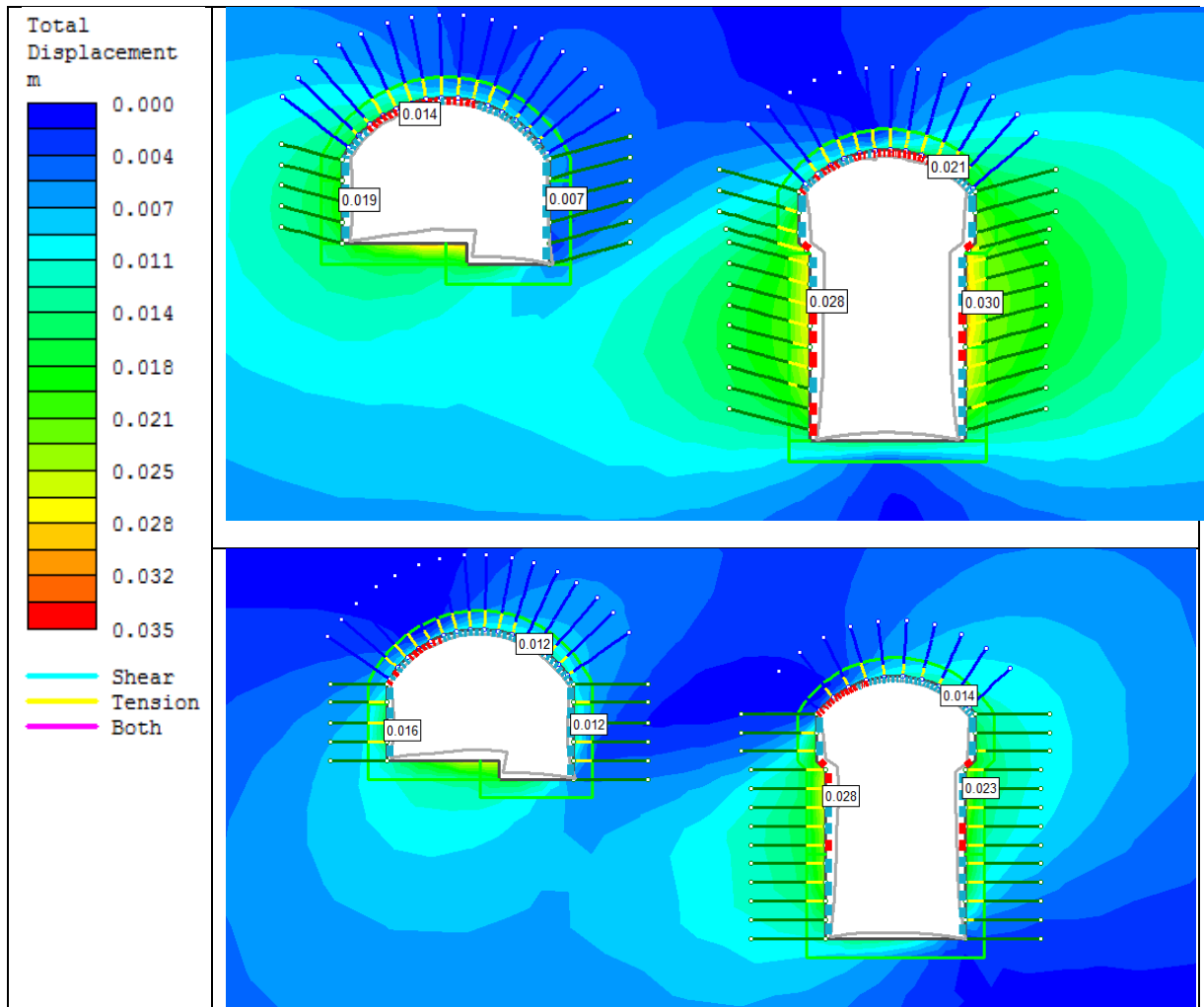


Figure 6. 19: Total displacement and installed support for the original placement (over) and the alternative placement (under). Yielded liner elements (red) and bolt elements (yellow) are displayed. Values in the roof and walls are labelled [m]. Deformation boundary is scaled 1:50.

6.4 Discussion on model results and sensitivity analysis

A numerical model is worthless without proper input parameters. It is important to understand that there are uncertainties in the input parameters, which will lead to inaccuracy in the model results. The laboratory results used as material properties will vary in the rock mass. In addition, the strength parameters applied in the model are a function of the geological strength index, which is a subjective classification tool (Section 3.5.2) and not an exact material property. The calculation of the strength parameters is carried out through the Hoek-Brown criterion, which is an empirical modification of the rock mass strength. From the strength parameters, residual parameters are calculated with empirical equations also involving the GSI value. The disturbance factor is also hard to predict, since it is dependent on the quality of the blasting.

Not only are there uncertainties in the material properties, the stress situation is an estimate and not an exact value. There are uncertainties in the hydraulic fracturing measurements (as shown in table 4.2) and in the extrapolation of the results to the cavern location. The model in the previous section is developed as a best estimate of the prevailing conditions. Because of the uncertainties described above, it is interesting to examine a situation where the conditions are

slightly worse. This is done as a simple sensitivity analysis where the following parameters are changed:

Table 6. 9: Parameters examined in the sensitivity analysis. Values that are most likely to occur (best estimate) and worst case estimates are given.

Parameter	Best estimate	Worst case
<i>GSI</i>	45	40
m_i	25	20
<i>UCS [MPa]</i>	84	60
<i>E-Modulus [GPa]</i>	112	70
<i>Disturbed zone [m]</i>	2	4
<i>Sigma 1</i>	19,7	28,5
<i>Sigma 2</i>	12,3	15,8

Worst case values for UCS and E-Modulus are collected from Multiconsult (2011), while the m_i parameter has a standard deviation implemented in RocLab. Sigma 1 and 2 corresponds to the largest stress levels from the hydraulic fracturing (Table 4.2). The extent of the disturbed zone and GSI value is set after consultation with supervisor (Panthi, 2015). Hoek-Brown parameters (peak and residual) are calculated with the same procedure and formulas described in section 6.1.4.

Table 6. 10: Rock mass properties for the worst case scenario.

Parameter	Peridotite	Disturbed zone
m_b	2,346	1,149
s	0,0012	0,0003
a	0,5114	0,5114
m_r	1,297	0,6349
s_r	0,0002	0,00005
a_r	0,5348	0,5348
$E_{rm} [GPa]$	11,2	5,4

Yielded elements and support are presented in figure 6.20 for the worst case scenario. The yielded zone is dramatically increased, and it is quite clear that the proposed support is not sufficient. Both locations represent clearly unstable situations.

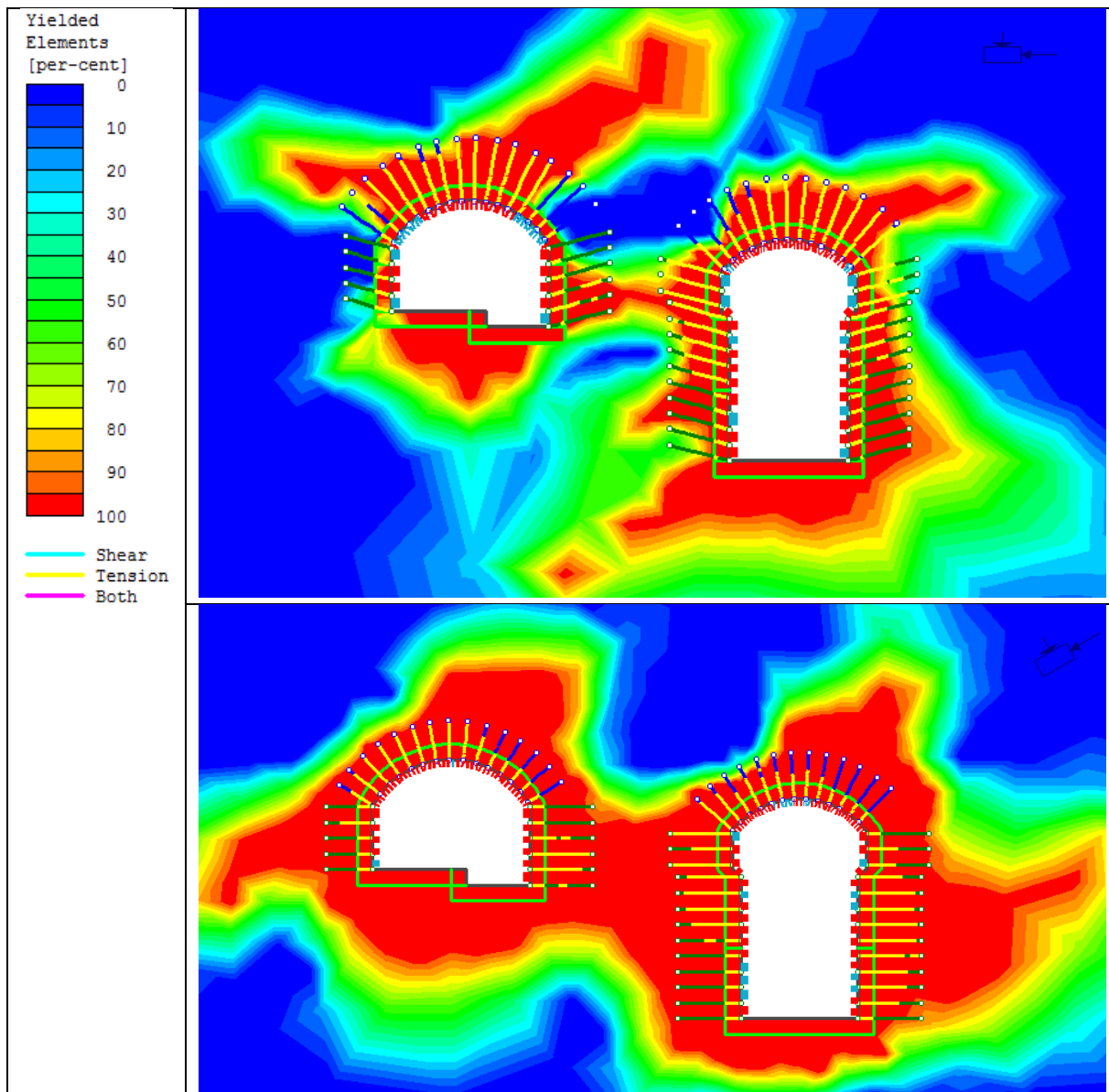


Figure 6. 20: Yielding in support and rock mass for the worst case scenario. Original placement (over) and alternative placement (under).

To see which of the parameters in table 6.9 has the greatest influence on the stability, a sensitivity analysis is carried out. The following parameters are set to worst case, one by one:

- GSI
- Stresses
- m_i
- UCS
- E-modulus
- Extension of disturbed zone

As a sensitivity measure, the increase in yielded mesh elements and maximum total displacement are analysed for an unsupported state.

Table 6. 11: Sensitivity analysis. Maximum total displacement, yielded mesh elements and increase of yielded mesh elements from the best estimate in % are given.

Description	Original placement		Alternative placement	
	Yielded mesh elements (% increase)	Maximum total displacement [cm]	Yielded mesh elements (% increase)	Maximum total displacement [cm]
<i>Best estimate</i>	836	3,2	845	2,9
<i>Worst case</i>	1208 (44)	15,7	1586 (88)	13,7
<i>GSI</i>	883 (6)	4,9	902 (7)	4,2
<i>Stresses</i>	1064 (27)	5,2	1075 (27)	4,4
<i>m_i</i>	879 (5)	3,6	930 (10)	3,3
<i>UCS</i>	937 (12)	3,6	972 (15)	3,3
<i>E-modulus</i>	806 (0)	5,2	838 (0)	4,5
<i>Disturbed zone</i>	939 (12)	4,5	918 (9)	3,8

The stress levels have the largest impact on the sensitivity analysis as a single parameter. These levels will be confirmed or adjusted once the additional stress measurements are carried out. GSI and E-modulus has little effect on the yielded elements, but are more influential on the amount of displacement. UCS and m_i are affecting the yielded elements more than the total displacement, relative to the other parameters.

The results from the best estimate model with support shows that the total closure of the walls of the powerhouse are at most 6,0 cm for the original placement without installed support. This yields a strain level of 0,4 %. Hoek (2001) suggests strain levels of approximately 1 % are the onset of instability and difficulties in providing adequate support. The alternative placement has a total closure of maximum 5,5 cm for the powerhouse wall without support, which corresponds to a strain level of 0,37 %. These levels of displacement is not menacing, considering the large span of the caverns.

Extension of the yielded zone is significant in the pillar, and from the query lines (Figure 6.9), the maximum stress is transferred close to the centre of the pillar. It should be noted that the yielding is coinciding with crack initiation and not total failure of the rock mass.

The yielded bolt elements are restrained to the disturbed zone, which constitute 1/3 of the bolt lengths at most. After consultation with supervisor (Panthi, 2015), this is not seen as critical for the global stability of the caverns. With 20 mm diameter bolts (tensile capacity of 0,15 MN), some of the bolts yielded over the whole bolt length in the walls for the original placement. The yielding in the roof were not that critical, but more extensive than for 33 mm bolts. Also for the alternative placement, the bolt yielding were considered too extensive with 20 mm bolts, although there were less yielding than for the original placement.

Due to high compressive stress in the roof and deformation in the walls, significant amounts of liner elements are yielded. This is especially widespread in the original placement, despite the increased shotcrete thickness. The compressive strength of the shotcrete is limited to 35 MPa,

because of difficulties in conducting concrete strength exceeding 35 MPa for shotcrete application (Panthi, 2015).

The dilation parameter has proven to have a large effect on the model results. An increased dilation will add a lot of displacement, which again will affect tensional yielding in both shotcrete and bolts. On the other hand, an increased dilation parameter will slightly reduce the amount of yielding in the rock mass surrounding the caverns. There seems to be no definite guidelines to determine the dilation parameter. Crowder & Bawden (2004) proposes that the value should be low for this kind of rock mass, but it is not quantified. Hence, this input parameter will add uncertainty to this analysis.

7. Discussion

7.1 Stress situation

Predicting the stress situation is vital to the quality of a stability analysis. Magnitude and orientation of in situ stresses will have great impact on the behaviour of the rock mass, when the caverns are excavated. The stress situation proved to be the parameter with the largest effect on the sensitivity analysis (section 6.4). Shut in pressure varies from 10 to 16,5 MPa for the hydraulic fracturing measurements (Table 4.2). Hence, the uncertainty of the values applied in the stability analysis is significant. In addition, the extrapolation of these results by the terrain model in section 6.1.3 involves factors of uncertainty (Section 6.4).

Applying equation [6.1.1] to project the principal stresses into the desired cross section is questionable due to its disregarding of shear stresses. That being said, the calculations from equation [6.1.1] only adjusted the stress values by 0,4 MPa. This is a rather small adjustment compared to the already existing uncertainties. Since the angle between the length axis of the caverns and the major principal stress is only 13°, it stands to reason that the magnitude of the projected stress is close to the magnitude of the principal stresses.

Assuming a constant field stress is also a simplification of the actual conditions. In reality, the vertical stresses will vary with depth. When the accuracy of the stress estimation is increased, it should be considered to implement a gravitational field stress to the model.

7.2 Placement and orientation of the caverns

In the analysis in this thesis, both location and orientation is different for the two reviewed alternatives. It is of course possible to combine location from one alternative and orientation from the other alternative. These combinations have not been analysed in detail, but placement and orientation are discussed individually in this section.

7.2.1 Placement

Considering geological conditions, such as jointing, weakness zones and rock mass quality, there are little difference between the two alternatives. The headrace tunnel will have a more parallel alignment to zone 2 for the alternative location. It is advisable to change the angle of the headrace tunnel when encountering this zone. Considering zone 1, the alternative placement has a more favourable orientation of the tailrace tunnel and the escape/cable tunnel. Before excavating the caverns, it must be certain that these excavations are not inflicted with any significant weakness zones.

The overburden is more favourable for the original placement and results in a higher safety factor pursuant to hydraulic splitting in the pressure tunnel. Still, the safety factor from the rules of thumb are satisfactory for both locations of the cone (Table 4.4). Lower overburden will also increase the probability of block downfall, but high horizontal stresses in the area has a stabilising effect regarding block downfall.

The main advantage of the alternative placement is the length reduction of the access tunnel and cable tunnel. Reducing the tunnel length will result in savings in costs and time. Moving

the portal of the escape/cable tunnel north is done so that the tunnel does not exceed an inclination that inflicts the practical feasibility. It will also shorten the road length in the valley side. The proposed length of the escape/cable tunnel is approximately 7°. When designing the tunnel system for this alternative in detail, this tunnel could be made even shorter.

7.2.2 Orientation

The rosette plot in figure 4.11 indicates that both the orientation in the original and the alternative placement has a favourable orientation with respect to joint directions. From the measurements closest to the power station (Figure 4.11), the alternative placement has slightly less joints aligned to the cavern length axis. On the other hand, from all the measurements in the ophiolite complex (Figure 4.7a), there are no such advantage.

The original placement is aligned nearly parallel to the minor horizontal stress. This is not optimal regarding concentration of stress in the roof of the caverns. Especially the powerhouse cavern will be subjected to high compressive stresses in the roof. It can be argued that the high horizontal stress will contribute to confining pressure and thereby stabilising the caverns. Still a horizontal stress of the size of the minor horizontal stress (12 MPa) should be sufficient to confine a span of 20 m. The shape of the powerhouse cavern will result in an anisotropic stress distribution when the horizontal stresses are higher than the vertical stresses.

To reduce the stress concentration in the roof, the alternative orientation has a low angle between the length axis and the major horizontal stress. If the length axis is parallel to the major horizontal stress, tensional jointing might develop along the length axis. To prevent this, the orientation is proposed with an angle of 13° with the major horizontal stress. This is in good understanding with theory from section 6.2.

If the caverns are aligned parallel to the valley side, it will cause a tilted stress situation in the cross section of the caverns due to topographical influence. This angle results in a stress concentration in the part of the roof that is facing the valley side. The other side of the roof will be relieved and the block fall hazard will increase, which will call for extra caution if this orientation is chosen. The original orientation will also be in a tilted stress situation, but this is out of plane for the cross section. Effects of the dip angle for the out of plane stress is not analysed, since the model only consists of a 2D analysis of the cross section.

7.3 Spacing between caverns

The goal for determination of pillar width was to obtain a pillar centre of competent rock mass. This is achieved by a pillar width of 22 m for the original placement and 26 m for the alternative placement. The maximum stress in the pillar is slightly higher for the alternative placement than the original, but the stress distribution is more favourable in the pillar for the alternative placement than the original (Figure 6.10). This is because the pillar stress has a peak closer to the centre for the original placement, which is an indication that the rock mass close to the walls is yielded and thereby carry less load.

It was found necessary to extend the pillar width for the alternative placement, compared to the original. This is mainly because of the tilted stress situation that has an unfavourable dipping angle with respect to pillar stability. In addition, the reduced overburden contributes to an increased stress anisotropy.

From figure 6.10 and 6.11, the maximum pillar stress has a dipping angle that calls for extra caution regarding joints that are dipping along with the trajectory of the maximum pillar stress.

Analysing of strength factor and yielded elements in the pillar has made the basis for the choice of pillar width. From a cost saving perspective, the pillar should be as narrow as possible, without it affecting the stability adversely. Myrvang (2001) proposes that increasing the pillar width beyond 1,5 times the diameter of the opening will result in a small reduction in maximum pillar stress. By that statement, a pillar width larger than 1,5 times the span has little effect on stability. It should be noted that this is for circular excavations, and the height of the powerhouse exceeds the suggested pillar widths. As presented in chapter 2.6, the distance between caverns should not be less than the height of the larger cavern to obtain satisfying stability. This criterion is applicable for weak rock masses, and since the rock quality at the location of the caverns are referred to as fair to good, a pillar width less than the height of the largest cavern is regarded as acceptable.

7.4 Stability analysis

7.4.1 Stress distribution

It is quite difficult to obtain accurate calculations of the stress distribution with empirical and analytical methods. This is mainly due to the irregular cavern shape and angle between the principal stresses and the horizontal and vertical axis. Hence, these results should be treated carefully as an indication of the stress magnitudes rather than exact values.

Stress distribution around the excavated caverns has been compared for the different methods and summarised in table 7.1.

Table 7. 1: Comparison of calculated stress distribution from analytical, empirical and numerical methods.

Description		Maximum tangential stress [MPa]			
		Kirsch's equations	Hoek & Brown (1980)	Numerical results	Numerical (no disturbed zone)
<i>Original placement</i>	<i>Transformer hall</i>	51,3	54,6	32,5	39,0
	<i>Powerhouse</i>	51,3	70,3	40,0	51,0
<i>Alternative placement</i>	<i>Transformer hall</i>	32,2	33,7	24,0	32,5
	<i>Powerhouse</i>	32,2	43,7	32,0	47,5

The stress values from the numerical model with a blast damage zone are generally lower than for the analytical and empirical methods. Since the disturbed zone has a lower rock mass E-modulus than the rest of the rock mass, it will transfer some of the stress radially into the less disturbed rock mass. This is supported by the numerical values from the model with no disturbed zone, which are higher for both situations.

In reality, the neighbouring cavern affects the stress situation. This influence is not implemented in the analytical and empirical method. As the Kirsch's solution does not take into account the excavation shapes, it will underestimate the value in the roof of the powerhouse, and slightly overestimate the value in the roof of the transformer hall. This method does not take into account rock mass properties that effect the radial distribution of the secondary stresses.

The empirical method proposed by Hoek & Brown (1980) produces higher stress values than the numerical modelling in the original placement. In the alternative placement, the values corresponds better. This method does not take into account the tilted stress situation in the alternative placement, which creates higher stress concentrations in more local areas in the roofs. In addition, the excavation shapes used in the empirical method are generalized and not adapted to each individual shape. As the method is developed for massive rock, it is probably more applicable for rock masses with higher GSI value than the peridotite in the Moglicë area.

7.4.2 Failure and extent

Due to the brittleness of the rock ($E_i=111,8$ MPa) and high horizontal stresses, spalling is expected to occur in the cavern roofs. The risk of rock burst is low, since this phenomenon requires more energy contained in the rock mass prior to failure. Jointing and rock strength are factors that probably will cause failure before the energy levels are high enough to result in rock burst.

Empirical predictions in section 3.5.3 proposes minor spalling for the alternative placement and orientation, and minor to severe spalling in the original placement. The depths of failure calculated from equation [3.5.12], [3.5.13] and [3.5.14] vary with the stress inputs. The stress values from Kirsch's equation under predicts the depth of failure compared to the numerical analysis (Table 7.2). On the other hand, the empirical stress calculation seems to overestimate the depth for the original placement, but it is coinciding well for the alternative placement.

Table 7. 2: Comparison of depth of failure from analytical/empirical and numerical methods.

Description		Depth of failure [m]		
		Kirsch's equations	Hoek & Brown (1980)	Numerical results
<i>Original placement</i>	<i>Transformer hall</i>	2,5	3,0	2,3
	<i>Powerhouse</i>	2,2	4,7	3,1
<i>Alternative placement</i>	<i>Transformer hall</i>	-	-	0,5
	<i>Powerhouse</i>	-	1,1	1,3

When the stress values from the numerical results (without blast damaged zone) are applied to the equations for depth of failure, they give shallower depth than the numerical results (0,5 m and 2,1 m) for the original placement. For the alternative placement, the results coincide well (0 m and 1,6 m).

With the uncertainties in both the numerical model and the input parameters in the equations for depth of failure (stresses, rock mass spalling strength and excavation radius), a certain

deviation is to be expected. Half the span is used as excavation radius, because the span is influencing the failure propagation in the roof. The excavation shape might be an uncertainty when choosing excavation radius for the analysis, but there are no clear indications that one of the shapes (transformer hall or powerhouse) yield more correct answers than the other.

The general trend is that the original orientation is more exposed to spalling than the alternative orientation. Due to the shape of the powerhouse, this is more exposed than the transformer hall. To minimize the impact of brittle failure, it would be favourable to align the cavern length axis such that the horizontal stresses decrease in the cross section (as the case is for the alternative orientation). The other measure would be to change the shape of the caverns. Reducing the height/span ratio of the powerhouse would ease the stress concentration in the roof, but due to practical limitations, this is rarely an option.

Quantification of rock mass failure due to low secondary stresses is done only through numerical analysis in this thesis. Areas with negative tangential stresses are detected in the walls of the powerhouse for both placements (Figure 6.12). The largest extension of this zone occurs in the powerhouse wall facing the pillar for the original placement. This zone has at most a range of approximately 5 m into the pillar. Failure in this zone is assumed to consist of horizontal joints due to the large horizontal virgin stress. This is the reason why the rock bolts in the walls are proposed installed with a 15 degree upward angle for the original placement.

The Hoek & Brown (1980) method for estimation of tangential stresses predicts negative tangential stresses in the powerhouse wall for both placements (table 5.2). It also predicts negative tangential stress in the transformer hall wall for the original placement, although this is not shown in the numerical model. This supports that this method might overestimate the magnitude of secondary stress anisotropy.

7.4.3 *Rock mass quality and rock support*

From the classification with the “little q” system, the rock mass can be characterized as fair to good. The RMR and Q-values calculated from the GSI value used in the numerical modelling describes the rock mass as poor to fair. This rough comparison indicates that the GSI value used in the modelling is conservative. Hence, the estimation of support from the RMR and Q system will be conservative.

As the rock support proposition from the “little q” system is very generalised, it is not suited as a tool to customise the support in detail. The support estimation from the RMR system are of limited value since it is accommodated to horseshoe shaped openings with 10 m span. This requirement does not fit the Moglicë caverns. It is more appropriate to use the Q-value chart to customise support, due to its higher level of details. Still there is a high level of uncertainty related to the Q-values obtained by converting the GSI value. In addition, rock mass classification systems are most applicable where instability is caused by block fall and not high stresses (Palmström & Stille, 2010).

Bolt lengths proposed by the Q-value chart (Table 5.11) are in good correspondence to the bolt lengths estimated from empirical formulas (Table 5.8). These methods suggests 4-6 m rock bolts. Proposed bolt lengths in the numerical model is mainly based on the extension of the yielded zone in the rock mass and bolts. From this analysis, 6-8 m bolts are seen as sufficient.

In the roof, the bolts are placed at least one meter into intact rock. 8 m long bolts seems to be enough to deal with the tensional yielded zone in the walls. Bolt spacing used in the numerical modelling (c/c: 1,5-2 m) is fairly coherent to the spacing proposed by the Q-value chart (c/c: 1,7-2 m).

Shotcrete thickness from the Q-value chart is proposed to 9-12 cm. To avoid extensive yielding of the beam elements, the thickness in the numerical model is set to 30 cm for the alternative placement and 40 cm for the original placement. Shotcrete does normally not exceed a compressive strength of 35 MPa (Panthi, 2015). Hence, the thickness was increased to minimise the yielding.

In general, the estimated support from the numerical modelling results are more conservative than the reinforcement proposals from the Q-system and the empirical formulas for bolt lengths. There could be several explanations for this:

- The reinforcement used in the numerical model is conservative, due to caution taken by the author.
- The majority of case histories in the Q-system are derived from hard jointed rocks, and there are few examples for values less than 1 (NGI, 2013). The Q-value used in the reinforcement estimation for the Moglicë caverns are on the limit of the value span that is most applicable for this system.
- The Q-value obtained from the GSI value, it is not adapted to the specific stress situation in the area of the powerhouse complex.
- The empirical formulas are not customized to specific rock mass properties and stress conditions for the relevant area.
- Uncertainties in the input parameters in the numerical model could be underestimating the rock mass strength.

8. Conclusions and further work

8.1 Conclusions

A secure and cost effective design of a powerhouse complex is of prime importance to the success of a hydropower project. This involves placement, orientation, pillar width and global stability of the caverns. Stability assessments involves detecting possible challenges and develop a support plan to deal with these challenges. Through the stability assessment of the Moglicë caverns, brittle failure in the cavern roof due to high horizontal stresses was detected. Tensile fracturing in the cavern walls due to negative secondary stresses might also be an issue.

Assessment of placement and orientation of the caverns has been carried out. The planned placement and orientation of the caverns are the basis for this assessment. To look at the possibility of reducing the length of appurtenant tunnels, an alternative placement are assessed and compared to the original. This alternative is located 150 m closer to the valley side in the direction of the original access tunnel. The length axis of the caverns are aligned approximately to the minor principal stress (according to hydraulic fracturing measurements) for the planned alternative. To reduce the stress concentration in the cavern roof, a different orientation (N48°E) are proposed for the alternative placement. Both alternatives has advantages and disadvantages regarding placement and orientation. The assessment of placement and orientation are concluded in the following:

- The original placement has a more favourable overburden, which increases the safety factor for the cone placement and it reduces the horizontal/vertical stress anisotropy.
- The alternative placement reduces the tunnel system with 163 m (from the sketch in Table 4.3).
- Both locations obtained a satisfactory factor of safety regarding placement of the cone, which means that the same penstock length can be applied for both alternatives.
- Little differs the two orientations considering joint directions and weakness zones.
- The original orientation has a horizontal major principal stress in the cross section of the caverns. This is favourable regarding the stresses acting on the pillar, and required pillar width is estimated to be 4 m less for the original orientation contra the alternative orientation.
- The length axis of the caverns in the alternative placement has a more advantageous angle to the major principal stress, considering stress concentration in the roof and tensile stress in the walls of the caverns.

During this work, analytical, empirical and numerical methods have been applied to document possible stability issues and estimate proper rock support. Conclusions from the stability analysis and the employed methods are summarized below:

- The empirical method from Hoek & Brown (1980) for calculating stress distribution seems to be over predicting the magnitude of maximum tangential stress compared to the numerical results, especially if the blast damaged zone is taken into account. Kirsch's equations has limitations when the shape of the excavation is not circular. The

method from Hoek & Brown (1980) are probably more applicable for rock masses with a higher GSI value.

- The original orientation will suffer from a larger extent of brittle failure in the cavern roof due to higher compressive stresses.
- The powerhouse is in general more exposed to brittle failure than the transformer hall.
- Numerical calculations of depth of brittle failure from the deviatoric stress criterion and the Hoek & Brown brittle parameters coincide well with each other. Compared to the empirical equations for spalling depth impact, the deviation depends on the input from the calculation of stress distribution. With stress values from the elastic numerical model (without disturbed zone) applied to the empirical equations, the depth of failure coincide well with the numerical results for the alternative placement, but underestimates the depth for the original placement.
- Bolt lengths proposed from the Q-system are in good correspondence to empirical formulas where excavation span is the input parameter. These methods suggests bolt lengths of 4-6 m, while bolt lengths of 6-8 m are applied in the numerical model. As a conservative estimate, 6-8 m is recommended.
- Shotcrete thickness recommended from the Q system is significantly less than the thickness applied in the numerical model. The numerical model displays yielded elements in the shotcrete with thickness of 30-40 cm. Hence, 30 cm is recommended for the alternative placement and 40 cm for the original placement.
- The worst case estimation of the input parameters to the numerical model results in a level of stability that is not acceptable for excavations of large scale caverns. Hence, it is necessary to make sure that the stress condition and rock mass properties are better than worst case before excavating the caverns.

All the methods applied in this assessment have their strength and weaknesses. It is important to be aware of the uncertainties in the methods and treat the results with caution. To obtain a high-quality stability analysis, it is necessary to combine several methods to achieve a broad foundation before making conclusions. Minimising the error in the input parameters is essential to the quality of a stability analysis. A good analysis tool is worthless without correct input parameters.

From the assessment, it would be allowable to move the powerhouse and transformer cavern 150 m closer to the valley side. This will result in savings in both cost and time. However, these findings must be approved by calibrating the analysis with updated stress values and rock material properties. Determining cavern orientation will be a choice between increasing the pillar width by approximately 4 m, or take consideration of more yielding in the support due to larger displacement and higher stress concentrations. The original orientation will also call for a thicker layer of shotcrete. This is a question of expenses, but it seems to the author that the alternative orientation overall will be more favourable regarding stress induced stability issues.

8.2 Further work

Recommended further work is summarized below:

- The scope of this study is an assessment of stress induced stability issues. To make the stability analysis complete, it is recommended to analyse any structurally controlled instabilities in detail. This is especially important if the alternative orientation is chosen, since that case showed stress relief in parts of the cavern roof.
- Before the alternative placement of the powerhouse caverns can be applied, the appurtenant tunnel system needs to be designed in detail.
- When additional stress measurement is carried out, the analysis must be adjusted to increase the level of accuracy in the analysis.

9. Bibliography

- Aagaard, B., 2015: *Personal correspondence with co-supervisor.*
- Aasen, O., Ødegaard, H., Palmström, A., 2013: *Planning of pressurized headrace tunnel in Albania.* In: Norwegian Hydropower Tunneling 2. Publication No.22. Norwegian Tunnelling Society.
- Aliaj, S., 2006: *The Albanian Orogen: Convergence zone between Eurasia and the Adria microplate.* The Adria Microplate: GPS Geodesy, Tectonics and Hazards. Earth and Environmental Sciences Volume 61, 2006, pp. 133-149.
- Allkja, S., 2013: *Report on geological and geotechnical investigations of upper part of the headrace of HPP Moglicë, BH-MO-13.* Altea & Geostudio 2000.
- Barton, N.R., 1995: *The influence of joint properties in modelling jointed rock masses.* Keynote lecture. 8. Congress of ISRM, Rotterdam Balkema, vol. 3.
- Barton, N.R., Lien, R., Lunde, J., 1974: *Engineering classification of rock masses for the design of tunnel support.* Rock Mech. 6(4), pp. 189-239.
- Beitnes, A., Langelid, A., Ødegaard, O.C., 2007: *Hanekleiva – What was Discovered in the Tunnels – Basis for Decisions.* Fjellsprengningsteknikk/Bergmekanikk/Geoteknikk (NJFF) pp. 16.1-16.14.
- Bieniawski, Z.T., 1976: *Rock mass classification in rock engineering.* Exploration for rock engineering, proc. of symp. 1, pp. 97-106. Cape Town: Balkema.
- Bieniawski, Z.T., 1989: *Engineering Rock Mass Classifications: A Complete Manual for Engineers and Geologists in Mining, Civil and Petroleum Engineering.* A Wiley-interscience publication, 251 p.
- Cai, M., Kaiser, K., 2014: *In-situ Rock Spalling Strength near Excavation Boundaries.* Rock Mech. Rock Eng. 47, pp. 659-675.
- Cai, M., Kaiser, P.K., Tasaka, Y., Minami, M., 2007: *Determination of residual strength parameters of jointed rock masses using the GSI system.* International Journal of Rock Mechanics & Mining Sciences 44, pp. 247-265.
- Crowder, J.J., Bawden, W.F., 2004: *Review of Post-Peak Parameters and Behaviour of Rock Masses: Current Trends and Research.* Available from: rocscience.com
- Devoll Hydropower, 2011: *Harnessing of Hydropower Potential of Devoll River, Geological Report Part III – HPP3 (Moglicë).* Unpublished.
- Devoll Hydropower, 2013: *Devoll Hydropower Project – grievance redress mechanism leaflet.*
- Devoll Hydropower, 2015: *Moglicë HPP – Project Overview.* URL: www.dhp.al/index.php/our-project/project-overview/moglice-hpp






- Diederichs, M.S., 2007: *The 2003 CGS Geocolloquium Adress: Damage and spalling prediction criteria for deep tunnelling*. Can. Geotech. J., Vol. 44, pp. 1082-1116.
- Diederichs, M.S., Carter, T., Martin C.D., 2010: *Practical rock spall prediction in tunnels*. Proceedings ITA World Tunnel Congress, Vancouver, 8 p.
- Eberhardt, E., 2012: *The Hoek-Brown Failure Criterion*. Rock Mech. Rock Eng. 45, pp. 981-988.
- Edvardsson, S., Broch, E., 2002: *Underground powerhouses and high pressure tunnels*. Hydropower development vol 14. Norwegian University of Science and Technology, Trondheim, 99 p.
- Erbach, G., 2015: *Negotiating a new UN climate agreement – Challenges on the road to Paris*. European Parliamentary Research Service (EPRS).
- Emdal, A., 2013: *Introduksjon til geoteknikk*. Institutt for bygg, anlegg og transport, NTNU. Tapir akademisk forlag, 191 p.
- Farmer, I.W., Shelton, P.D., 1980: *Factors that affect underground rock bolt reinforcement systems*. Trans. Inst. Min. Metall. 89, pp. A68-A83.
- Hammett, R.D., Hoek, E., 1981: *Design of large underground caverns for hydroelectric projects with particular reference to structurally controlled failure mechanisms*. ASCE Spring Convention, New York, pp. 192-206.
- Hoek, E., 1994: *Strength of rock and rock masses*. ISRM News J, 2(2), pp. 4-16.
- Hoek, E., 2000: *Large Powerhouse caverns in weak rock*. In: Rock Engineering, Ch. 13. Balkema Publishers.
- Hoek, E., 2001: *Big Tunnels in Bad Rock 2000 Terzaghi Lecture*. ASCE Journal of Geotechnical Engineering. Vol. 127, No.9, pp. 726-740.
- Hoek, E., 2007: *Practical rock engineering – 2007 Edition*. Hoek's corner. Rocscience Inc. URL: www.rocscience.com/education/hoeks_corner.
- Hoek, E., Brown, E.T., 1980: *Underground Excavation in Rock*. The Institution of Mining and Metallurgy, London, 527 p.
- Hoek, E., Brown, E.T., 1997: *Practical estimates of rock mass strength*. International Journal of Rock Mechanics and Mining Sciences, Vol 34, No 8, pp. 1165-1186.
- Hoek, E., Carranza-Torres, C., Corkum, B., 2002: *Hoek-Brown failure criterion – 2002 Edition*. Proceedings of the fifth North American rock mechanics symposium, Toronto, Canada, Vol. 1, pp. 267-273.
- Hoek, E., Kaiser, P.K., Bawden, W.F., 1995: *Support of underground excavations in hard rock*. Mining Research Directorate and Universities Research Incentive Fund, 300 p.
- Hutchinson, D.J., Diederichs, M.S., 1996: *Cablebolting in underground mines*. BiTech Publishers Ltd., Richmond, 406 p.

- iC consulenten ziviltechniker GesmbH, 2014: *Devoll Hydropower HPP Moglicë – Headrace Tunnel. Statement Headrace Tunnel Excavation Method*. Unpublished.
- International Institute for Sustainable Development (IISD), 2014: *Climate Summit Bulletin – A Summary Report of the UN Climate Summit 2014*.
- ISRM, 1978: *Suggested methods for the quantitative description of discontinuities in rock masses*. Int. J. Rock Mech. Min. Sci. & Geomech. pp. 319-368.
- Jacobs Consulting Geologists, 2011: *Harnessing of Hydropower Potential of Devoll River, Geological Report HPP Moglicë*. Unpublished.
- Lang, T.A., Bischoff, J.A., 1984: *Stability of reinforced rock structure. Design and performance of underground excavations*. London: British Geotechnical Society, pp. 11-18.
- Kaiser, P.K., Tannant, D.D., McCreath, D.R., 1996: *Canadian rockburst support handbook*. Geomechanics Research Centre, Laurentian University, Sudbury, 314 p.
- Marinos, P., Hoek, E., 2000: *GSI – A geologically friendly tool for rock mass strength estimation*. Proc. GeoEng2000 Conference, Melbourne, pp. 1422-1442.
- Marinos, V., Marinos, P., Hoek, E., 2005: *The geological strength index: applications and limitations*. Bulletin of Engineering Geology and the Environment, Vol. 64, pp. 55-65.
- Marinos, P., Hoek, E., Marinos, V., 2006: *Variability of the engineering properties of rock masses quantified by the geological strength index: the case of ophiolites with special emphasis on tunnelling*. Bulletin of Engineering Geology and the Environment, Vol 65, pp. 129-142.
- Marcher, T., Saurer, E., 2013: *Design and verification challenges of hydropower plant caverns*. ILF Consulting Engineers Ltd.
- Martin, C.D., 1997: *Seventeenth Canadian Geotechnical Colloquium: The effect of cohesion loss and stress path on brittle rock strength*. Can. Geotech. J. Vol. 34, pp. 698-725.
- Martin, C.D., Christainsson, R., 2009: *Estimating the potential for spalling around a deep nuclear waste repository in crystalline rock*. Int. J. Rock Mech. Mining Sciences, Vol. 46, pp. 219-228.
- Martin, C.D., Kaiser, P.K., McCreath, D.R., 1999: *Hoek-Brown parameters for predicting the depth of brittle failure around tunnels*. Can. Geotech. J. Vol. 36. NRC Canada.
- Multiconsult, 2011: *Design report – Numerical modelling of underground caverns for Moglicë*. Devoll Hydropower Project. Unpublished.
- Myrvang, A., 2001: *Bergmekanikk*. Institutt for geologi og bergteknikk. Norges teknisk-naturvitenskapelige universitet, Trondheim.
- Nilsen, B., Broch, E., 2011: *Ingeniørgeologi-berg grunnkurskompendium*. Norges teknisk-naturvitenskapelige universitet, Trondheim, 292 p.
- Nilsen, B., Palmström, A., 2000: *Handbook nr.2: Engineering Geology and Rock Engineering*. Norwegian Group of Rock Mechanics, 249 p.

- Nilsen, B., Thidemann, A., 1993: *Rock Engineering*. Hydropower Development, volume 9. Norwegian Institute of Technology, Trondheim, 156 p.
- Norconsult, 2011: *HPP Moglicë Power station, Rock support*. Project drawings. Unpublished.
- Norconsult/Multiconsult, 2011: *Engineering Geological Summary Report HPP3*. Devoll Hydropower Project Engineering Services. Unpublished.
- Norwegian Geotechnical Institute, 2013: *Using the Q-system*. Handbook: Rock mass classification and support design, 54p.
- Palmström, A., Broch, E., 2006: *Use and misuse of rock mass classification systems with particular reference to the Q-system*. Tunnelling and Underground Space Technology, Vol. 21, pp. 575-593.
- Palmström, A., Stille, H., 2010: *Rock engineering*. Thomas Telford Limited, London, 408 p.
- Panthi, K.K., 2006: *Analyses of engineering geological uncertainties related to tunnelling in Himalayan rock mass conditions*. Doctoral thesis. Norwegian University of Science and Technology, Trondheim.
- Panthi, K.K., 2012: *Evaluation of rock bursting phenomena in a tunnel in the Himalayas*. Bulletin of Engineering Geology and the Environment, Vol. 71, pp. 761-769.
- Panthi, K.K., 2014: *Norwegian Design Principle for High Pressure Tunnels and Shafts: Its Applicability in the Himalaya*. Hydro Nepal: Journal of Water Energy and Environment, issue no. 14, pp. 36-40.
- Panthi, K.K., 2015: Personal correspondence with supervisor.
- Rocscience, 2014a: *Phase2 product sheet*.
- Rocscience, 2014b: *RocLab, Rock Mass Strength Analysis using the Generalized Hoek-Brown failure criterion*. Rocscience Inc.
- Rocscience, 2015: *Phase2 v8.0 webhelp*.
- SINTEF, 2010: *Hydraulic Fracturing Tests in the Devoll Hydropower Project, Albania*. Unpublished.
- Statkraft, 2015: *Devoll*. URL: <http://www.statkraft.com/aboutstatkraft/Projects/albania/devoll/>
- Trinh, Q.N., 2015: *Personal correspondence regarding Phase² model*.
- U.S. Army Corps of Engineers, 1980: *Engineering and design: Rock reinforcement*. Engineering Manual EM 1110-1-20907. In: Hutchinson & Diederichs, 1996.
- VIKØrsta, 2012: *CT-Bolt M33*. Product sheet.
- World Stress Map, 2008: *Mediterranean region including topography*.
- Zhao, J., 2000: *Applicability of Mohr-Coulomb and Hoek-Brown strength criteria to the dynamic strength of brittle rock*. Int. J. Rock Mech. & Mining Sciences, Vol. 37, pp. 1115-1121.

Appendices

Appendix A: Guidelines for estimating disturbance factor D (Hoek, 2007)

Appearance of rock mass	Description of rock mass	Suggested value of D
	Excellent quality controlled blasting or excavation by Tunnel Boring Machine results in minimal disturbance to the confined rock mass surrounding a tunnel.	D = 0
	Mechanical or hand excavation in poor quality rock masses (no blasting) results in minimal disturbance to the surrounding rock mass. Where squeezing problems result in significant floor heave, disturbance can be severe unless a temporary invert, as shown in the photograph, is placed.	D = 0 D = 0.5 No invert
	Very poor quality blasting in a hard rock tunnel results in severe local damage, extending 2 or 3 m, in the surrounding rock mass.	D = 0.8
	Small scale blasting in civil engineering slopes results in modest rock mass damage, particularly if controlled blasting is used as shown on the left hand side of the photograph. However, stress relief results in some disturbance.	D = 0.7 Good blasting D = 1.0 Poor blasting
	Very large open pit mine slopes suffer significant disturbance due to heavy production blasting and also due to stress relief from overburden removal. In some softer rocks excavation can be carried out by ripping and dozing and the degree of damage to the slopes is less.	D = 1.0 Production blasting D = 0.7 Mechanical excavation

Appendix B: The RMR-system and guidelines for support (Hoek, 2007)

A. CLASSIFICATION PARAMETERS AND THEIR RATINGS									
Parameter		Range of values							
1	Strength of intact rock material	Point-load strength index	>10 MPa	4 - 10 MPa	2 - 4 MPa	1 - 2 MPa	For this low range - uniaxial compressive test is preferred		
		Uniaxial comp. strength	>250 MPa	100 - 250 MPa	50 - 100 MPa	25 - 50 MPa	5 - 25 MPa	1 - 5 MPa	< 1 MPa
Rating			15	12	7	4	2	1	0
2	Drill core Quality RQD		90% - 100%	75% - 90%	50% - 75%	25% - 50%	< 25%		
	Rating			20	17	13	8		3
3	Spacing of discontinuities		> 2 m	0.6 - 2 . m	200 - 600 mm	80 - 200 mm	< 60 mm		
	Rating			20	15	10	8		5
4	Condition of discontinuities (See E)		Very rough surfaces Not continuous No separation Unweathered wall rock	Slightly rough surfaces Separation < 1 mm Slightly weathered walls	Slightly rough surfaces Separation < 1 mm Highly weathered walls	Slickensided surfaces Gouge < 5 mm thick or Separation 1-5 mm Continuous	Soft gouge >5 mm thick or Separation > 5 mm Continuous		
	Rating			30	25	20	10		0
5	Groundwater	Inflow per 10 m tunnel length (l/m)	None	< 10	10 - 25	25 - 125	> 125		
		(Joint water press/ (Major principal σ))	0	< 0.1	0.1 - 0.2	0.2 - 0.5	> 0.5		
		General conditions	Completely dry	Damp	Wet	Dripping	Flowing		
		Rating		15	10	7	4		0
B. RATING ADJUSTMENT FOR DISCONTINUITY ORIENTATIONS (See F)									
Strike and dip orientations		Very favourable		Favourable	Fair	Unfavourable	Very Unfavourable		
Ratings	Tunnels & mines	0		-2	-5	-10	-12		
	Foundations	0		-2	-7	-15	-25		
	Slopes	0		-5	-25	-50			
C. ROCK MASS CLASSES DETERMINED FROM TOTAL RATINGS									
Rating	100 ← 81		80 ← 61	60 ← 41	40 ← 21	< 21			
Class number	I		II	III	IV	V			
Description	Very good rock		Good rock	Fair rock	Poor rock	Very poor rock			
D. MEANING OF ROCK CLASSES									
Class number	I		II	III	IV	V			
Average stand-up time	20 yrs for 15 m span		1 year for 10 m span	1 week for 5 m span	10 hrs for 2.5 m span	30 min for 1 m span			
Cohesion of rock mass (kPa)	> 400		300 - 400	200 - 300	100 - 200	< 100			
Friction angle of rock mass (deg)	> 45		35 - 45	25 - 35	15 - 25	< 15			
E. GUIDELINES FOR CLASSIFICATION OF DISCONTINUITY conditions									
Discontinuity length (persistence)	< 1 m		1 - 3 m	3 - 10 m	10 - 20 m	> 20 m			
Rating	6		4	2	1	0			
Separation (aperture)	None		< 0.1 mm	0.1 - 1.0 mm	1 - 5 mm	> 5 mm			
Rating	6		5	4	1	0			
Roughness	Very rough		Rough	Slightly rough	Smooth	Slickensided			
Rating	6		5	3	1	0			
Infilling (gouge)	None		Hard filling < 5 mm	Hard filling > 5 mm	Soft filling < 5 mm	Soft filling > 5 mm			
Rating	6		4	2	2	0			
Weathering	Unweathered		Slightly weathered	Moderately weathered	Highly weathered	Decomposed			
Rating	6		5	3	1	0			
F. EFFECT OF DISCONTINUITY STRIKE AND DIP ORIENTATION IN TUNNELLING**									
Strike perpendicular to tunnel axis				Strike parallel to tunnel axis					
Drive with dip - Dip 45 - 90*		Drive with dip - Dip 20 - 45*		Dip 45 - 90*		Dip 20 - 45*			
Very favourable		Favourable		Very unfavourable		Fair			
Drive against dip - Dip 45-90*		Drive against dip - Dip 20-45*		Dip 0-20 - Irrespective of strike*					
Fair		Unfavourable		Fair					

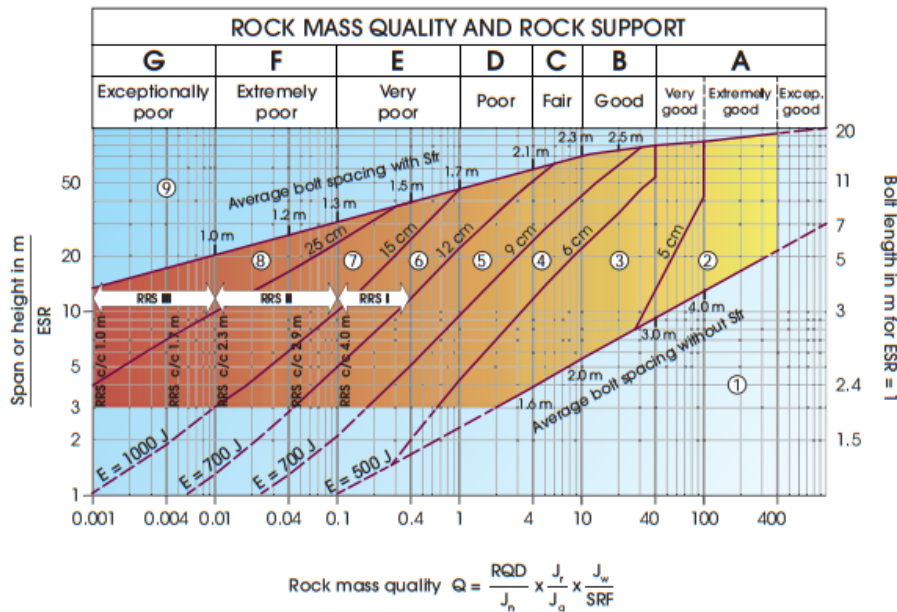
* Some conditions are mutually exclusive. For example, if infilling is present, the roughness of the surface will be overshadowed by the influence of the gouge. In such cases use A.4 directly.

** Modified after Wickham et al (1972).

Rock mass class	Excavation	Rock bolts (20 mm diameter, fully grouted)	Shotcrete	Steel sets
I - Very good rock <i>RMR</i> : 81-100	Full face, 3 m advance.	Generally no support required except spot bolting.		
II - Good rock <i>RMR</i> : 61-80	Full face , 1-1.5 m advance. Complete support 20 m from face.	Locally, bolts in crown 3 m long, spaced 2.5 m with occasional wire mesh.	50 mm in crown where required.	None.
III - Fair rock <i>RMR</i> : 41-60	Top heading and bench 1.5-3 m advance in top heading. Commence support after each blast. Complete support 10 m from face.	Systematic bolts 4 m long, spaced 1.5 - 2 m in crown and walls with wire mesh in crown.	50-100 mm in crown and 30 mm in sides.	None.
IV - Poor rock <i>RMR</i> : 21-40	Top heading and bench 1.0-1.5 m advance in top heading. Install support concurrently with excavation, 10 m from face.	Systematic bolts 4-5 m long, spaced 1-1.5 m in crown and walls with wire mesh.	100-150 mm in crown and 100 mm in sides.	Light to medium ribs spaced 1.5 m where required.
V – Very poor rock <i>RMR</i> : < 20	Multiple drifts 0.5-1.5 m advance in top heading. Install support concurrently with excavation. Shotcrete as soon as possible after blasting.	Systematic bolts 5-6 m long, spaced 1-1.5 m in crown and walls with wire mesh. Bolt invert.	150-200 mm in crown, 150 mm in sides, and 50 mm on face.	Medium to heavy ribs spaced 0.75 m with steel lagging and forepoling if required. Close invert.

(Developed for 10 m span rock tunnels)

Appendix C: The Q-system (NGI, 2013)



Support categories

- ① Unsupported or spot bolting
- ② Spot bolting, **SB**
- ③ Systematic bolting, fibre reinforced sprayed concrete, 5-6 cm, **B+Sfr**
- ④ Fibre reinforced sprayed concrete and bolting, 6-9 cm, **Sfr (E500)+B**
- ⑤ Fibre reinforced sprayed concrete and bolting, 9-12 cm, **Sfr (E700)+B**
- ⑥ Fibre reinforced sprayed concrete and bolting, 12-15 cm + reinforced ribs of sprayed concrete and bolting, **Sfr (E700)+RRS I+B**
- ⑦ Fibre reinforced sprayed concrete >15 cm + reinforced ribs of sprayed concrete and bolting, **Sfr (E1000)+RRS II+B**
- ⑧ Cast concrete lining, **CCA** or **Sfr (E1000)+RRS III+B**
- ⑨ Special evaluation

Bolts spacing is mainly based on Ø20 mm

E = Energy absorption in fibre reinforced sprayed concrete

ESR = Excavation Support Ratio

Areas with dashed lines have no empirical data

RRS - spacing related to Q-value

- I** S130/6 Ø16 - Ø20 (span 10m)
D40/6+2 Ø16-20 (span 20m)
- II** S135/6 Ø16-20 (span 5m)
D45/6+2 Ø16-20 (span 10m)
D55/6+4 Ø20 (span 20m)
- III** D40/6+4 Ø16-20 (span 5m)
D55/6+4 Ø20 (span 10m)
D70/6+6 Ø20 (span 20m)

S130/6 = Single layer of 6 rebars,
30 cm thickness of sprayed concrete

D = Double layer of rebars

Ø16 = Rebar diameter is 16 mm

c/c = RRS spacing, centre - centre

In rock masses of good quality	Q > 10	The actual Q-value is multiplied by 5
For rock masses of intermediate quality	0.1 < Q < 10	The actual Q-value is multiplied by 2.5 (in cases of high stresses the actual Q-value is used)
For rock masses of poor quality	Q < 0.1	The actual Q-value is used

$$Q = \frac{RQD}{J_n} \times \frac{J_f}{J_a} \times \frac{J_w}{SRF}$$

$$\frac{\text{Span or height in m}}{ESR} = \text{Equivalent dimension}$$

For the types of excavation B, C and D, it is recommended to use ESR = 1.0 when Q < 0.1. The reason for that is that the stability problems may be severe with such low Q-values, perhaps with risk for cave-in. ESR together with the span (or wall height) gives the Equivalent dimension in the following way:

Type of Excavation	ESR
A Temporary mine openings, etc.	ca. 3-5
B Vertical shafts: j) circular sections k) rectangular/square section * Dependent of purpose. May be lower than given values.	ca. 2.5 ca. 2.0
C Permanent mine openings, water tunnels for hydro power (exclude high pressure penstocks), water supply tunnels, pilot tunnels, drifts and headings for large openings.	1.6
D Minor road and railway tunnels, surge chambers, access tunnels, sewage tunnels, etc.	1.3
E Power houses, storage rooms, water treatment plants, major road and railway tunnels, civil defence chambers, ports, intersections, etc.	1.0
F Underground nuclear power stations, railways stations, sports and public facilities, factories, etc.	0.8
G Very important caverns and tunnels with a long lifetime, = 100 years, or without access for maintenance.	0.5

1 RQD (Rock Quality Designation)		RQD
A	Very poor	< 27 (joints per m ²)
B	Poor	(20-27 joints per m ²)
C	Fair	(13-19 joints per m ²)
D	Good	(8-12 joints per m ²)
E	Excellent	(0-7 joints per m ²)

Note: 1) Where RQD is reported or measured as ≤ 10 (including 0) the value 10 is used to evaluate the Q-value

2) RQD-intervals of 5, i.e. 100, 95, 90, etc., are sufficiently accurate

2 Joint set number		J _n
A	Massive, no or few joints	0.5-1.0
B	One joint set	2
C	One joint set plus random joints	3
D	Two joint sets	4
E	Two joint sets plus random joints	6
F	Three joint sets	9
G	Three joint sets plus random joints	12
H	Four or more joint sets, random heavily jointed "Sugar cube", etc	15
J	Crushed rock, earth like	20

Note: 1) For tunnel intersections, use 3 x J_n

2) For ponds, use 2 x J_n

3 Joint Roughness Number		J _r
a) Rock-wall contact, and		
b) Rock-wall contact below 10 cm of shear movement		
A	Discontinuous joints	4
B	Rough or irregular, undulating	3
C	Smooth, undulating	2
D	Slickensided, undulating	1.5
E	Rough, irregular, planar	1.5
F	Smooth, planar	1
G	Slickensided, planar	0.5

Note: 1) Description refers to small scale features and intermediate scale features, in that order

c) No rock-wall contact when sheared		
H	Zone containing clay minerals thick enough to prevent rock-wall contact when sheared	1

Note: 2) RQD1 if the mean spacing of the relevant joint set is greater than 3 m (dependent on the size of the underground opening)

3) J_n = 0.5 can be used for planar slickensided joints having lineations, provided the lineations are oriented in the estimated sliding direction

4 Joint Alteration Number		J _a	J _a approx.
a) Rock-wall contact (no mineral fillings, only coatings)			
A	Tightly bedded, hard, non-softening, impervious filling, i.e. quartz or epidote.		0.75
B	Unaltered joint walls, surface staining only.		1
C	Slightly altered joint walls. Non-altering mineral coatings, sandy particles, clay-free disaggregated rock, etc.		2
D	Silty or sandy clay coatings, small clay fraction (non-staining).		3
E	Softening or low friction clay mineral coatings, i.e. kaolinite or mont. Also chlorite, talc, gypsum, graphite, etc., and small quantities of swelling clays.		4

b) Rock-wall contact below 10 cm shear (thin mineral fillings)			
F	Sandy particles, clay-free disaggregated rock, etc.	25-30°	4
G	Strongly over-consolidated, non-altering, clay mineral fillings (continuous, but < 2mm thickness).	16-24°	6
H	Medium or low over-consolidation, softening, clay mineral fillings (continuous, but < 2mm thickness).	12-16°	8
J	Swelling-clay fillings, i.e. montmorillonite (continuous, but < 2mm thickness). Value of J _a depends on percent of swelling clay-size particles.	6-12°	8-12

c) No rock-wall contact when sheared (thick mineral fillings)			
K	Zones or bands of dehydrated or crushed rock. Strongly over-consolidated.	16-24°	6
L	Zones or bands of clay, dehydrated or crushed rock. Medium or low over-consolidation or softening fillings.	12-16°	8
M	Zones or bands of clay, dehydrated or crushed rock. Swelling clay. J _a depends on percent of swelling clay-size particles.	6-12°	8-12
N	Thick continuous zones or bands of clay. Strongly over-consolidated.	16-24°	10
O	Thick, continuous zones or bands of clay. Medium to low over-consolidation.	12-16°	13
P	Thick, continuous zones or bands with clay. Swelling clay. J _a depends on percent of swelling clay-size particles.	6-12°	13-20

5 Joint Water Reduction Factor		J _w
A	Dry excavations or minor inflow (turbid or a few drops)	1.0
B	Medium inflow, occasional outwash of joint fillings (many drops/m ²)	0.66
C	Jet inflow or high pressure in competent rock with unfilled joints	0.5
D	Large inflow or high pressure, considerable outwash of joint fillings	0.33
E	Exceptionally high inflow or water pressure decaying with time. Causes outwash of material and perhaps cone in	0.2-0.1
F	Exceptionally high inflow or water pressure confining without noticeable decay. Causes outwash of material and perhaps cone in	0.1-0.05

Note: 1) Factors C for are crude estimates, increase J_w if the rock is drilled or grouting is carried out

2) Special problems caused by ice formation are not considered

6 Stress Reduction Factor		SRF
a) Weak zones intersecting the underground opening, which may cause loosening of rock mass		
A	Multiple occurrences of weak zones within a short section containing clay or chemically dehydrated, very loose surrounding rock (any depth), or long sections with incompetent (weak) rock (any depth). For squeezing, see 4L and 6M	10
B	Multiple shear zones within a short section in competent clay-free rock with loose surrounding rock (any depth)	7.5
C	Single weak zones with or without clay or chemical dehydrated rock (depth $\leq 50m$)	5
D	Loose, open joints, heavily jointed or "sugar cube", etc. (any depth)	5
E	Single weak zones with or without clay or chemical dehydrated rock (depth $> 50m$)	2.5

Note: 1) Reduce these values of SRF by 25-50% if the weak zones only influence but do not intersect the underground opening

b) Competent, mainly massive rock, stress problems				
F	Low stress, near surface, open joints	$\sigma_1/\sigma_3 > 200$	$\sigma_1/\sigma_3 < 101$	SRF 2.5
G	Medium stress, favourable stress condition	200-10	101-43	1
H	High stress, very tight structure. Usually favourable to stability. May also be unfavourable to stability dependent on the orientation of stresses compared to parting/weakness planes*	10-5	43-10	0.5-2
J	Moderate spalling and/or sloughing after > 1 hour in massive rock	5-3	10-5	5-50
K	Spalling or rock burst after a few minutes in massive rock	3-2	5-1	50-200
L	Heavy rock burst and immediate dynamic deformation in massive rock	< 2	> 1	200-400

Note: 1) For strongly anisotropic virgin stress field (measure σ_1 when $5 \leq \sigma_1/\sigma_3 \leq 10$, reduce σ_1/σ_3 to 0.75 σ_1/σ_3 . When $\sigma_1/\sigma_3 > 10$, reduce σ_1/σ_3 to 0.15 σ_1/σ_3 , where σ_1 = unconfined compression strength, σ_3 and σ_1 are the major and minor principal stresses, and σ_3 = maximum tangential stress (estimated from elastic theory)

2) When the depth of the crown below the surface is less than the span, suggest SRF increase from 2.5 to 5 for such cases (see F)

c) Squeezing rock, plastic deformation in incompetent rock under the influence of high pressure			
M	Mild squeezing rock pressure	1-5	5-10
N	Heavy squeezing rock pressure	> 5	10-20

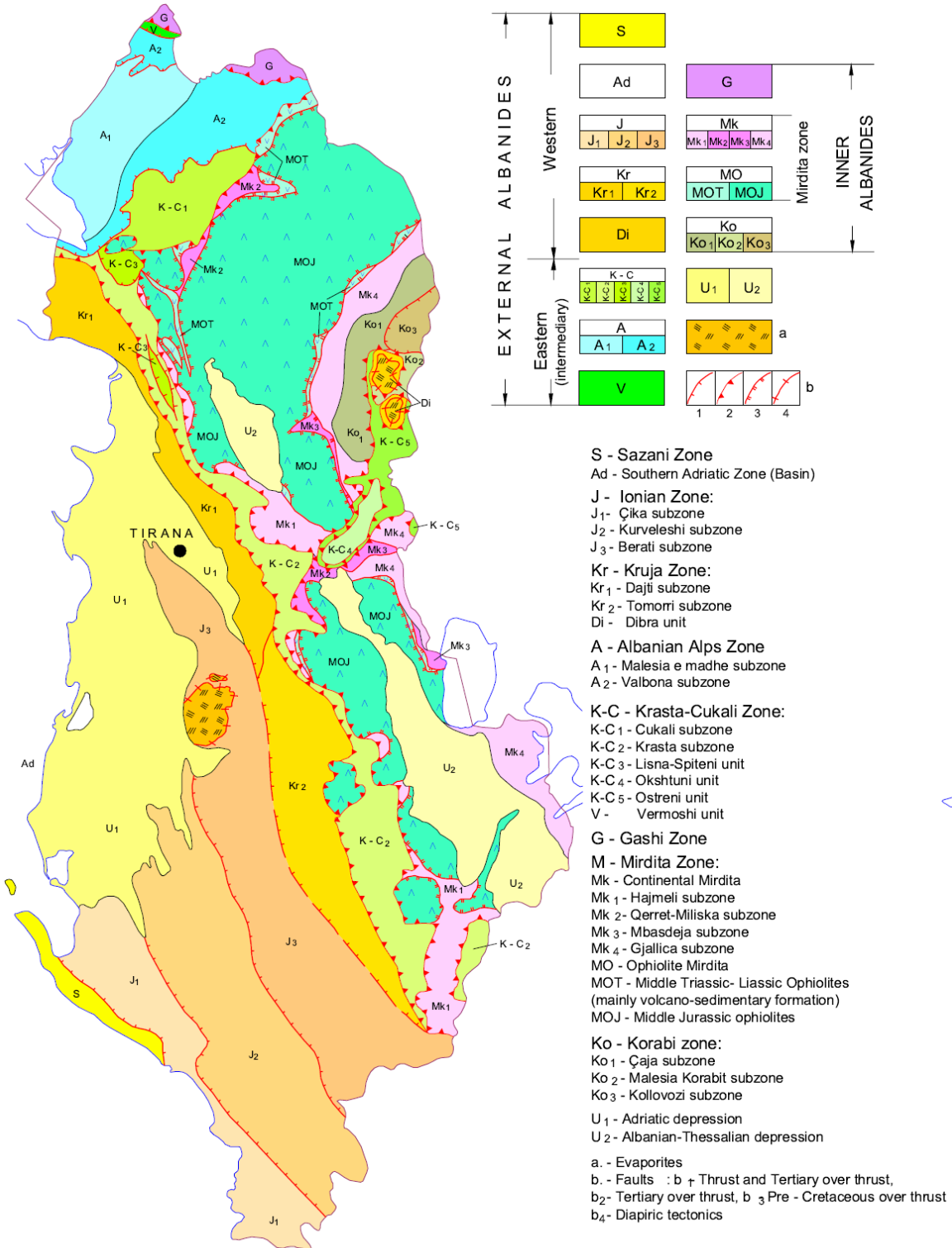
Note: 1) Determination of squeezing rock conditions must be made according to relevant literature (i.e. Singh et al., 1972 and Brown and Gerstlitz, 1996)

d) Swelling rock, chemical swelling actively depending on the presence of water			
O	Mild swelling rock pressure		SRF 5-10
P	Heavy swelling rock pressure		10-15

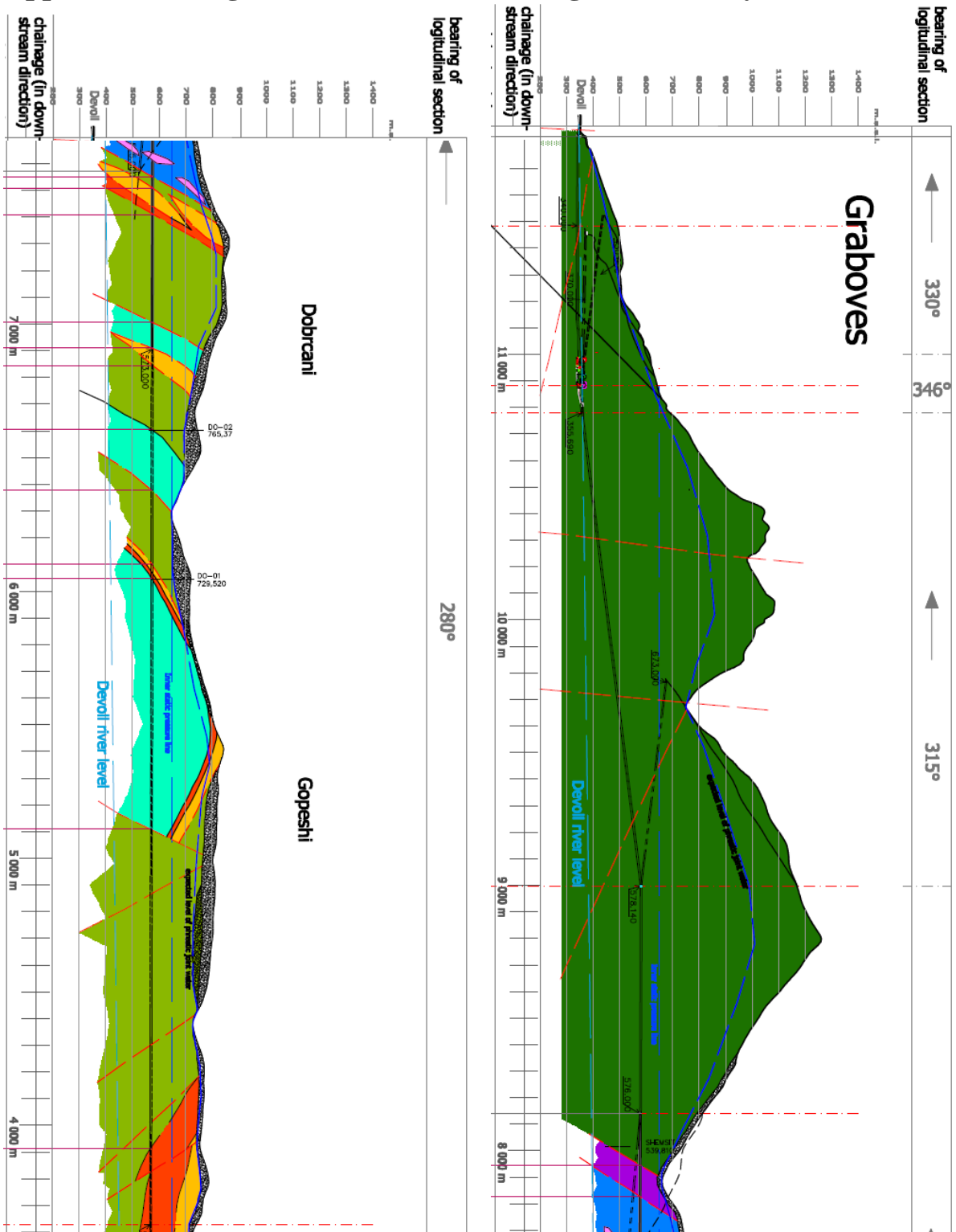
Note:

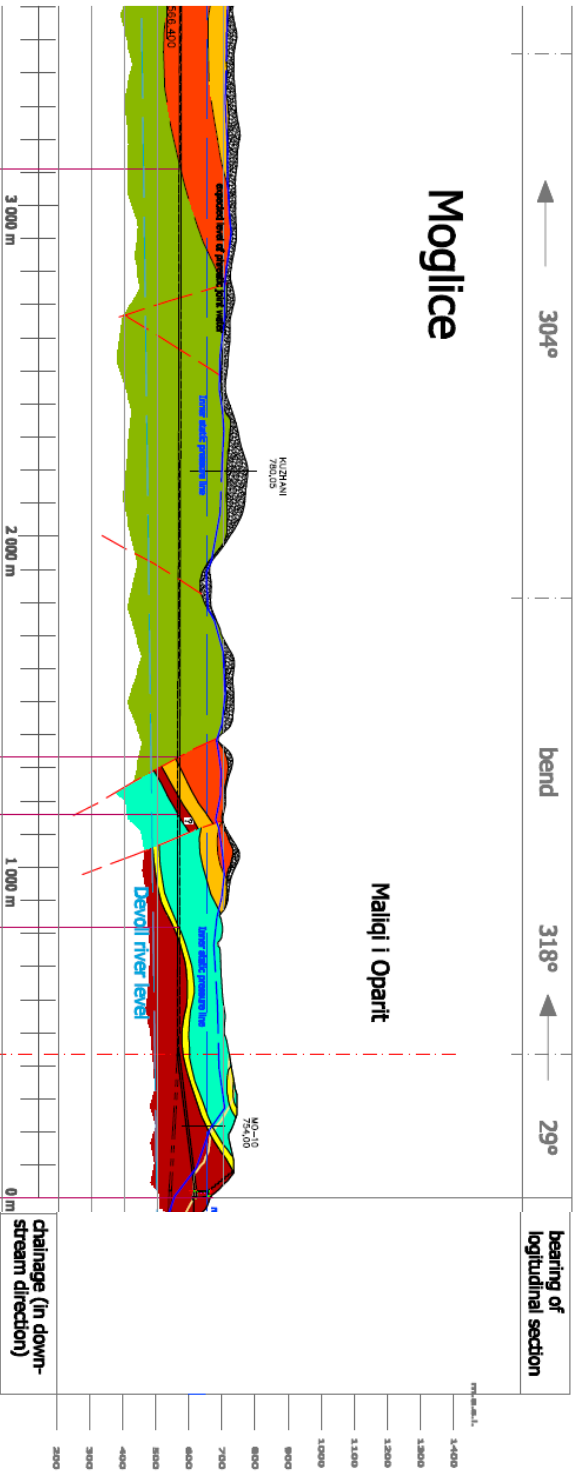
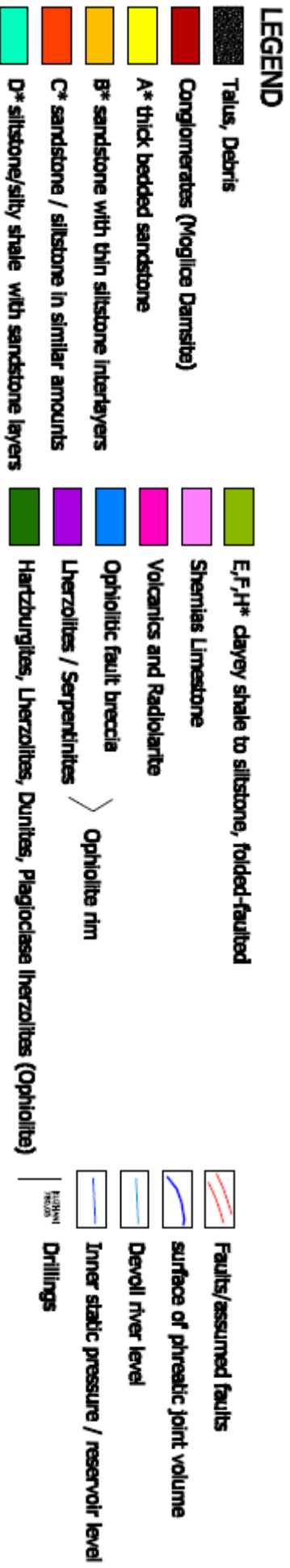
The values for J_n and J_r should be chosen based on the orientation and shear strength, τ , (where $\tau = \sigma \tan(\phi + J_r)$) of the joint or discontinuity that gives the most unfavourable stability for the rock mass, and along which failure most likely will occur.

Appendix D: Tectonic scheme of the Albanides (DHP, 2011)

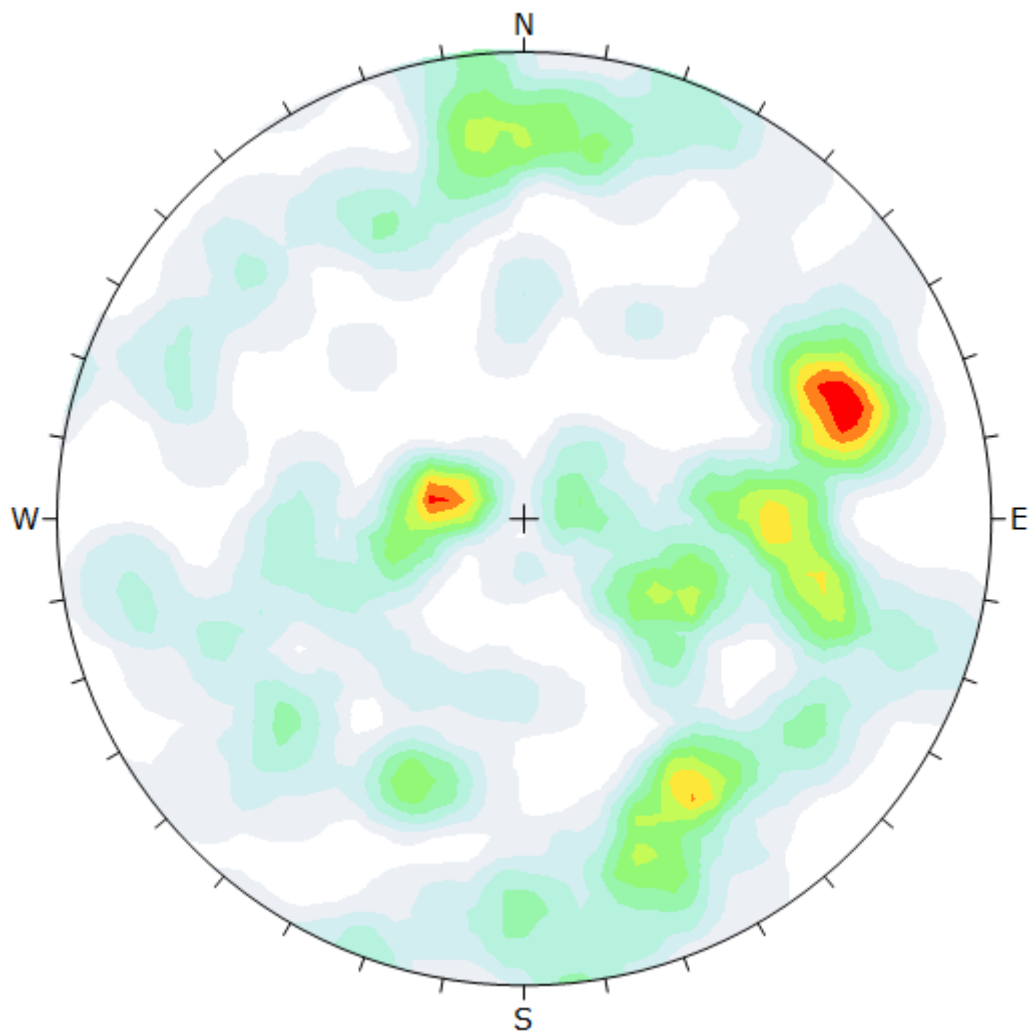


Appendix E: Longitudinal section of the Moglicë waterway (DHP, 2011)



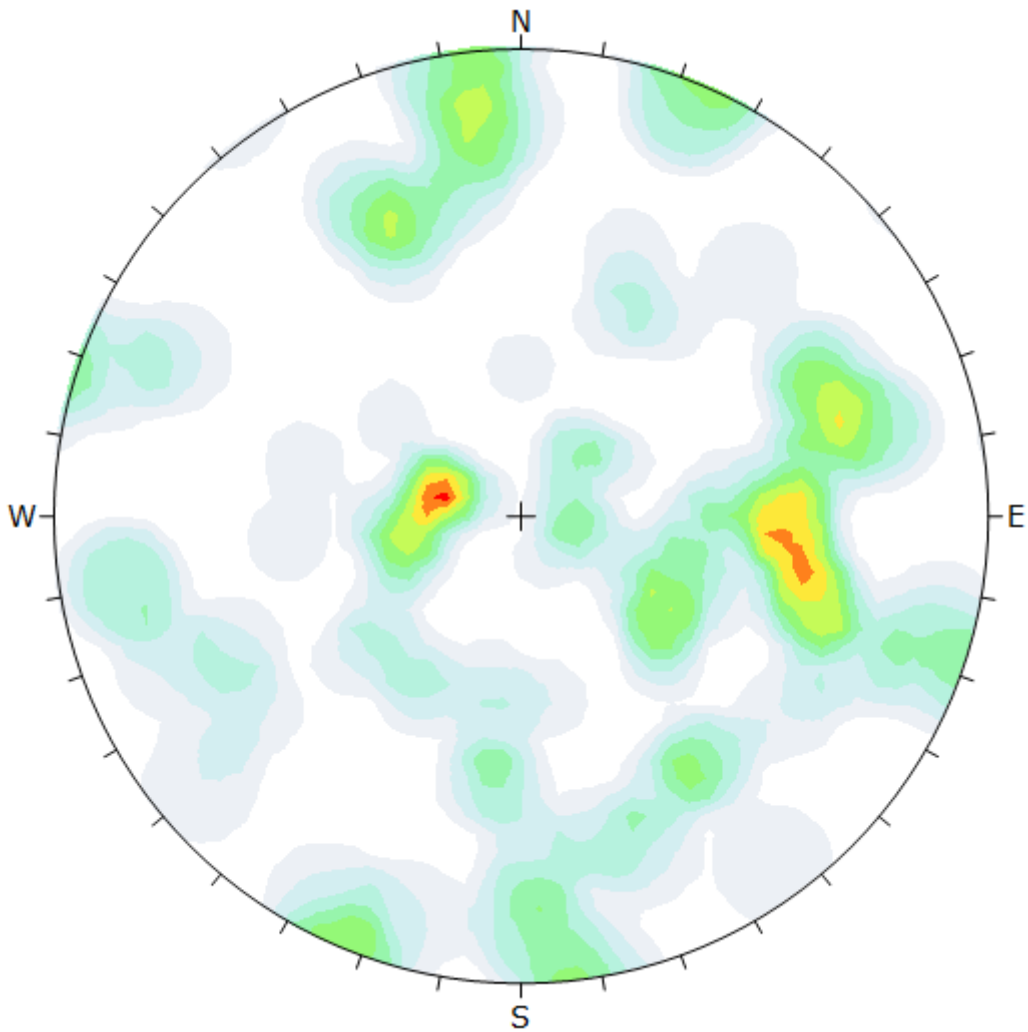


Appendix F: Stereo plots of joints in the ophiolite complex



Color	Density Concentrations
	0.00 - 0.45
	0.45 - 0.90
	0.90 - 1.35
	1.35 - 1.80
	1.80 - 2.25
	2.25 - 2.70
	2.70 - 3.15
	3.15 - 3.60
	3.60 - 4.05
	4.05 - 4.50
Maximum Density	4.36%
Contour Data	Pole Vectors
Contour Distribution	Fisher
Counting Circle Size	1.0%
Plot Mode	Pole Vectors
Vector Count	145 (145 Entries)
Hemisphere	Lower
Projection	Equal Angle

Stereo plot of all joints in the ophiolite complex. Corresponding to figure 4.7a.



Color	Density Concentrations
	0.00 - 0.55
	0.55 - 1.10
	1.10 - 1.65
	1.65 - 2.20
	2.20 - 2.75
	2.75 - 3.30
	3.30 - 3.85
	3.85 - 4.40
	4.40 - 4.95
	4.95 - 5.50
Maximum Density	5.10%
Contour Data	Pole Vectors
Contour Distribution	Fisher
Counting Circle Size	1.0%
Plot Mode	Pole Vectors
Vector Count	92 (92 Entries)
Hemisphere	Lower
Projection	Equal Angle

Stereo plot of the joint measurements closest to the powerhouse complex. Corresponding to figure 4.7b.

Appendix G: Values of the constant m_i for intact rock (Hoek, 2007)

Rock type	Class	Group	Texture			
			Coarse	Medium	Fine	Very fine
SEDIMENTARY	Clastic		Conglomerates* (21 ± 3)	Sandstones 17 ± 4	Siltstones 7 ± 2	Claystones 4 ± 2
			Breccias (19 ± 5)		Greywackes (18 ± 3)	Shales (6 ± 2) Marls (7 ± 2)
	Non-Clastic	Carbonates	Crystalline Limestone (12 ± 3)	Sparitic Limestones (10 ± 2)	Micritic Limestones (9 ± 2)	Dolomites (9 ± 3)
		Evaporites		Gypsum 8 ± 2	Anhydrite 12 ± 2	
		Organic				Chalk 7 ± 2
METAMORPHIC	Non Foliated		Marble 9 ± 3	Hornfels (19 ± 4) Metasandstone (19 ± 3)	Quartzites 20 ± 3	
	Slightly foliated		Migmatite (29 ± 3)	Amphibolites 26 ± 6		
	Foliated**		Gneiss 28 ± 5	Schists 12 ± 3	Phyllites (7 ± 3)	Slates 7 ± 4
IGNEOUS	Plutonic	Light	Granite 32 ± 3 Granodiorite (29 ± 3)	Diorite 25 ± 5		
		Dark	Gabbro 27 ± 3 Nontite 20 ± 5	Dolerite (16 ± 5)		
	Hypabyssal		Porphyries (20 ± 5)		Diabase (15 ± 5)	Peridotite (25 ± 5)
	Volcanic	Lava		Rhyolite (25 ± 5) Andesite 25 ± 5	Dacite (25 ± 3) Basalt (25 ± 5)	Obsidian (19 ± 3)
		Pyroclastic	Agglomerate (19 ± 3)	Breccia (19 ± 5)	Tuff (13 ± 5)	

* Conglomerates and breccias may present a wide range of m_i values depending on the nature of the cementing material and the degree of cementation, so they may range from values similar to sandstone to values used for fine grained sediments.

** These values are for intact rock specimens tested normal to bedding or foliation. The value of m_i will be significantly different if failure occurs along a weakness plane.